# Soft Robot with New Pneumatic Rubber Actuators for Medical Assisting Device

**2016, 3**

**Mohamed Najib bin Ribuan**

**Graduate School of**

**Natural Sciences and Technology**

**(Doctor`s Course)**

**OKAYAMA UNIVERSITY**

# Abstract

Soft robots came into focus after for a long time the coexistence between human and conventional robot has never been an achievement. Unlike hard robot, soft robot has the potential to be more adaptable, capable, and safer devices especially in conditions where the robot has a close contact with human in unstructured environment such as in homes, offices, and public places. However, actuating soft robot is a challenging task as any rigid mechanism and electrical motor will impair the soft and safe characteristics of the robot. Therefore, pneumatic and/ or fluidic type of actuation became common for robot operation.

Basically, the motion generated from soft material such as rubber and silicone, is by the deformation of the soft structure when pneumatic pressure is applied. Only 1 and/ or 2 degree of freedom (DOF) can be achieved through this soft actuator mechanism. Nevertheless, to produce a significant motion of actuation, large deformation is necessary resulting a slow and rough movement if such actuators are to be employed in soft robot as a means of locomotion. In this research, a novel mechanism of fast response and an omnidirectional soft actuator is proposed. The actuators serve as soft robot legs with 6 DOFs for omnidirectional, smooth and precise locomotion ability.

One interesting application of such soft robot; and taking the advantage of transparence characteristic of silicone material, is in fluoroscopy examination. In this examination, an X-ray is used to scan a small lesion and polyps inside stomach as an early detection of stomach cancer. Due to shrinking nature of stomach, it has to be compressed from an external force in order to expose any concealed lesion. Normally, radiologist used a commercialized compression paddle and folded towel as an assisting medical device, positioned manually under the patient stomach to give a pressure to the stomach. The adjustment of the device is bothersome to the patient and here the soft robot has the opportunity to be employed and operated remotely without being detected by the X-ray image.

The development of soft actuator as pneumatic rubber leg for our robot begins with the idea, operating principle and the design of the leg. The design parameters were identified and simulation was conducted to achieve the optimum design from the construction of the leg. For elastomeric material simulation, Finite Element Analysis (FEA) was employed with several prototype designs were simulated until the optimum results is achieved for the specific design

parameters. In addition, simulation works provides better understanding of the leg motion and any modification can possibly be made before fabrication of the prototype.

Then, the fabrication of the prototype took place based on the optimum results obtained in the simulation works. Computer Aided Design (CAD) was used to design the leg and silicone molds of the leg. The information in CAD was then used in Computer Aided Manufacturing (CAM) for rapid prototyping and the silicone mold was produced using polyester resin plate. Two-component Room Temperature Vulcanizing (RTV) silicone rubber were used to produce the rubber leg where the process involves mixing of the silicone material, bubble elimination, and heating. Since the fabrication of the leg was layer by layer, the assembly of the layer was done before tubes were connected to the chambers inside the leg.

The leg prototype was then tested in experimental works in order to achieve the characteristics of the leg prototype. Leg displacement and deflection in vertical, sideway and diagonal direction were measured with different pressure ranging from 0 to 150 kPa. The results were compared with simulation works and show an agreement between the experiment and simulation data thus validating the static analysis characteristics of the leg. In addition, force generated from the deflection in sideway and diagonal direction was also measured using force gauge to identify leg ability in climbing a slope, a condition that may require the robot to perform during the fluoroscopy examination.

An achievement in establishing the leg prototype and its characteristic led to the design of soft robot. Eight legs were arranged in square to form a square-shaped walking soft robot without a leg at the center as the center leg will provide unnecessary analysis during locomotion. The locomotion gait was identified to generate a thrusting force for robot movement. Four stages of locomotion gait was achieved and corresponding pressurized chambers were identified in order to control the pneumatic valve for locomotion direction. The information is crucial in developing the programming of valve activation that dictates the direction of robot locomotion. Furthermore, locomotion pattern were decided where the legs were categorized into two groups in order to achieve static stability locomotion.

Afterwards, the development of soft robot that involve fabrication and control system setup were accomplished. The fabrication process was principally the same as in the fabrication of leg prototype. However, the new molds were produced as the soft robot was fabricated in one complete unit instead of combining each single leg together as it was time consuming and energy wasting. Forty pneumatic valves were used to control the pressure to the chambers where Digital Input Output (DIO) card was connected to the valve via Darlington's circuit as electronics interface between a PC and the valves. The human interface was developed in Microsoft Visual Studio (MVS) 2005 environment using C programming where the user able to control the robot via command prompt window. The characteristics of robot locomotion was investigated through experiment and omnidirectional locomotion ability, locomotion speed, traction force and maximum payload were able to establish.

Finally, the adaptation of soft robot and pneumatic pillow was confirmed with several experiments. The pillow was implanted on top of the robot and robot movement was observed. The ability of the robot to carry the pillow and remain stable after the inflation of the pneumatic pillow 7 times higher than the height of the robot without fall aside confirm a successful coordination between the soft robot and pneumatic pillow to serve as medical assisting device in fluoroscopy examination.

As a conclusion, we managed to produce a new pneumatic rubber leg able to perform omnidirectional motion from a unique mechanism. The characteristics of the leg was validated through experiment and simulation results. The combination of eight legs were used to form a soft robot square in shape to carry a pneumatic pillow as the transparence property of the robot and pneumatic pillow is an advantage of not being detected under X-ray examination. With the omnidirectional locomotion ability, adequate locomotion speed, smooth and precise locomotion ability; the soft robot has the potential to replace the commercialized compression paddle and folded towel as medical assisting device in fluoroscopy examination as an early detection of stomach cancer.

# Dedication

To my dear parents, and my loving family;
*Zanariyah binti Ab Karim*
*Muhammad Afiq Hakimi, 11*
*Nuralisya Hani, 9*
*Muhammad Affan Haikal, 5*
*Muhammad Afdhal Hafiz, 3*
*Nuramira Hafsah, 4 month*

## Acknowledgement

I would like to take this opportunity to commemorate my dearest former supervisor, Professor Koichi Suzumori for his guidance and assistant during my early year of study. His idea and suggestion really open my eyes and broaden my knowledge to cultivate research culture as common practise inside myself. Thank you very much for those enjoying days yet in a short period of time.

I would also like to express my gratitude to my supervisor, Associate Professor Takefumi Kanda for his support and valuable advice in order for me to produce satisfying research outcome. His constructive comments improved the level of my investigation and educate me to generate quality results.

My appreciation also goes to Associate Professor Shuichi Wakimoto, who critically response to the outcomes of my study. I learn a lesson to view things from different perspective in finding solution to a problem during conducting the research. Also to Professor Shibuya, from Shikata Medical Campus, Okayama University for the opportunity to use the facilities under his observation.

To my fellow System Integration Laboratory students and staffs, thank you very much for your help and hospitality during my time in Okayama University. The friendship and togetherness are so worthy from a lot of activities we involve with, that still fresh in my mind.

Finally, to examiners; Professor Yamazaki, Professor Gofuku, and Professor Watanabe for the advices and comments, for the sake of my research betterment.

# Contents

| | | Page |
|---|---|---|
| Title | | i |
| Abstract | | iii |
| Dedication | | vi |
| Acknowledgement | | vii |
| Contents | | viii |
| List of figures | | xi |
| List of tables | | xiv |

**Chapter**

| | | |
|---|---|---|
| **1** | **Introduction** | |
| 1.1 | Introduction | 1 |
| 1.2 | Soft Actuator | 1 |
| 1.3 | Soft Robot | 2 |
| 1.4 | Fluoroscopy Medical Examination | 3 |
| | 1.4.1 Procedure | 3 |
| | 1.4.2 Medical assisting device | 4 |
| 1.5 | Research Purpose | 7 |
| | 1.5.1 Aim and objectives | 7 |
| | 1.5.2 Thesis contribution | 8 |
| 1.6 | Thesis outline | 8 |
| **2** | **Review on Soft Actuator, Soft Robot and Stomach Fluoroscopy** | |
| 2.1 | Introduction | 10 |
| 2.2 | Soft Actuator and Its Application | 10 |
| 2.3 | Development in Soft Robot | 20 |
| 2.4 | Cancer Threat and Stomach Fluoroscopy | 25 |
| 2.5 | Summary | 28 |
| **3** | **New Pneumatic Rubber Actuator** | |
| 3.1 | Introduction | 29 |
| 3.2 | Design Concept | 29 |
| | 3.2.1 Basic structure | 29 |
| | 3.2.2 Working principle | 30 |
| 3.3 | Finite Element Analysis (FEA) Design Optimization | 32 |
| | 3.3.1 Design Prototypes | 32 |
| | 3.3.2 Simulation results | 35 |
| 3.4 | Fabrication Process | 36 |
| | 3.4.1 Computer Aided Design (CAD) | 36 |
| | 3.4.2 Computer Aided Manufacturing (CAM) | 39 |
| | 3.4.3 Silicone mixing | 40 |
| | 3.4.4 Pouring | 41 |

3.4.5 Air bubble elimination 41
3.4.6 Heating and curing 42
3.4.7 Assembly 43
3.5 Experiments 44
3.5.1 Vertical displacement 45
3.5.2 Sideway displacement 46
3.5.3 Diagonal displacement 46
3.6 Results and Discussion 47
3.6.1 Vertical displacement 47
3.6.2 Sideway displacement 48
3.6.3 Diagonal displacement 49
3.7 Summary 50

**4 Omnidirectional Locomotion Soft Robot**

4.1 Introduction 52
4.2 Design and Operation 52
4.2.1 Structure of soft robot 52
4.2.2 Soft robot operation 55
4.3 Soft Robot Development 56
4.3.1 Gait and Locomotion Pattern 56
4.3.2 Fabrication Process 58
4.4 Control System Development 60
4.4.1 Hardware development 60
4.4.1.1 Pneumatic systems 60
4.4.1.2 Valves 59
4.4.1.3 Darlington circuit 61
4.4.1.4 DIO card and connections 61
4.4.2 Software development 63
4.4.2.1 Microsoft Visual Studio (MVS) 2005 63
4.4.2.2 C Programming 64
4.5 Experiments 69
4.5.1 Omnidirectional locomotion 69
4.5.2 Operating frequency and locomotion speed 70
4.5.3 Traction force 70
4.5.4 Payload 70
4.6 Results and Discussion 71
4.6.1 Omnidirectional locomotion ability 71
4.6.2 Locomotion speed 72
4.6.3 Traction force 73
4.6.4 Maximum payload 74
4.7 Summary 75

**5 Soft Robot and Pneumatic Pillow Integration for Medical Assisting Device**

5.1 Introduction 76
5.2 Pneumatic Pillow 76
5.2.1 Design and working principle 77

5.2.2 Specification 77
5.3 Integration and Adaptability 78
5.4 X – ray compatibility 78
5.5 Results and Discussion 79
5.5.1 Mobile stomach compression medical assisting device 79
5.5.2 X – ray traceability 80
5.6 Summary 82

**6 Conclusion and Future Works**

6.1 Summary of Contribution 83
6.2 Future works 84

References 86
Publications 95
Appendix A 96
Appendix B 109

# List of Figures


| Figure | Page |
|---|---|
| **Figure 1.1:** Tensile modulus for selected materials [8]. | 3 |
| **Figure 1.2:** Environment of fluoroscopy examination where patient is slanted for clear image output. | 4 |
| **Figure 1.3:** Compression paddle used to press the stomach. | 5 |
| **Figure 1.4:** (a) Folded towel located under patient's stomach, (b) way of folding the towel, (c) uncompressed stomach, and (d) compressed stomach with clear image. | 6 |
| **Figure 2.1:** Classification of elastic actuator according to Volder, 2010 [13]. | 10 |
| **Figure 2.2:** Pneumatic soft actuator classification and method of classification. | 11 |
| **Figure 2.3:** PAM and its application in in-pipe inspection mobile robot by Fukuda, 1989[1]. | 11 |
| **Figure 2.4:** Pneumatic Artificial Muscles generating rotational motion from Noritsugu, 1997 [15]. | 12 |
| **Figure 2.5:** Use of PAMs in human power assist system by Sasaki, 2005 [20]. | 12 |
| **Figure 2.6:** Knee rehabilitation using PAMs by Park, 2014 [25]. | 13 |
| **Figure 2.7:** Device produced using PAMs. | 13 |
| **Figure 2.8:** Continuum limb from PAMs by Suzumori, 2013 [42]. | 13 |
| **Figure 2.9:** Structure of FMA and its application produced by Suzumori, 1991[44]. | 14 |
| **Figure 2.10:** FMAs as conveyor carrying glass plate by Suzumori, 1994 [46]. | 14 |
| **Figure 2.11:** FMAs as medical device by Chishiro, 2013 [49]. | 15 |
| **Figure 2.12:** Linear motion from PBA by Hayakawa, 2003 [53]. | 15 |
| **Figure 2.13:** Bending motion using PBA presented by Konishi, 2001 [67]. | 15 |
| **Figure 2.14:** Rotational motion from PBAs demonstrated by He, 2013 [68]. | 16 |
| **Figure 2.15:** Ankle rehabilitation device using PBAs by Saga, 2011 [78]. | 16 |
| **Figure 2.16:** Linear motion from employment of bellow by Sasaki, 2012 [79] and Chang, 2015 [82]. | 17 |
| **Figure 2.17:** Bellow-type actuator for bending motion by Konishi, 2002 [83], Choi, 2009 [84] and Meng, 2015 [84]. | 17 |
| **Figure 2.18:** (a) Twisting motion by Gorissen, 2014 [90], (b) rotational motion by Niiyama, 2014 [91], and (c) helical motion by Amase, 2015 [92]. | 18 |
| **Figure 2.19:** Therapy device by Wilkening, 2011 [95] and miniature manipulator from Wakimoto, 2011 [101]. | 18 |
| **Figure 2.20:** Rolling motion from jamming type actuator by Steltz, 2009 [103]. | 19 |
| **Figure 2.21:** Granular jamming used as robotic exoskeleton by Bean, 2015 [107]. | 19 |
| **Figure 2.22:** Soft robots using PAMs by Cai, 2009 [110], Koizumi, 2012 [111], and Godage, 2012 [113]. | 20 |
| **Figure 2.23:** Soft robot from FMAs by Suzumori, 1996 [114], 2007 [115] and Takeshima, 2015 [116]. | 21 |
| **Figure 2.24:** Example of soft robot using PBAs by Suzumori, 1996 [117], Weymouth, 2015 [123], Ni, 2015 [124] and Best, 2015 [125]. | 22 |
| **Figure 2.25:** Gripper using bellow type actautor by Noritsugu, 2000 [126] and Ilievski, 2011 [127]. | 22 |
| **Figure 2.26:** Variation of locomotion ability from soft robot by Shepherd, 2011 [128], Florez, 2014 [129], Tolley, 2014 [131], and Onal, 2011 [132] and 2012 [133]. | 23 |
| **Figure 2.27:** Peristaltic locomotion soft robot from combination of PBA and | |

bellow type of actuator by Dario, 2004 [139] and Yanagida, 2013 [141]. 23
**Figure 2.28:** Colour changing and camouflage ability from soft robot by Suzumori, 2011 [142] and Morin, 2012 [143]. 24
**Figure 2.29:** Type of cancer incidence in Japan in 2007 for male and female [146]. 26
**Figure 2.30:** Type of cancer incidence based on age for male (top) and female (bottom) in Japan in 2007 [146]. 27
**Figure 2.31:** Cancer type and estimation cases in 2011 [148]. 28
**Figure 3.1:** (a) Side view and (b) top view. 30
**Figure 3.2:** Leg mechanism for omnidirectional, fast response and millimetre range pace. 30
**Figure 3.3:** (a) to (f) Leg trajectories with associated deformed chambers. Note the dark colour indicates a pressurized chamber. 31
**Figure 3.4** Design parameters *a*, *b* and *c*. 33
**Figure 3.5:** Simulation for vertical, (a – b), side (c – d) and diagonal (e – f). 35
**Figure 3.6:** Four layers to form the prototype. 36
**Figure 3.7:** Mould designs with corresponding designation. 37
**Figure 3.8:** Details dimension of soft actuator. 38
**Figure 3.9:** Roland milling machine for rapid prototyping. 39
**Figure 3.10:** Fabricated block moulds. 39
**Figure 3.11:** Flow process of flexible leg fabrication. 40
**Figure 3.12:** Mixing 2 components of silicone rubber material. 40
**Figure 3.13:** Conditioning vacuum mixer. 41
**Figure 3.14:** Proper amount of compound poured into block moulds. 41
**Figure 3.15:** Pressing the mould before heating. 42
**Figure 3.16:** Natural convection oven for curing. 43
**Figure 3.17:** Complete prototype of flexible leg. 44
**Figure 3.18:** (a) Flexible leg and (b) cross section of prototype. 44
**Figure 3.19:** Force measurement. 45
**Figure 3.20:** Vertical deformation at 150kPa. 46
**Figure 3.21:** Sideway deformation at 150 kPa. 46
**Figure 3.22:** Diagonal deformation at 150 kPa. 47
**Figure 3.23:** Displacement (mm) vs. pressure (kPa). 47
**Figure 3.24:** Magnitude, *r* (mm) vs. pressure (kPa). 48
**Figure 3.25:** Deflection angle (°) vs. pressure (kPa). 48
**Figure 3.26:** Magnitude, *r* (mm) vs. pressure (kPa). 49
**Figure 3.27:** Deflection angle (°) vs. pressure (kPa). 50
**Figure 4.1:** Soft robot design and dimension. 53
**Figure 4.2:** Details dimension of soft robot in (a) side view and (b) top view. 54
**Figure 4.3:** Proposed soft robot operation in stomach fluoroscopy examination. 55
**Figure 4.4:** Overview of proposed complete system. 56
**Figure 4.5:** Locomotion pattern of soft robot with 180˚ phase shift different. 58
**Figure 4.6:** Mould drawing for the soft robot with the assembly mould. 59
**Figure 4.7:** Fabricated prototype of soft robot. 59
**Figure 4.8:** Valve type. 60
**Figure 4.9:** 7-channel Darlington Sink Driver. 61
**Figure 4.10:** DIO card PCI-2746C from Interface. 61
**Figure 4.11:** Connection between DIO's terminal, Darlington's Sink Driver circuit and valves. 62
**Figure 4.12:** Chamber numbering based on chamber position. 62
**Figure 4.13:** Valves assigning with corresponding chambers using

colour coding to differentiate the chamber position. 63
**Figure 4.14** Chamber condition and binary value representation. 65
**Figure 4.15:** Command prompt window for operating the soft robot. 68
**Figure 4.16:** System configuration. 68
**Figure 4.17:** Omnidirectional locomotion. 69
**Figure 4.18:** Traction force experimental setup. 70
**Figure 4.19:** Payload experimental setup. 71
**Figure 4.20:** Locomotion ability in (a) straightway, (b) diagonal, and (c) rotational. 71
**Figure 4.21:** Locomotion speed in straightway direction. 72
**Figure 4.22:** Locomotion speed in diagonal direction. 73
**Figure 4.23:** Locomotion speed in rotational direction. 73
**Figure 4.24:** Locomotion speed with payload in linear direction. 74
**Figure 4.25:** Locomotion speed with payload in rotational direction. 75
**Figure 5.1:** Sponge Core Soft Rubber Actuator in matrix arrangement, (a) initial state, and (b) pressurized state [97]. 76
**Figure 5.2:** Design of pneumatic bag actuator from (a) resin film, and (b) cloth cover [98]. 77
**Figure 5.3:** 2 actuators stacking with gusset [98]. 77
**Figure 5.4:** Pressurized single actuator [98]. 78
**Figure 5.5:** Double actuator with (a) pressurized single actuator, and (b) pressurized both actuator [98]. 78
**Figure 5.6:** Dimension of soft material sample. 79
**Figure 5.7:** Fabricated sample. 79
**Figure 5.8:** (a) Initial position, and (b) pressurized mobile stomach compression medical assisting device. 80
**Figure 5.9:** X – ray image of pneumatic pillow and soft material sample with different thickness. 80
**Figure 5.10:** Sample with edge cut at certain angle. 81
**Figure 5.11:** X-ray image of sample which its edge was slanted. 81

# List of Tables


**Table** **Page**

**Table 3.1:** Design optimization for 18 possible models. 34
**Table 4.1:** Gait locomotion and corresponding pressurized chamber. 57
**Table 4.2** Pin assignment with corresponding chamber. 63
**Table 4.3:** Forward locomotion sequence. 66
**Table 4.4** Simplified hexadecimal value for programming development. 67
**Table 5.1:** Pneumatic bag actuator specification. 77

# Chapter 1

## Introduction

### 1.1 Introduction

This chapter gives a brief idea of soft actuator, soft robot and fluoroscopy medical examination. It begins with the introductory of actuator, its type and the advent of soft actuator. Then, the arrival of soft robot is briefly explained as a results of to spur the coexistence between human and robot in social life. Next part introduces the fluoroscopy medical examination, where the soft robot has a potential application as medical assisting device. Finally, the purpose and contribution of the thesis is presented.

### 1.2 Soft Actuator

Basically, actuator converts an energy into a motion. The source of energy comes from many forms including electrical current, hydraulic fluid pressure, pneumatic pressure, thermal and magnetic field. Meanwhile, the motion generated from these energies are fundamentally the same. Motion such as linear, rotation, and oscillatory motion are the examples of type of motion produced by the actuator in order to generate a movement for a mechanical system that provide solution to any specific mechanical problem.

However, the selection of actuator depends on the type of actuator used. Four main types of actuators are electrical, mechanical, hydraulic, and pneumatic actuator. Electrical actuator such as motor and valve are widely used due to their cleanliness and readily available for any application. Mechanical actuator that involves gears, rails, pulley, chain, etc. converts a rotary motion into linear motion and normally this actuator is combined with the rest of type of actuator. Hydraulic actuator, consisting of cylinder or fluid motor utilizes liquid such as an oil to generate linear, rotary and oscillatory motion. Similarly, pneumatic actuator applied the same concept as in hydraulic actuator except the compressed gas is used instead of an oil.

Among these type of actuators, the advantages of cleanliness, quick response, easily constructed, high power to weight ratio, lightweight and economical set up is provided by pneumatic actuator. More importantly, these attributions made pneumatic actuator more adaptable to soft structure. For example, soft materials that can be easily deformed such as polymers, foams, granular materials, rubber, etc. can only be actuated using a compress air or vacuum; the domain solely under pneumatic system operationalization. The utilization of soft materials in pneumatic actuator, or referred as soft actuator offers a good human interaction as it can be safe by its compliance property and its ability to absorb the force if collision accidentally happen during the close interaction between human and robot.

Nevertheless, the combination of rigid structure implanted within the soft material is also possible to produce the soft actuator. For example, Shaped Memory Alloy (SMA), Ionic polymer metal composite (IPMC), Ionic Conducting Polymer Film (ICPF), Electroactive Polymer Actuator (EPA), Dielectric Elastomer Actuator (DEA), Ferro fluid, cable, wire and composite granular embedded inside soft material structure can generate motions from input such as electrical and mechanical energy.

## 1.3 Soft Robot

Ever since the discovery of the word ‘robot’ used by Czech writer, Karel Capek in 1921, the world has been seen a tremendous explosion of robot technology in every aspect of human life. Although the word was referred to ‘automata’, originated from a great history and evidences - dated back as far as circa 270 BC, until today the progressive of invention of robot has never been at its peak. The pace of innovation continues in tandem with technological advancement in several areas particularly in design, construction, operation, application of robot, computer system, control system, sensory feedback and information processing, where these areas are referred as ‘robotics’.

Although the two fathers of robotics, Isaac Asimov and Joseph Engelberger have made a significant contribution in the robotics field, perhaps the effort itself confines the robot into limited human interaction. Isaac Asimov, science fiction writer, introduced Three Laws of Robotics in 1942 as follow,

1. A robot may not injure a human, or, through inaction, allow a human being to come to harm.
2. A robot must obey the orders given it by human beings excepts where such orders would conflict with the First Law.
3. A robot must protect its own existence as long as such protection does not conflict with the First or Second Law.

Meanwhile, Engelberger started the first robotics company, Unimation in 1961 for the famous industrial robot, Unimate that widely used in automotive industry. Yet the dispersion of robots are only common in industrial and research area where human population could not taste the direct impact and benefits from its existence.

Due to this limitation of safety requirement and possible human error, soft robots were introduced quite recently and still in infancy stage [1] with substantial progress are now happening in all over the world. Although some researchers tend to mix up the bio-inspired and/or biomimetic as 'soft' robot [2-11] where a solid-structure was embedded under soft material as a means of actuation, we agree on the definition where soft robot is composed exclusively from soft material with stiffness in the range of soft biological materials [12]. This is because of our interest to maintain the compliance property of the robot for human interaction and with the existence of solid structure in the system will jeopardize the safety and reliability of the robot. Figure 1.1 shows the tensile modulus (Young's modulus) for certain material including biological materials.

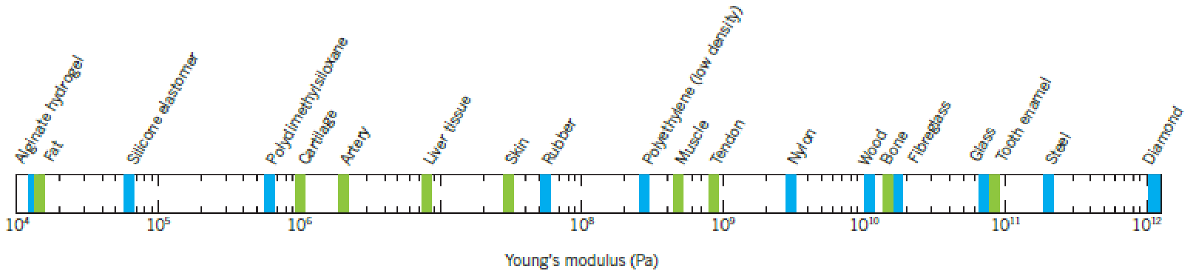


**Figure 1.1:** Tensile modulus for selected materials [12].

## 1.4 Fluoroscopy Medical Examination

### 1.4.1 Procedure

Fluoroscopy is a kind of medical imaging intended to examine specific area in the body such as bones, muscles, joints; and an internal organs such as heart, lung, kidney and stomach. In the case of patient whom undergoing stomach fluoroscopy test, he/she will be asked to drink a contrast media or "dye" such as barium prior to the examination. During the test, a continuous wide beam of X-ray is exposed to the patient`s stomach. Exam table where patient is located in prone or supine position will be tilted at several angles to allow the barium coating the stomach wall. This will results in an excellent video image throughput. However, along the process to discover any abnormality during the examination, patient is required to hold his/her breath and some intervention from radiologist is necessary to compress the abdomen. As stomach just like a balloon which is shrinking in nature, the compression of the stomach will expose and spread the barium hence revealing the small ulcer and polyps which identified as the root cause of stomach cancer. This procedure took about 15 to 30 minutes to complete with different position of patient as well as tilting angle of the exam table.

Figure 1.2 shows the condition of patient during fluoroscopy examination. The patient is in the exam room while the radiologist whose operate the machine is in separate room, namely control room. The exam table is controlled by the radiologist in order to incline the patient at specific angle to thorough investigation of any abnormality inside the stomach based on the output image from the display.

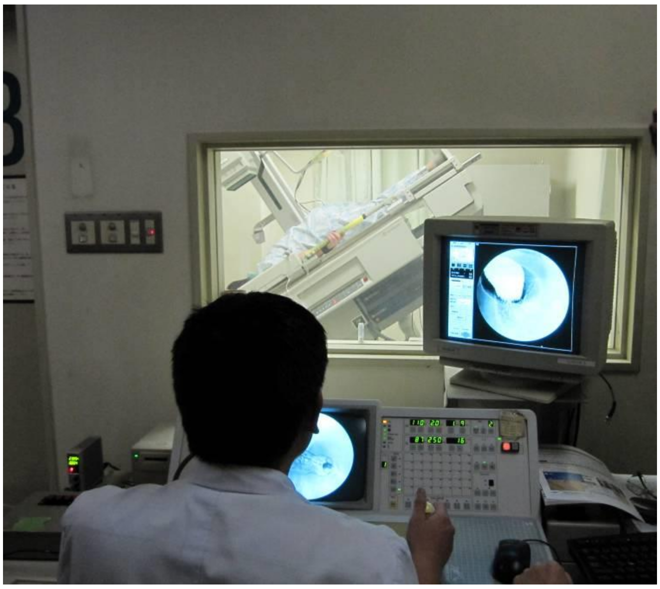

**Figure 1.2:** Environment of fluoroscopy examination where patient is slanted for clear output image.

### 1.4.2 Medical assisting device

A commercialized compression paddle and folded towel has been widely used as a compressing device, which is placed between the exam table and patient's stomach to push the stomach at specific area. They work to prevent superimpose of the image since both the compression paddle and bath towel are X-ray transparent. Figure 1.3 shows the usage of compression paddle and Figure 1.3 (a) shows the pressurized compression paddle while Figure 1.3 (b) shows compression paddle under normal condition.

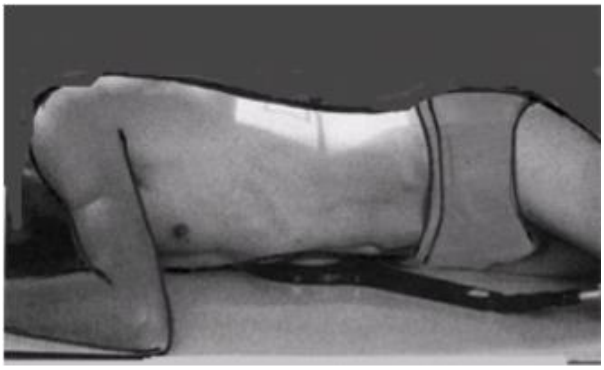

(a)

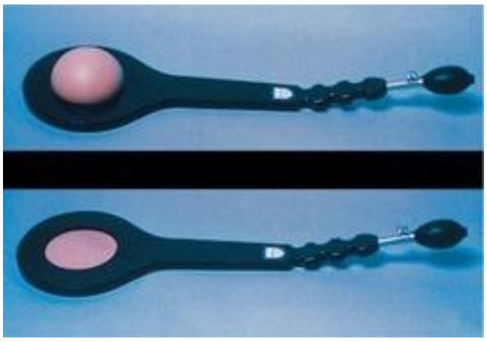

(b)

**Figure 1.3:** Compression paddle used to press the stomach. *http://www.auntminnie.com/index.aspx?sec=ser&sub=def&pag=dis&ItemID=53089* (a) Compression paddle is pressurized, and (b) compression paddle in normal condition. https://o.quizlet.com/Ng-DGkzRQAz-U0b09STl5g_m.jpg

Meanwhile, the employment of folded towel has been practised by some radiologist and can be seen as in Figure 1.4 (a). Figure 1.4 (b) shows the way how the towel is folded and placed between the patient stomach and the exam table. From the improvisation, Figure 1.4 (c) and Figure 1.4 (d) show the comparison between an X-ray images of stomach without compress and stomach being compressed respectively using the folded towel. The orange box highlight the area of the compressed stomach with clear image at the specific area.

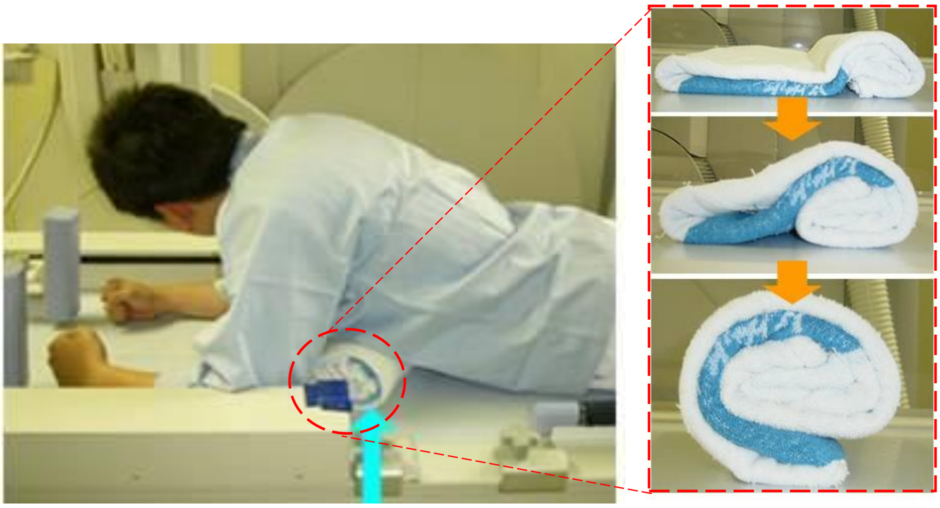

(a) (b)

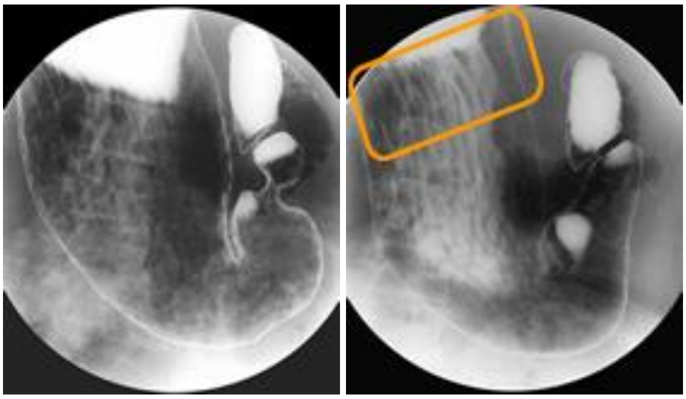

(c) (d)

**Figure 1.4:** (a) Folded towel located under patient's stomach, (b) way of folding the towel, (c) uncompressed stomach, and (d) compressed stomach with clear image. http://www.syoukaki-kensinseido.jp/index.html

Nevertheless, frequent intervention by radiologist during the adjustment of the assisting device to the specific location around the stomach can be bothersome for the patient. This includes the radiologist have to enter the examination room, asking the patient to lift his/her body, adjusting the assisting device manually, exit the examination room and continue operating the fluoroscopy machine. This process will repeat several times for different stomach area and besides uncomfortable to the patient, the level of radiation exposure also increase both to the patient and the radiologist.

## 1.5 Research Purpose

The purpose of this study is to establish a soft actuator with X-ray transparent property able to perform higher DOF of actuation that includes linear extension and oscillatory motion in different direction. This gives the actuator an omnidirectional ability which is useful for locomotion if the actuator serves as the legs for a soft robot. The design property of the actuator which dictates the output performance need to be identified in order to obtain the characteristics of the actuator.

Once the soft actuator is established, the investigation continues to develop the soft robot in term of realizing the omnidirectional locomotion. Components such as locomotion stability, traveling speed, distance and ability to carry a load need to be identified in order to evaluate the soft robot performance. Furthermore, the potential ability of replacing the existing medical assisting device need to be confirmed as well as its workability to ensure the safety and reliability of the soft robot during its operation.

### 1.5.1 Aim and objectives

Based on the requirement of X-ray transparency and distraction experienced by the patient, this study aims to produce a soft robot able to transfer a pneumatic pillow as an assisting medical device. This device will be serve as stomach compression during stomach fluoroscopy examination as a means to eradicate human intervention and radiation risks. The soft robot is constructed from soft actuator made from silicone rubber to form a horizontal platform for pneumatic pillow transportation to the specific location with omnidirectional locomotion ability. The soft robot operates pneumatically and remotely controlled thus eliminating radiologist intervention during the medical examination.

Following are the objectives of the study to ensure the aim is achievable,

1. To establish an actuator with omnidirectional mechanism from soft materials exhibits properties such as translucent, safe and human compliance.
2. To produce a prototype of soft robot, based on the established actuator to perform omnidirectional locomotion and operate in clean and quiet environment, e.g. Healthcare centre and hospital.
3. To develop the control system of soft robot in order to govern the locomotion direction.

4. To evaluate the characteristics and parameters associated with the performance of the soft robot.
5. To incorporate pushing mechanism on the soft robot for stomach fluoroscopy examination and confirm its workability as medical assisting device.

### 1.5.2 Thesis contribution

The principal contribution of this thesis are as follow,

1. The establishment of new soft actuator with linear and oscillatory motion in different direction for higher degree-of-freedom (DOF).
2. Based on the soft actuator, an omnidirectional locomotion soft robot is realized eliminating a complex mechanism for turning and changing direction.
3. The property of stiffness and thickness of soft material, specifically a silicone rubber towards the detection of an X-ray is established.

## 1.6 Thesis Outline

The thesis is divided into five chapters. In Chapter 1, which is the Introduction, the background of the study is discussed. It covers the explanation of soft actuator, soft robot and fluoroscopy medical examination, where the problem statement is identified and how the soft robot can be potentially employed to facilitate the medical procedure. In addition, the introduction of soft actuator and soft robot are also delivered to give a general idea about the branch of actuator and robot. Besides explanation of research purpose, this chapter also highlight the aim and contribution of this research to be acknowledged and appreciated.

In the second chapter of the thesis, represented by Chapter 2, a review on the development of soft actuator, soft robot and issue regarding stomach fluoroscopy examination are presented. The soft actuator, which hold the basic mechanism for the soft robot movement is the main subject of this study and required a complete review. From the review, any gap and disadvantage of existing actuator is identified and stem the idea to create a new mechanism for the new soft actuator. Then, the literature on soft robot is explained to provide the current progress in soft robotics field. The final part of Chapter 2 discusses the impact of stomach fluoroscopy examination towards life threatening cancer with case study conducted in Japan.

Chapter 3 discussed the development of soft actuator. It covers the design of the soft actuator, its operating principle and parameters associated with the design. The simulation works are described in order to achieve the optimum design of the actuator which assists the fabrication process. Afterwards, the description of fabrication process is presented including Computer Aided Design (CAD), mould design, Computer Aided Machining (CAM), etc. until the prototype of the actuator is obtained. Then, the validation of all the theory and hypotheses from the previous works is demonstrated through series of experimental works.

In Chapter 4, the development of soft robot is discussed. The discussion focused on the design and operation of the soft robot. This includes the theory of locomotion gait and locomotion pattern in order to identify the thrusting force and robot ability to perform the omnidirectional locomotion. Then, fabrication process is explained until the prototype of the soft robot is achieved. In order to control the soft robot, the development of both software and hardware are presented. From the configuration, a series of experiments managed to be performed and explained in this chapter. The results from the experiments contribute to the characteristics and behaviour of the robot based on input parameters applied to the control system.

Chapter 5 reports on the works of combining the soft robot with pneumatic pillow as medical assisting device in stomach fluoroscopy examination. The pneumatic pillow which has been tested under X-ray examination and confirmed its workability, is implanted on the top of the robot. The compatibility between the two subjects is investigated through a series of experiments. Results from the experiments provide the evidence for potential ability of the combination of soft robot and pneumatic pillow, to be used as medical assisting device in fluoroscopy examination.

The final Chapter 6 summarizes the works and outcome of the investigation. The accomplishment of the research is compared to the previous aim and objectives in order to reflect the achievement of the works. In addition, any drawback in every aspect during the study is addressed and possible improvement is suggested. This benefits the future works of the study and to ensure a continuous and active research progress in the area of soft robotics.

# Chapter 2

## Review on Soft Actuator, Soft Robot and Stomach Fluoroscopy

### 2.1 Introduction

This chapter begins with a review on soft actuators and their corresponding mechanism that generates several motions. Then, the application of the actuators is briefly explained. Afterwards, a review on soft robot is presented to update the current progress in the field of soft robot. These information provide the niche area where the soft robot has never yet been explored. The final part discusses the relation between stomach cancer and fluoroscopy examination based on case study in Japan.

### 2.2 Soft Actuator and Its Application

The classification of Elastic Fluidic Microactuators can be seen as in Figure 2.1 based on Volder [13]. However, with the intensive research and fast progress in soft actuators, the categorization of soft actuator can be expanded.

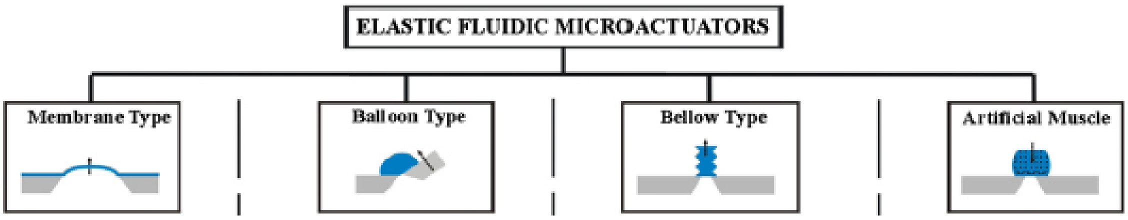


**Figure 2.1:** Classification of elastic actuator according to Volder, 2010 [13].

In general, pneumatic soft actuator can be divided into five categories: Pneumatic Artificial Muscles (PAMs), Flexible Micro Actuators (FMAs), Pneumatic Balloon Actuators (PBAs), bellows, and composite granular jamming. Figure 2.2 shows the division of soft actuator and the categorization method as guidance for the classification.

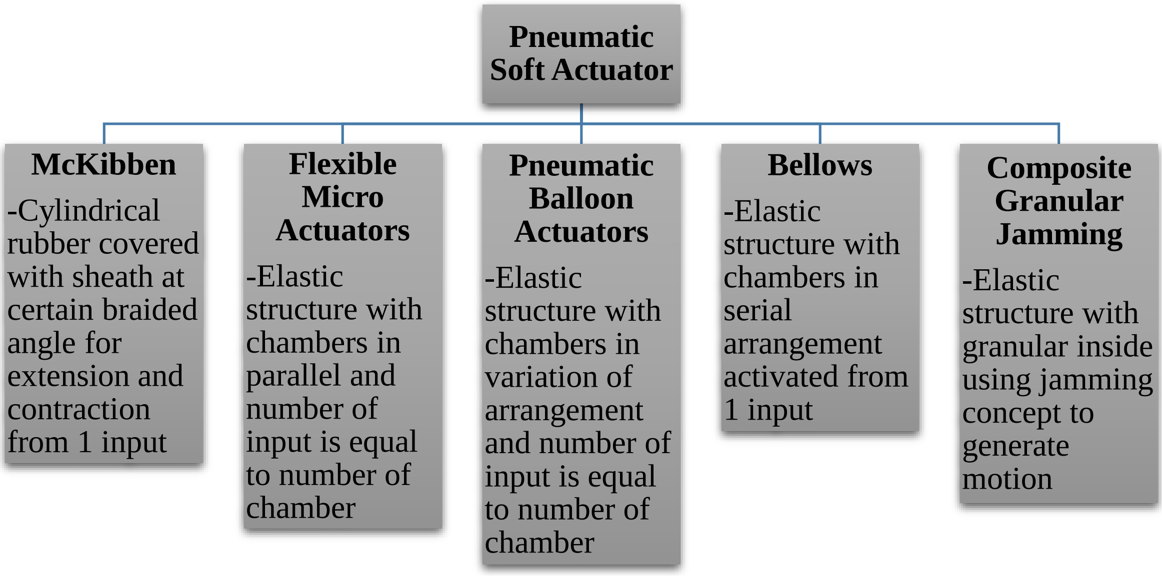


**Figure 2.2:** Pneumatic soft actuator classification and method of classification.

In principle, McKibben or PAMs or Pneumatic Muscle Actuators (PMAs) is constructed from a rubber and covered by sheath or nylon sleeves with specific braid angle to allow an extension and contraction when pressurized. This mechanism allows one Degree-Of-Freedom (1-DOF) linear motion as well as bending, and rotation, depending on the arrangement of the actuators. For linear motion, the actuator is arranged with both ends are located in straight position as in Figure 2.3 (a). The bending motion is realized when several actuators are arranged in parallel as in Figure 2.3 (b). These configuration was established by Fukuda for his in-pipe inspection robot [14]. In rotational motion, two actuators are arranged and connected to roller as in Figure 2.4 where the actuator works antagonistically.

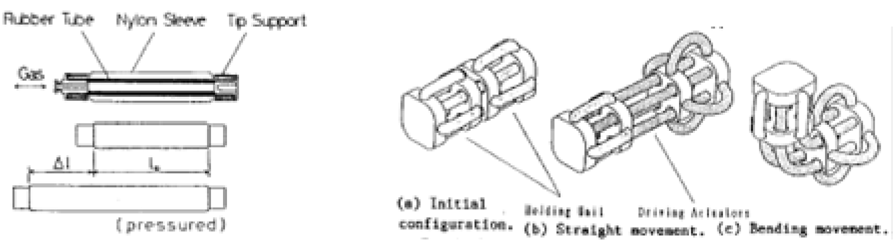


(a) (b)

**Figure 2.3:** PAM and its application in in-pipe inspection mobile robot by Fukuda, 1989 [14].

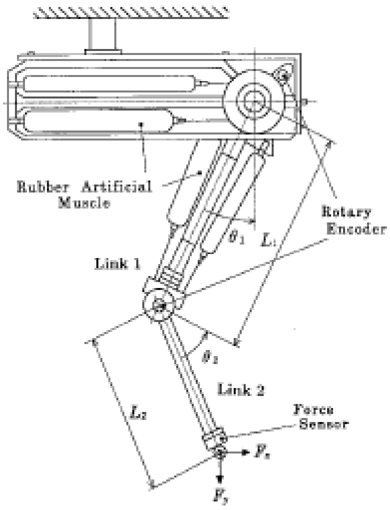


**Figure 2.4:** Pneumatic Artificial Muscles generating rotational motion from Noritsugu, 1997 [15].

Several researchers have demonstrated variation of arrangements to achieve similar motion of linear, bending and rotational based on their application. In power assist and exoskeleton system, PAMs are used as demonstrated in [16 – 22] as can be seen in Figure 2.5.

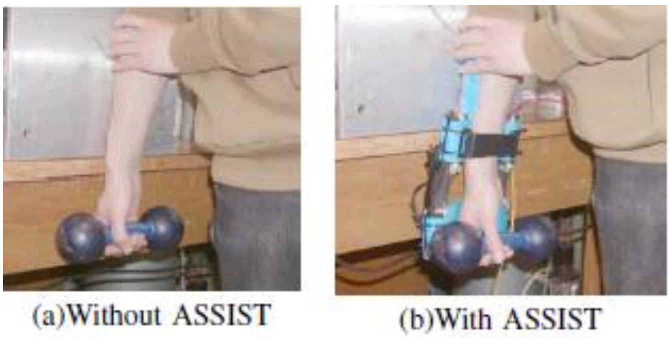


**Figure 2.5:** Use of PAMs in human power assist system by Sasaki, 2005 [20].

Another application which close to power assist is rehabilitation where PAMs are widely used as reported in [23 – 27]. Among favourite body parts for rehabilitation are hand finger, ankle and knee as in Figure 2.6.

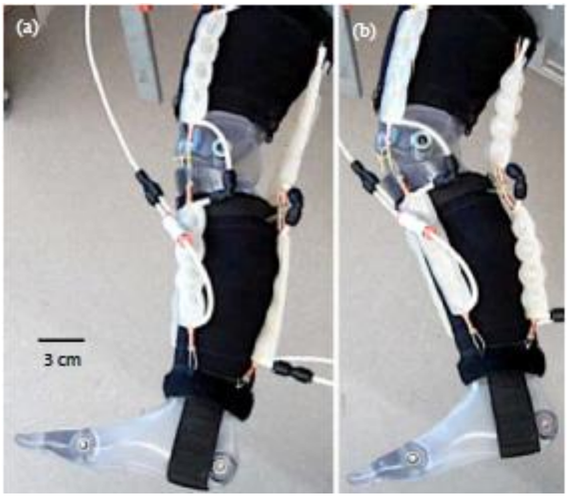


**Figure 2.6:** Knee rehabilitation using PAMs by Park, 2014 [25].

Nevertheless, invention of device based on PAMs showed intensive progress as described in [28 – 40]. Device such as endoscope, minimal invasive surgery tool and robot actuator were among the device produced as in Figure 2.7.

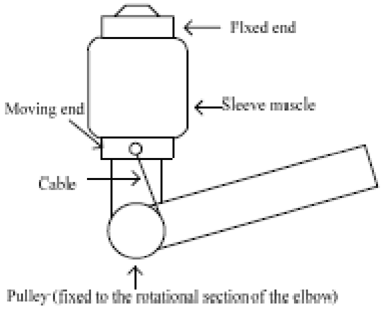


Wakimoto [29] Volder [32] Driver [35]

**Figure 2.7:** Device produced using PAMs.

Another application which PAMs are used is in producing continuum limb. Although several continuum limbs has been demonstrated, the pneumatically operated continuum limb has been established in [41 – 42] as in Figure 2.8.

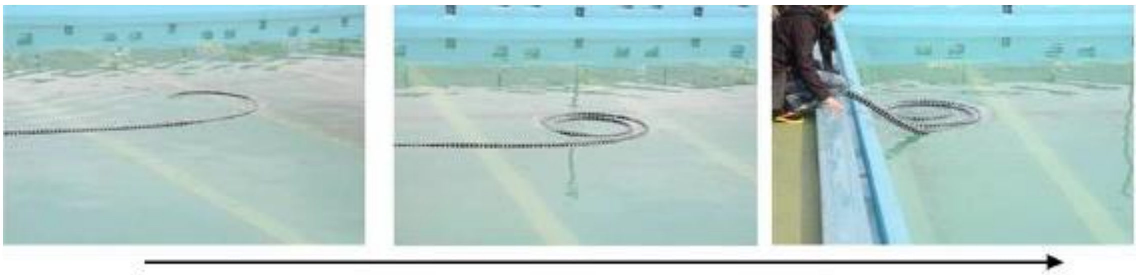

**Figure 2.8:** Continuum limb from PAMs by Suzumori, 2013 [42].

An FMA consists of several chambers arranged in parallel within one elastic structure with or without sleeve and the sleeve do not determine the contraction and extension of the actuator as in PAM. It was first developed by Suzumori where the structure and application can be seen in Figure 2.9 [43 – 47]. For linear motion, all the chambers are pressurized whilst bending motion can be achieved by pressurizing one of the chamber. Nevertheless, rotational motion is difficult for this kind of actuator.

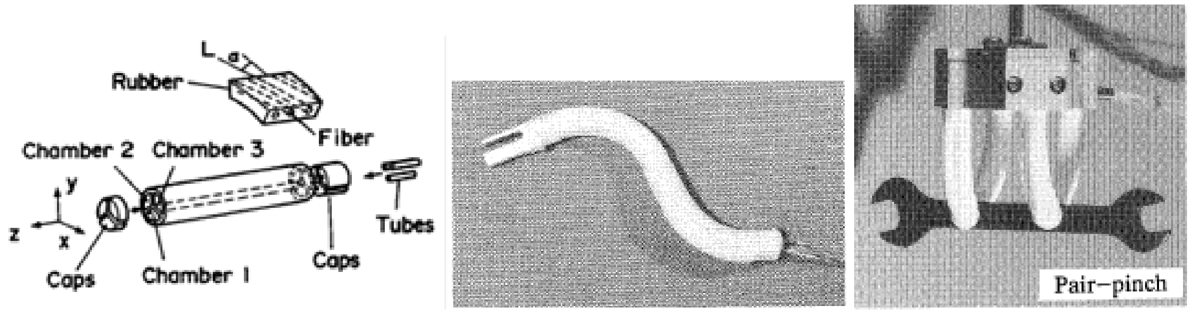


**Figure 2.9:** Structure of FMA and its application produced by Suzumori, 1991[44].

Most of the application of FMA are as manipulator and device for medical purpose [48 – 52]. Interestingly, besides as manipulator as demonstrated by Suzumori previously, it also be used as conveyor as in Figure 2.10.

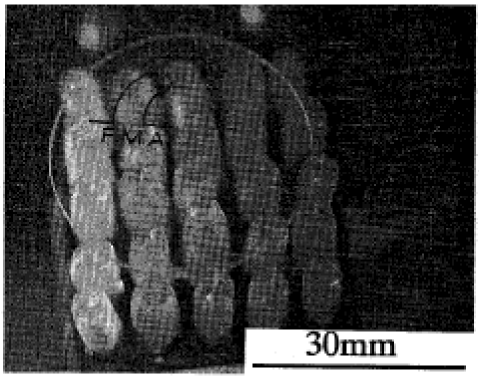


Fig.10 Example of 5x5 array FMA carrying a glass plate; post-assembled device after stereo lithography for each FMA)

**Figure 2.10:** FMAs as conveyor carrying glass plate by Suzumori, 1994 [46]

Figure 2.11 shows the application of FMAs as mechanism to be used with forceps during medical surgery as well as endoscope.

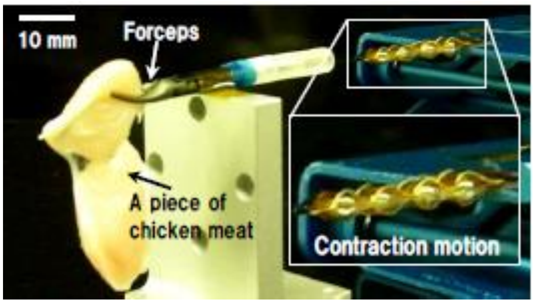


**Figure 2.11:** FMAs as medical device by Chishiro, 2013 [49].

By using simple mechanism of balloon deformation, PBA is constructed from elastic material with chamber independently operated whilst the arrangement is not parallel as in FMA. The simple linear motion was described in [53 – 55] by pressurizing the chamber as in Figure 2.12. In fact, most of the employment of PBAs are taking the advantage of the linear motion as demonstrated in [56 – 66].

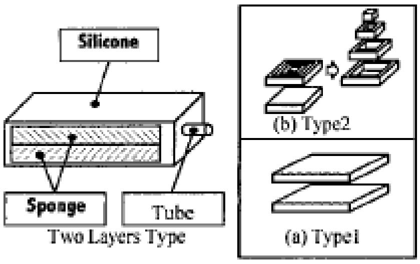


Fig.5 Structure of Silicon Outer Fence Mold Actuator

**Figure 2.12:** Linear motion from PBA by Hayakawa, 2003 [53].

Bending motion can be obtained by using different thickness of material or different elasticity of material as in Figure 2.13. For rotational motion, the arrangement of PBAs are in series as in Figure 2.14.

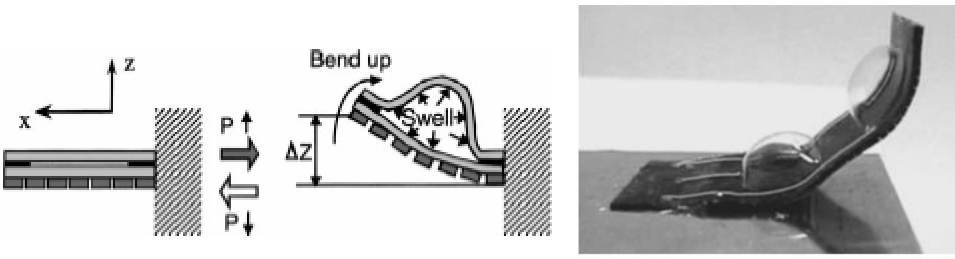


Fig. 2. Working principle of an end-effector using a PBA.

Fig. 13. 2-DOF end-effector with two pneumatic balloons.

**Figure 2.13:** Bending motion using PBA presented by Konishi, 2001 [67].

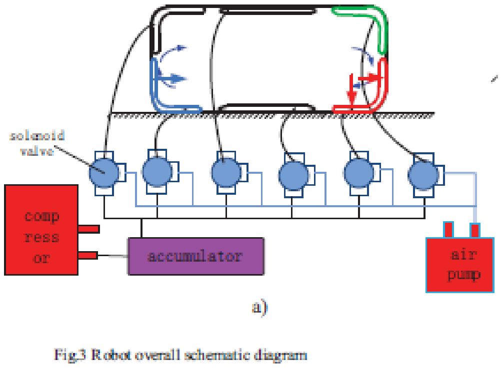


**Figure 2.14:** Rotational motion from PBAs demonstrated by He, 2013 [68].

Due to its versatility, PBAs are widely used to produce devices for wide range of applications. For example, by sequencing the pressurized chambers PBAs can be used as micro pump as demonstrated in [69 – 70] as well as sorting table as in [71 – 73] and mimicry of esophageal [74]. However, rehabilitation device remains the preference of application of PBAs among researchers and Figure 2.15 shows an example of rehabilitation device [75 – 78].

**Figure 2.15:** Ankle rehabilitation device using PBAs by Saga, 2011 [78].

Another category of pneumatic soft actuator, bellow type actuator is constructed from elastic materials with chambers arranged in series within one structure and pressurized only from one input. A large displacement and bending angle can be obtained from bellows mechanism with single input hence linear motion seldom be applied in application except in [79 – 82] as in Figure 2.16.

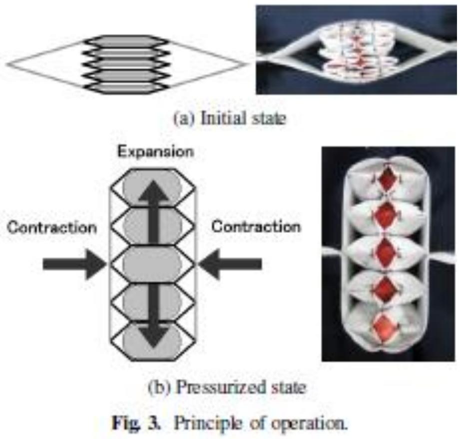


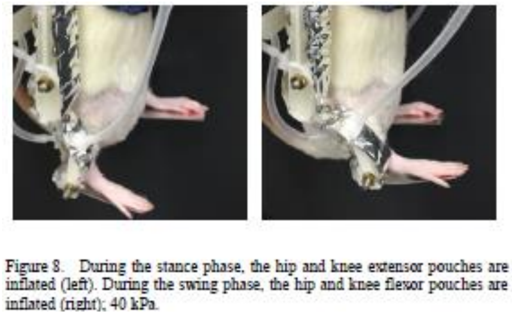


Sasaki[79] Chang[80]

**Figure 2.16:** Linear motion from employment of bellow by Sasaki, 2012 [79] and Chang, 2015 [82].

Many researches have been conducted by taking the advantage of bending motion ability from bellow-type of actuator [83 – 89] as in Figure 2.17.

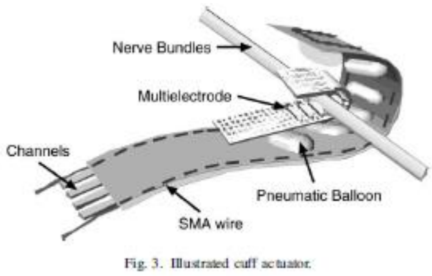


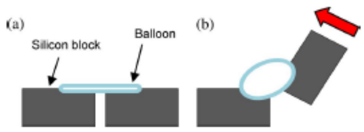


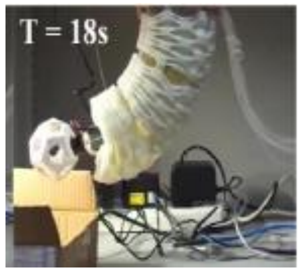


Konishi[83] Choi[84] Meng[86]

**Figure 2.17:** Bellow-type actuator for bending motion by Konishi, 2002 [83], Choi. 2009 [84] and Meng, 2015 [84].

Interestingly, rotational motion and a few difficult motion can be produced using bellow-type actuator [90 – 92]. Figure 2.18 (a), (b) and (c) show the twisting, rotational and helical motion respectively generated from bellow-type of actuator.

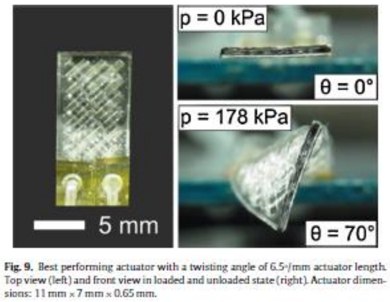


(a)

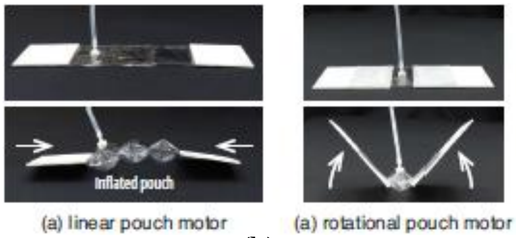


(b)


(c)

**Figure 2.18:** (a) Twisting motion by Gorissen, 2014 [90], (b) rotational motion by Niiyama, 2014 [91], and (c) helical motion by Amase, 2015 [92].

Bellow-type actuator are mostly used for medical device purposes as mentioned in previous reviews and in [93 – 97]. Nevertheless, it also been used for producing manipulator in [98 – 102] and Figure 2.19 shows the example of medical assisting device and miniature manipulator.

Wilkening[95] Wakimoto[101]

**Figure 2.19:** Therapy device by Wilkening, 2011 [95] and miniature manipulator from Wakimoto, 2011 [101].

Although the previous discussed pneumatic soft actuators are based on each category, there are investigation that combined two category of the actuator to produce a motion such as peristaltic. This will be discussed in soft robot development in the next chapter. The final type of pneumatic soft actuator which is granular jamming is constructed from elastic materials with granular are filled inside the chamber. The generated motion depends on the unjamming skin and membrane as in Figure 2.20. In addition, construction shape of the actuator also determine the type of motion that include rolling, linear and bending motion. [103 – 105].

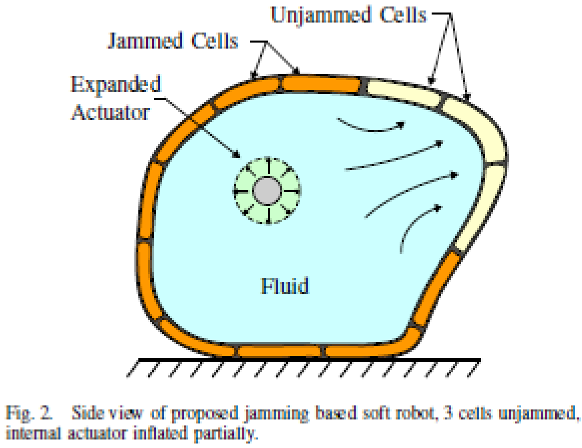


**Figure 2.20:** Rolling motion from jamming type actuator by Steltz, 2009 [103].

Due to its high ability to change stiffness, granular jamming is used in exoskeleton and manipulator for invasive surgery [106 – 108]. Figure 2.21 shows an example of granular jamming used robotic exoskeleton.

**Figure 2.21:** Granular jamming used as robotic exoskeleton by Bean, 2015 [107].

Nevertheless, the review of pneumatic soft actuator potentially used in medical application has been studied by Greef [109]. The term pneumatic soft actuator was referred as flexible fluidic actuator in the study and in the report, he summarized the mechanism for achieving bending and rotation motion as both are crucial to produce higher degree of freedom (DOF) medical instrument.

In order to generate a locomotion ability, the actuator need to have the ability to create linear and oscillatory motion. These motions will provide a gait or step-like motion that pushes the soft robot to one direction. In addition, how the robot changes its direction or makes a turn to arrive to its destination is also an important point of consideration. An omnidirectional ability will provide simple and fast motion for the robot to change its direction. Although previous literatures have shown some example of locomotion from FMA, PBA and PAM type of actuator, we can anticipate that the locomotion is sluggish due to the time taken for the soft material to deform and make a step. Furthermore, buckling is experienced for a long leg if a load is applied to the robot.

Therefore, a new mechanism of soft actuator with fast response and efficient leg length is required. In order to achieve fast response, parameters such as type of soft material, stiffness and thickness play an important role to the actuator performance. Similarly, to avoid buckling effect the determination of the leg length with correct stiffness and thickness is crucial hence both smooth and fast locomotion can be achieved successfully.

## 2.3 Development in Soft Robot

Based on several type of pneumatic soft actuators, soft robot was introduced as an approach to promote the coexistence between human and robot. The research area has become intensify these several years with intriguing product and uniqueness.  PAM type of actuator was exploited in early work by Fukuda [14] with inchworm locomotion technique by stretching and shrinking of twelve rubber actuators in two inches inner diameter pipeline inspection. The employment of PAM underwater was presented with swimming ability [110] by robotic fish. An interesting application of PAM was demonstrated in [111] with rolling tensegrity robot while locomotion robot using PAMs was described in [112 – 113]. Figure 2.22 shows some examples of soft robot using PAMs as a means of movement.

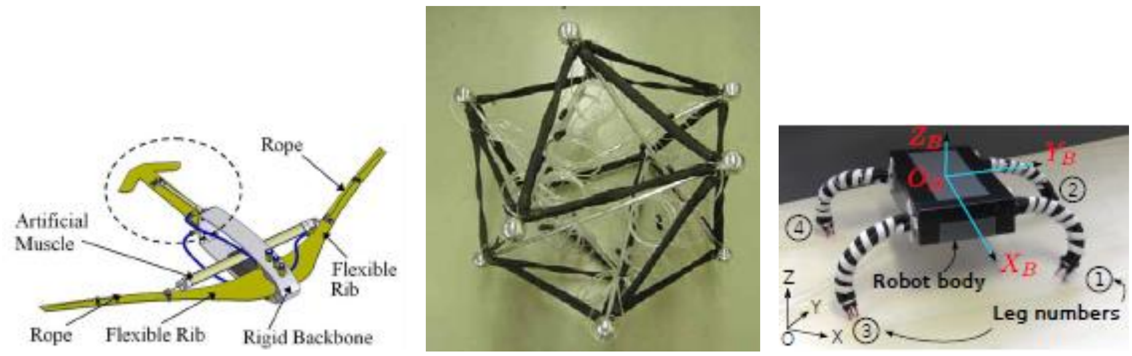


Cai[110] Koizumi[111] Godage[113]

**Figure 2.22:** Soft robots using PAMs by Cai, 2009 [110], Koizumi, 2012 [111], and Godage, 2012 [113].

The implementation of FMA in soft robot was kind of similar to PAM where the applications include locomotion and swimming of soft robot [114 – 115]. However, one of unique and brilliant approach of utilizing FMAs for soft robot was presented in [116] where six FMAs were braided to produce in-pipe locomotion robot. By sequentially pressurized the FMAs, forward locomotion is achieved and able to turn in elbow shape pipe. Figure 2.23 shows the examples of the soft robots.


Suzumori [114] Suzumori[115] Takeshima[116]

**Figure 2.23:** Soft robot from FMAs by Suzumori, 1996 [114], 2007 [115] and Takeshima, 2015 [116].

The PBA type of pneumatic soft actuator receives diverse kind of application. Suzumori introduced Bubbler by sequentially pressurized twelve chambers that created linear motion, and by pairing them, steering motion was achieved as mobile robot base [117]. Based on the principle, Suzumori applied the concept to colonoscopy assisting device with multi-room rubber tube and Bubbler tape that was twisted around colonoscope [118]. The improvement of such mechanism in colonoscopy assisting device were continued until number of chambers were reduced to three whilst traveling speed was increased [119 – 122]. Underwater application was demonstrated in [123] where the deflation of balloon from its elasticity releasing the fluid inside hence thrusting the robot forward. The fast inflation of balloon with high pressure was used as jumping robot as described in [124] and complete humanoid soft robot was presented in [125]. Figure 2.24 shows an examples of these robot based on PBAs.

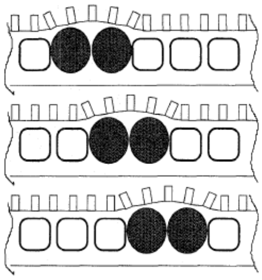
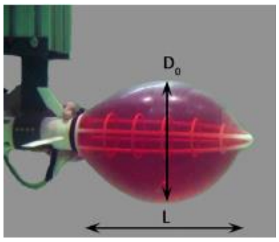

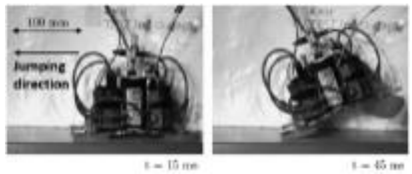


Suzumori[117] Weymouth[123] Ni[124]


Best[125]

**Figure 2.24:** Example of soft robot using PBAs by Suzumori, 1996 [117], Weymouth, 2015 [123], Ni, 2015 [124] and Best, 2015 [125].

Meanwhile, the research on soft robot using bellow type of pneumatic soft actuator mostly focused on gripper and locomotion type of robot. Considering the merit of large bending angle [126 – 127], the gripper demonstrates ability to hold soft and delicate object such as elastic ball and an egg as in Figure 2.25.

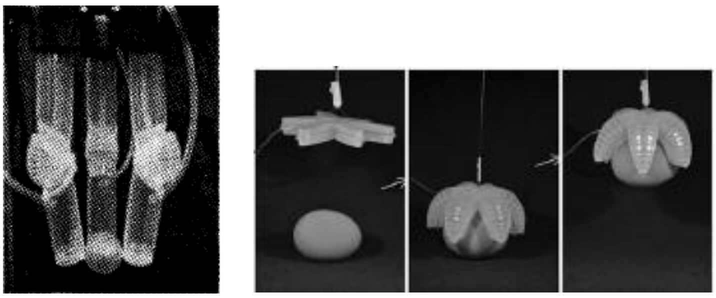

**Figure 2.25:** Gripper using bellow type actautor by Noritsugu, 2000 [126] and Ilievski, 2011 [127].

For locomotion type of soft robot [128 – 134], various configurations of bellow were exploited to produce different type of locomotion. Walking soft robot with bellows served as the legs of the robot was achieved to slip under short gap and for search and rescue robot as in Figure 2.26.

Jumping robot was also demonstrated using bellow type actuator as well as rolling and snake-like locomotion as depicted in the figure.

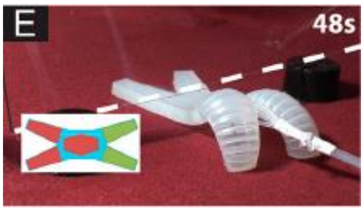


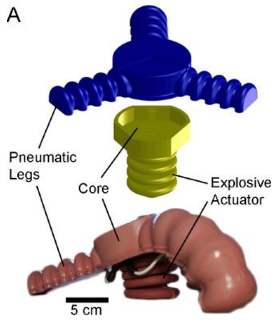


Shepherd[128] Florez[129] Tolley[131]

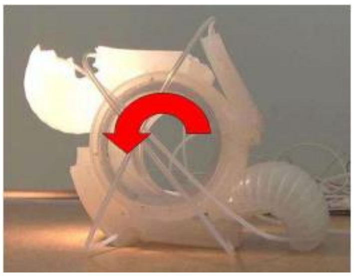

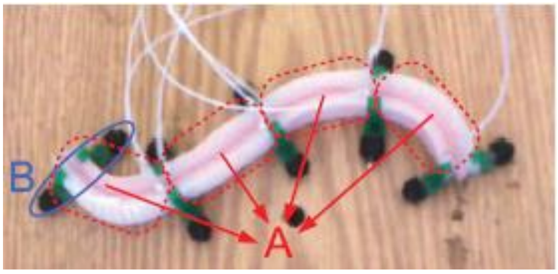


Onal[132] Onal[133]

**Figure 2.26:** Variation of locomotion ability from soft robot by Shepherd, 2011 [128], Florez, 2014 [129], Tolley, 2014 [131], and Onal, 2011 [132] and 2012 [133].

Although each type of soft actuator can be employed individually to produce soft robot, some researchers have demonstrated a combination of type of pneumatic soft actuator to generate a soft robot. However, the innovation confined to one locomotion pattern and application [135 – 141]. The combination of PBA and bellow type of actuator for realizing peristaltic locomotion for endoscopic application has long been investigated and the example of such soft robot can be seen as in Figure 2.27.


Dario[139] Yanagida[141]

**Figure 2.27:** Peristaltic locomotion soft robot from combination of PBA and bellow type of actuator by Dario, 2004 [139] and Yanagida, 2013 [141].

Nevertheless, these locomotion of soft robots restricted to linear motion with 1 and/ or 2 degree-of-freedom (DOF) while some required steering capability that made it impossible to achieve an omnidirectional locomotion. The only omnidirectional locomotion from soft actuator were discussed by few researchers including Suzumori whose demonstrated omnidirectional walking and turning robot from FMA [114], while Shepherd established locomotion with combination of crawling and undulations motion based on pneu-net (PN) architecture [128], and Godage with quadruped robot using continuum limbs [113]. Steering type of turning mechanism can be achieved by reducing operating pressure of one of the front leg of six legged soft robot [129].

One interesting application that took an advantage of silicone rubber transparent was demonstrated by colour changing and camouflage ability with soft diffraction grating and injecting colour fluid in microfluidic network [142 – 143] as in Figure 2.28

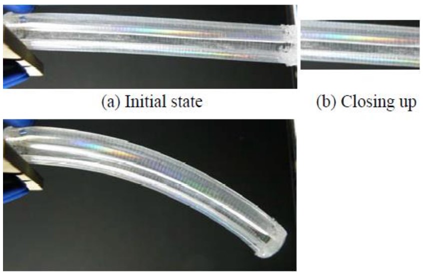



Suzumori, 2011[142]                    Morin, 2012[143]

**Figure 2.28:** Colour changing and camouflage ability from soft robot by Suzumori, 2011 [142] and Morin, 2012 [143].

Although an omnidirectional locomotion from soft robot has been presented, the traveling speed was sluggish in PN whilst using FMA, the long size of actuator affects the stability of the platform or robot base. Meanwhile, if any rigid structure is to be employed for accurate and fast response of locomotion, it will impair the compliance of the soft actuator. Therefore, an exclusively soft robot with fast, smooth and omnidirectional locomotion ability have yet to be established.

The previous paragraphs have demonstrated some efforts to promote the symbiosis between human and robot through soft robot in various kind of applications. Although the nearest example of close interaction between human and soft device was possibly presented by colonoscopy and endoscopy assisting device, the favourite equipment for the procedure still dominated by solid structure device as reviewed by Beasley [144]. While soft materials are arguably weak to be employed for rough and precise application, the resistant to mechanical damage is very strong as demonstrated by Martinez [145].

Nevertheless, the big potential of soft robot for it compliance property is never been doubt the only characteristic own by soft material that offers safe and reliable interaction with human being. One area that soft robot should progress intensively in order to close the gap is in medical field. Current researches have contributed to exoskeleton and rehabilitation where soft actuators are widely involved. Another region that a soft robot can plays the role is in assistive device, where besides being compliance the transparent property should also be taking the advantage. For example, an extreme examination in medical investigation which involves an X-ray and/or magnetic field where any solid and metal objects are prohibited provides a great chance for soft robot to offer her service. Thus, it creates another scope to expand the employment of robot for human interaction.

## 2.4 Cancer Threat and Stomach Fluoroscopy

Cancer disease is one of the leading causes of mortality rate worldwide. According to World Cancer Report 2014, about 14 million new cases and 8.2 million death toll had been reported in 2012. Japan – one of the well-developed countries with cutting-edge medical facilities, excellent medical care and the longest life expectancy listed by World Health Organization in 2012, has no exception to the lethal threat. Stomach cancer was top of the list of types of cancer in male category with 80,211 cases recorded while breast cancer led the list of types of cancer in female category with 56,289 cases both in 2007 data produced by Monitoring of Cancer Incidence in Japan (MCIJ) Project [146]. Figure 2.29 shows the case of cancer incidence based on type of cancer for male and female while Figure 2.30 shows the type of cancer incidence based on age for both male and female.

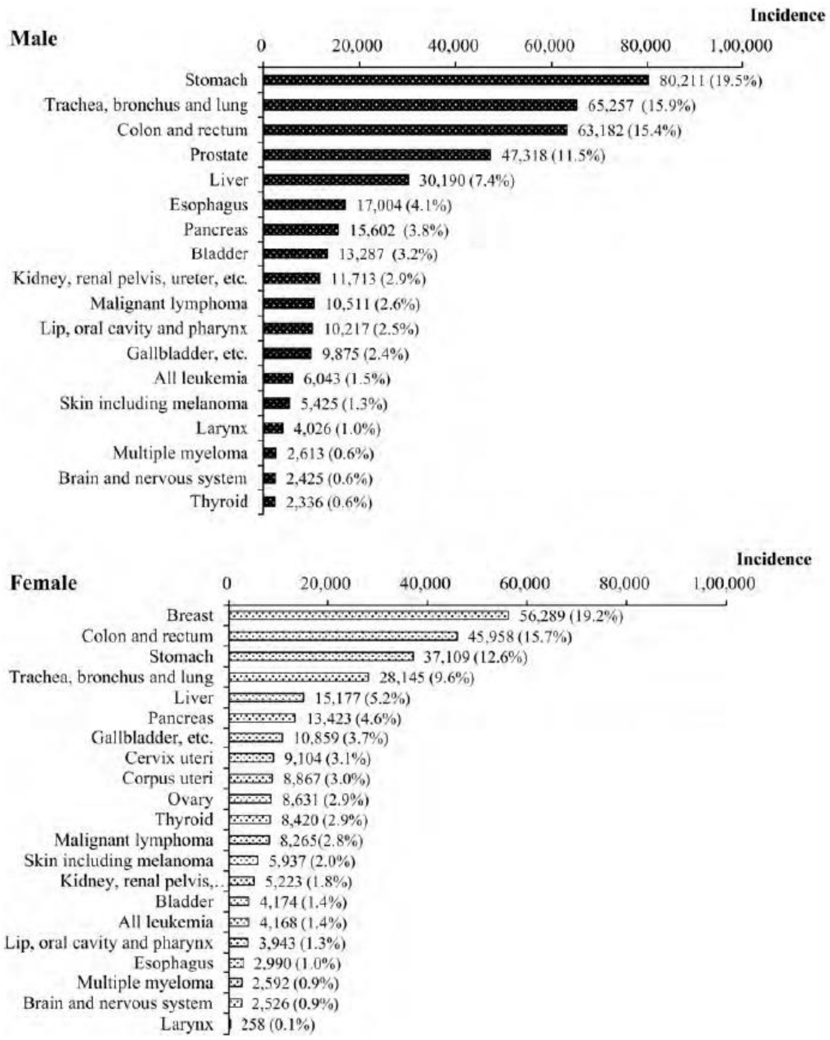


**Figure 2.29:** Type of cancer incidence in Japan in 2007 for male and female [146].

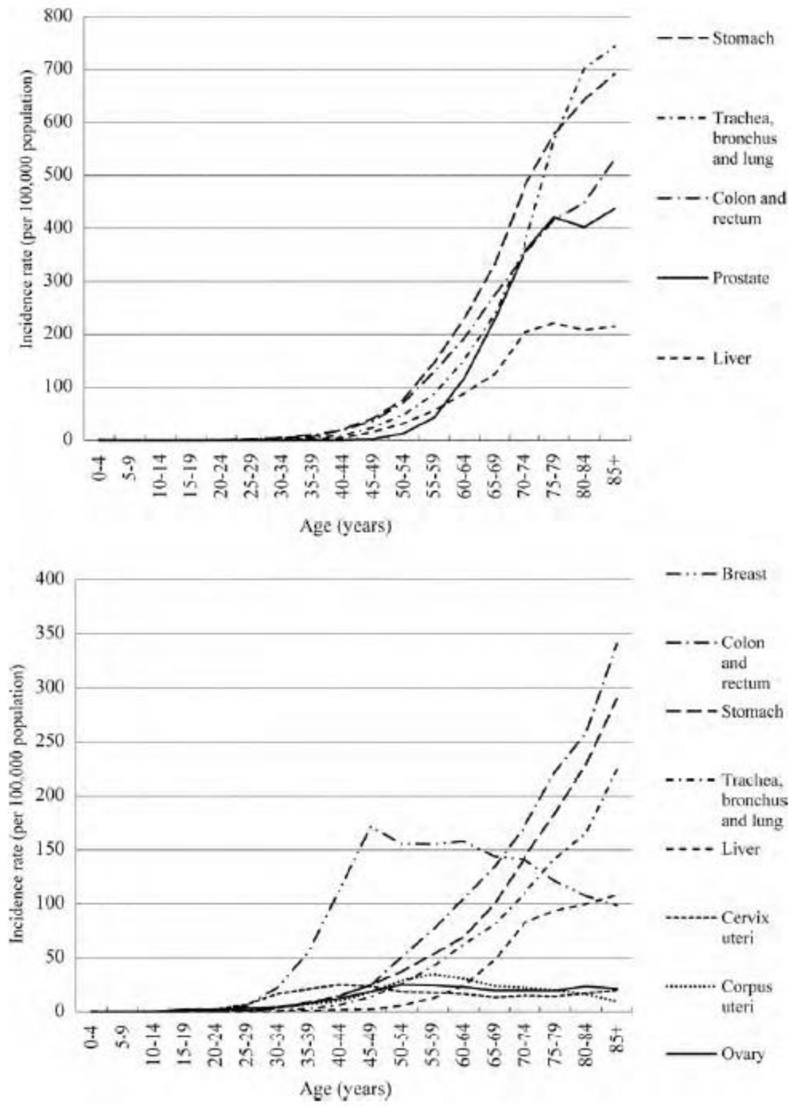


**Figure 2.30:** Type of cancer incidence based on age for male (top) and female (bottom) in Japan in 2007 [146].

Meanwhile, stomach cancer was in fourth place for new cases and third place in death cases worldwide estimated in 2011 [147]. Figure 2.31 shows the statistic of the estimation. Nevertheless, early detection of cancer cell is believed to reduce the death risk, and in Japan screening of stomach cancer using fluoroscopy may have reduced the mortality rates [148].

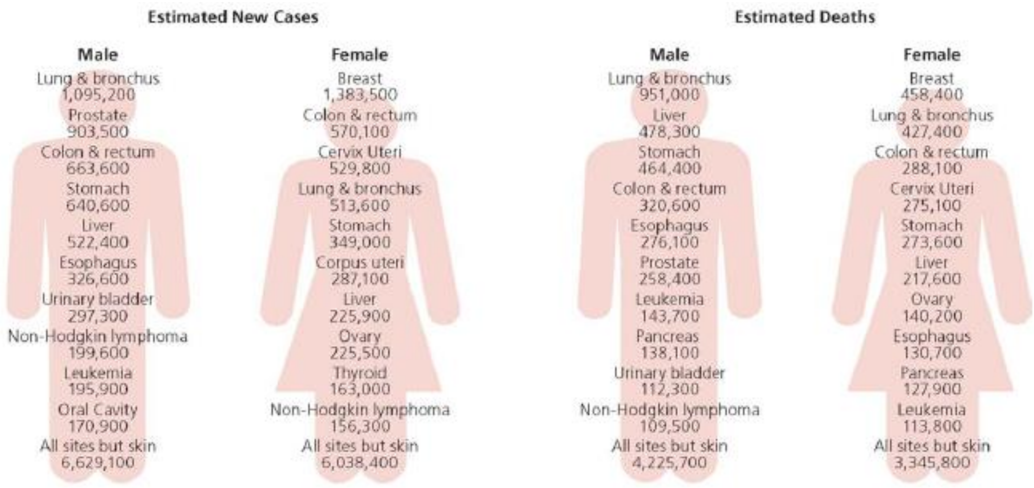


**Figure 2.31:** Cancer type and estimation cases in 2011 [148].

## 2.5 Summary

In this chapter, current progress of pneumatic soft actuator, soft robot and stomach fluoroscopy examination was presented. Various kind of configurations from soft actuator that creates linear, rotation and oscillatory motion can be understood. Furthermore, the advantage of soft robot should be noticed as its potential application can be explored to in order to close the gap for human interaction. Finally, the threat of stomach cancer was described and potential employment of soft robot in fluoroscopy examination can be clearly seen.

# Chapter 3

## New Mechanism Soft Actuator

### 3.1 Introduction

This chapter discuss the development of new mechanism soft actuator. The design, working principle, simulation works, fabrication and experiments are explained in details. The explanation includes software, machines and equipment involved in order to produce the prototype of the soft actuator.

### 3.2 Design concept

Theoretically, omnidirectional locomotion can be achieved if the leg possesses a minimum of three DOFs in its direction of swing: forward, sideways and diagonal. This will allow in various walking patterns such as forward and backward, sideways walking, diagonal walking, circling, and rotating. The perfect example of such a mechanical system is a ball joint, which permits any movement within the case or cup structure. At the same time, it also have to have fast response and millimetre range movement for accurate positioning thus became the design requirement of the actuator.

In order to realize such motions for flexible fluidic actuator, the employment of one chamber with a leg or stud will achieve a camshaft-like motion, whereas the manipulation of four chambers will obtain an active ball joint-like spherical motion, which will lead to omnidirectional locomotion for the leg. The following sub-sections will elaborate further on the conceptual design and construction of such a leg.

#### 3.2.1 Basic structure

Figure 3.1 (a) and (b) shows the side and top views of the structure of the leg, respectively. It consists of five chambers with equal volumes. Four chambers are arranged in a square on the bottom layer, and another chamber is located on top of the centre point of the bottom four chambers. The dimensions of the chamber, top layer, and bottom layer were kept at the minimum specifications except for the length and width of the bottom layer, which was 20 mm × 20 mm. The minimum specifications are based on adopted fabrication method considered the fabrication time, resources, and materials. Nevertheless, the minimum specification could be increased, and the results and performance of a larger unit could be calculated by multiplying the existing results by the expansion ratio.

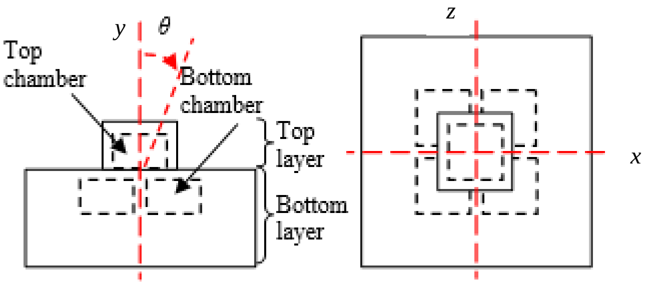


(a) (b)

**Figure 3.1:** (a) Side view and (b) top view.

A large material thickness below the bottom chambers was used to accommodate the air supply for the five chambers. Off-the-shelf industrial tubing (1 mm in diameter) was used to connect the unit to the pneumatic air supply.

Reference axes *x*, *y*, and *z* are represented by the broken lines, with the point of origin located between the top and bottom layers. The deflection angle θ was calculated from the displacement of the tip of the top layer with respect to the *x* and/or *z* direction.

### 3.2.2 Working principle

The operation of the pneumatic rubber leg can be described by referring to Figure 3.2. The designation C1 is used for the top chamber, with the other four chambers called C2, C3, C4, and C5. Theoretically, by applying pneumatic pressure to a rubber chamber, the deformation shape is dictated by the wall thickness, where a thin wall experiences intense expansion relative to a thick wall.

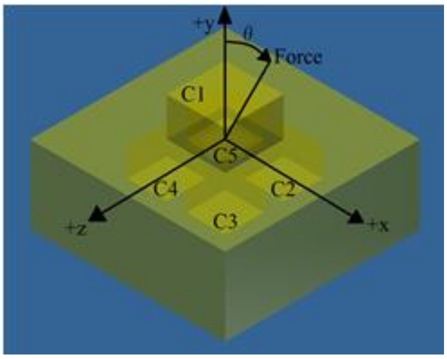


**Figure 3.2:** Leg mechanism for omnidirectional, fast response and millimetre range pace.

This principle is applied to the leg mechanism, where the expansion of the bottom chamber will push the top layer in several directions, depending on which chamber is pressurized. At the same time, the deflection of the top layer due to the expansion of the bottom chamber will generate a propelling force against the ground. This movement provides a swing-like motion with a propelling force for the leg to create a stride and initiate locomotion. This swing motion is in fact the leg trajectory and is measured by the deflection angle $\theta$, as can be seen in Figure 3.2.

To move the body vertically, chambers C1, C2, C3, C4, and C5 are pressurized simultaneously, which causes the leg to extend in the $y$ direction and slightly lifts the body before making a stride during locomotion. Hereafter, top chamber C1 is continuously pressurized to prevent a buckling effect.

By using several legs, i.e., 4, 6, or 8 legs, omnidirectional locomotion can be achieved based on the stride capability of a single leg. For example, forward and backward locomotion can be obtained by moving the leg in the $+z$ and $-z$ directions. This can be realized by simultaneously pressurizing chambers C2 and C5 to move the leg in the $+z$ direction and simultaneously pressurizing chamber C3 and C4 to move the leg in the $-z$ direction. Figure 3.3 (a) to Figure 3.3 (f) shows leg trajectory examples, with the associated deformed chambers.

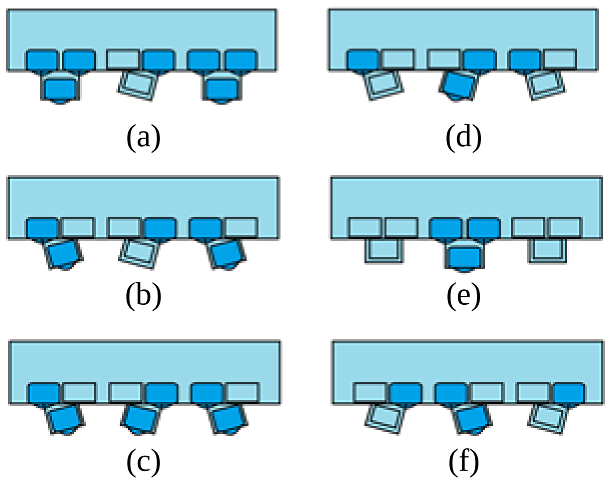


**Figure 3.3:** (a) to (f) Leg trajectories with associated deformed chambers. Note the dark colour indicates a pressurized chamber.

The same principle is applied to realize sideways motion – in this case, in the $+x$ and $-x$ direction. In order to realize right and left locomotion using several legs, a leg has to be moved in the $+x$ direction by simultaneously pressurizing chambers C4 and C5. In contrast, the leg has to be moved in the $-x$ direction by simultaneously pressurizing chambers C2 and C3.

Meanwhile, diagonal locomotion is obtained by moving several legs in a diagonal direction. By pressurizing three of the bottom chambers, four leg directions can be achieved to realize diagonal motion, namely, the $+x$ $+z$ direction, $-x$ $-z$ direction, $+x$ $-z$ direction, and $-x$ $+z$ direction. For the leg to move in the $+x$ $+z$ direction, chambers C2, C4 and C5 are pressurized simultaneously. To move in the $-x$ $-z$ direction, chambers C2, C3, and C4 are pressurized simultaneously. Similarly, to move perpendicular to that motion, the leg can be moved in the $+x$ $-z$ direction by pressurizing chambers C3, C4, and C5. Leg movement in the $-x$ $+z$ direction can be obtained by pressurizing chambers C2, C3, and C5 simultaneously. Furthermore, by combining the linear and diagonal motions from several legs operated sequentially, it is possible to attain rotational movement, as well as spinning. Hence omnidirectional locomotion can be realized.

## 3.3 Finite Element Analysis (FEA) Design Optimization

Based on the design structure, a model of the rubber leg was developed in an FEA environment because of the hyperelastic characteristic of rubber. This allowed its behaviour to be predicted and its geometric nonlinearity, material nonlinearity, and boundary condition nonlinearity to be calculated and performed in the fastest, simplest, and most practical manner. Marc and Mentat from MSC Software was used to perform the analysis. This is because the availability of elastomeric material selection in its advanced nonlinear simulation solution.

The simulation was divided into two parts: optimization and characteristic evaluation. The aim of the optimization was to achieve an optimum design from several possible models. The optimum design was then evaluated in terms of its characteristics when different pressures were applied. This process is described extensively in the following sections.

### 3.3.1 Design prototypes

***Design parameters***

The output characteristics of the unit were identified based on several factors. However, the wall thickness remains the reference in determining the deformation scale, where a thinner wall thickness will result in a larger deformation and a thicker wall will produce a smaller deformation.

Three design parameters were identified that will dictate the performance of the rubber leg. Figure 3.4 shows these three parameters: *a*, the dimension of the top chamber; *b*, the distance between the bottom chambers; and *c*, the distance between the top and bottom chambers.

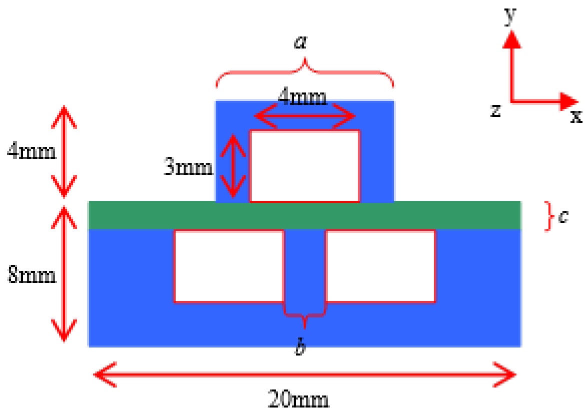


**Figure 3.4** Design parameters *a*, *b* and *c*.

***Evaluation parameters***

The output characteristics of the rubber leg were measured using the evaluation parameters. The displacements of the reference point at the tip of the leg in the vertical, sideways, and diagonal directions were recorded. This information was used to calculate the evaluation parameters, which were the magnitude and deflection angle of the rubber leg.

Because of the single dimension of the vertical displacement, the magnitude of the displacement was equal to the displacement on the *y* axis. However, for the two 2 dimensional sideways deformation, namely, along the *x* axis and *y* axis, trigonometry was used to obtain the magnitude and deflection angle of the rubber leg.

Similarly, for the three dimensional diagonal deformation, where deflection occurred along the *x* axis, *y* axis, and *z* axis, the magnitude and angle of the deflection were calculated using trigonometry as follows,

$$\text{Magnitude}, r = \sqrt{x^2+y^2+z^2}$$

$$\text{Deflection angle}, \theta = sin^{-1}\left(\frac{\sqrt{x^2+z^2}}{r}\right)$$

### *Design optimization*

A total of 18 possible models were simulated based on design parameters *a*, *b*, and *c*. All 18 models were simulated at 180 kPa based on the maximum pressure obtained from a burst investigation. From the simulation results, deformation coordinates were recorded for the vertical, sideways, and diagonal movements as *Y*, (*Xs*, *Ys*), and (*Xd*, *Yd*, *Zd*) respectively. Table 3.1 lists the models with the consecutive design parameters, as well as the recorded coordinates.

**Table 3.1:** Design optimization for 18 possible models.

| Model | ***a*** (mm) | ***b*** (mm) | ***c*** (mm) | ***Y*** (mm) | ***Xs*** (mm) | ***Ys*** (mm) | ***Xd*** (mm) | ***Yd*** (mm) | ***Zd*** (mm) |
|---|---|---|---|---|---|---|---|---|---|
| **P1** | 8x8 | 1.5 | 1.0 | 2.9 | 0.76 | 2.23 | 0.37 | 2.56 | 0.39 |
| **P2** | 7x7 | 1.5 | 1.0 | 3.33 | 1.02 | 2.47 | 0.49 | 2.90 | 0.48 |
| **P3** | 6x6 | 1.5 | 1.0 | 3.54 | 1.18 | 3.03 | 0.54 | 3.62 | 0.53 |
| **P6** | 8x8 | 2.0 | 1.0 | 2.79 | 0.86 | 2.18 | 0.42 | 2.5 | 0.42 |
| **P5** | 7x7 | 2.0 | 1.0 | 3.16 | 1.09 | 2.39 | 0.52 | 2.79 | 0.52 |
| **P4** | 6x6 | 2.0 | 1.0 | 3.34 | 1.25 | 3.01 | 0.55 | 3.15 | 0.55 |
| **P7** | 8x8 | 3.0 | 1.0 | 2.48 | 0.87 | 2.01 | 0.43 | 2.25 | 0.43 |
| **P8** | 7x7 | 3.0 | 1.0 | 2.67 | 1.00 | 2.14 | 0.49 | 2.42 | 0.49 |
| **P9** | 6x6 | 3.0 | 1.0 | 3.29 | 1.09 | 2.78 | 0.53 | 3.13 | 0.53 |
| **P10** | 8x8 | 1.5 | 0.5 | 2.79 | 1.09 | 1.97 | 0.52 | 2.26 | 0.55 |
| **P11** | 7x7 | 1.5 | 0.5 | 2.91 | 1.29 | 1.97 | 0.57 | 2.31 | 0.59 |
| **P12** | 6x6 | 1.5 | 0.5 | 2.98 | 1.51 | 2.12 | 0.67 | 2.60 | 0.69 |
| **P13** | 8x8 | 2.0 | 0.5 | 2.60 | 1.19 | 1.82 | 0.55 | 2.09 | 0.55 |
| **P14** | 7x7 | 2.0 | 0.5 | 2.87 | 1.50 | 1.86 | 0.64 | 2.18 | 0.64 |
| **P15** | 6x6 | 2.0 | 0.5 | 2.86 | 1.50 | 1.89 | 0.73 | 2.38 | 0.73 |
| **P16** | 8x8 | 3.0 | 0.5 | 2.42 | 1.23 | 1.62 | 0.62 | 1.91 | 0.62 |
| **P17** | 7x7 | 3.0 | 0.5 | 2.33 | 1.36 | 1.60 | 0.64 | 1.87 | 0.64 |
| **P18** | 6x6 | 3.0 | 0.5 | 2.36 | 1.30 | 1.67 | 0.66 | 1.99 | 0.66 |

An analysis of the results suggested that the optimum design was achieved by model P15 because it had the maximum deflection angle. Although the vertical displacement was slightly small compared with model P3, the maximum deflection angle, both in the sideways and diagonal directions, justified the selection of model P15 as the optimum design.

### 3.3.2 Simulation Results

Model P15 was further analyzed to determine its characteristics. A simulation was performed with the model from 0 to 120 kPa. Three types of deformations were observed to obtain its characteristics, namely, vertical, sideways, and diagonal deformations. The displacement of the tip of the top layer for each deformation was recorded in terms of the coordinate system, the magnitude and deflection angle were calculated by means of trigonometry. Fig. 3.5 shows the simulation results at 60 and 120 kPa for the three types of deformations.

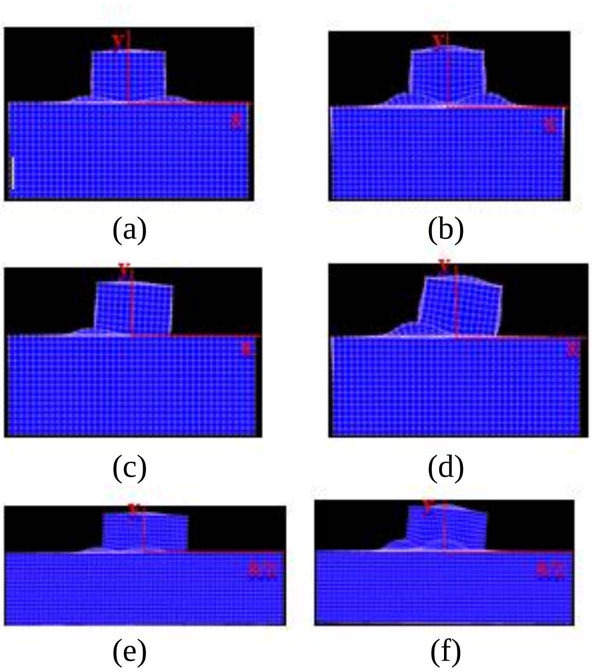

(a) (b) (c) (d) (e) (f)

**Figure 3.5:** Simulation for vertical, (a – b), side (c – d) and diagonal (e – f).

In the vertical deformations, as seen in Figure 2.11(a) and (b), all of the chambers (C1, C2, C3, C4 and C5) are pressurized at 60 or 120 kPa, respectively. The displacement of the tip of the top layer in the *y* direction was recorded.

In the sideways deformations as depicted in Figure 2.11(c) and (d), only the top chamber C1 and two bottom chambers C4 and C5 are pressurized at 60 or 120 kPa, respectively. The displacements of the tip of the top layer in the *y* and *x* directions were recorded.

In the diagonal deformations shown in Figure 2.11(e) and (f), the top chamber C1 and three bottom chambers C2, C4, and C5 are pressurized at 60 or 120 kPa respectively. The displacements of the tip of the top layer in the *y* and *x*/*z* directions were recorded.

## 3.4 Fabrication Process

### 3.4.1 Computer Aided Design (CAD)

In order to form a prototype using silicone liquid material, a mold is needed. Fabrication of the prototype began firstly with a drawing of the flexible leg in the CAD environment. For this purpose, Autodesk Inventor Professional 2010 was employed. Then, a rubber leg mold drawing was created based on the prototype drawing. In order to fabricate the prototype using a mold, the prototype was divided into four layers, as shown in Figure 3.6. Note that the dimension are all in mm.

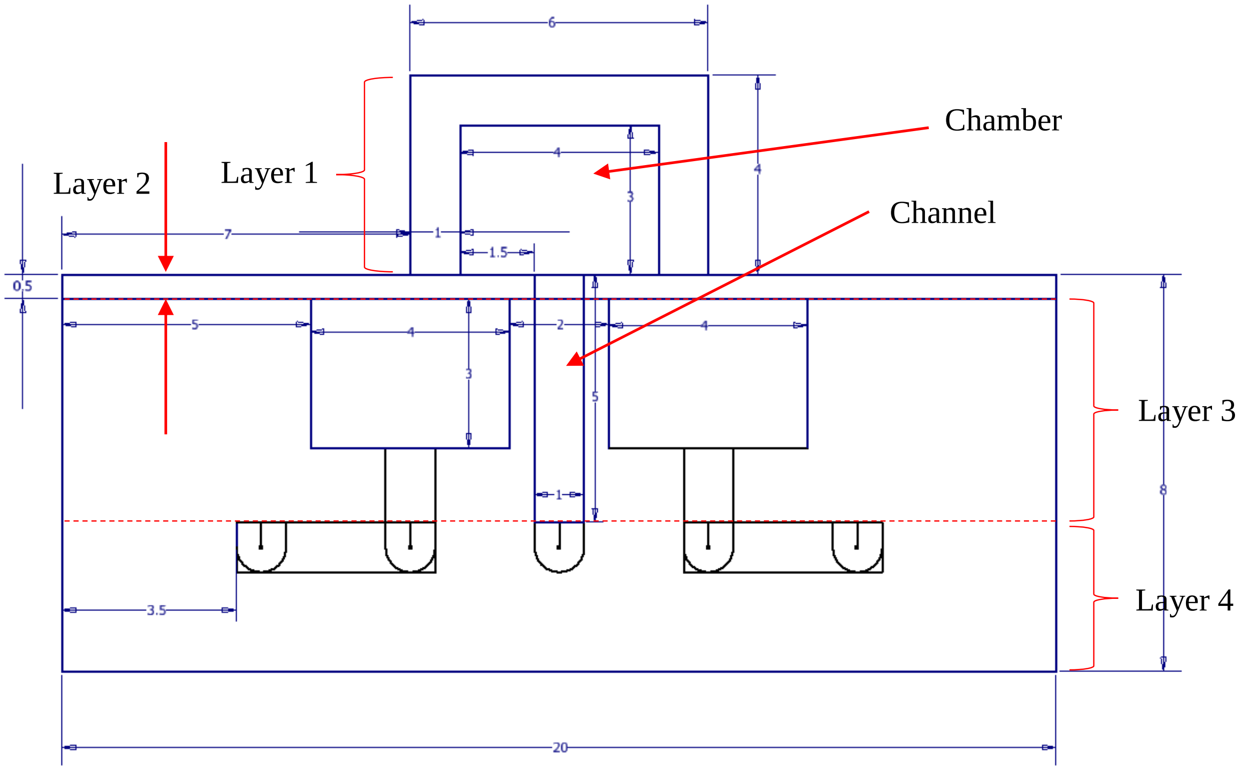


**Figure 3.6:** Four layers to form the prototype.

Figure 3.7 shows the drawing of eight block molds. Molds 1 (M1) and 2 (M2) were used to fabricate layer 1. Molds 3 (M3) and 4 (M4) were used to fabricate layer 3 and layer 4, respectively. Mold 5 (M5) was used to fabricate layer 2, and the remaining molds were used to assemble the layer into the complete prototype (M6 – M8). Figure 3.8 shows the detail dimension of soft actuator as a base for the mold drawing for (a) top view, (b) front view, and (c) side view. Note that all the dimensions are in mm. Next, the fabrication of molding took place and will be described in the following paragraph.

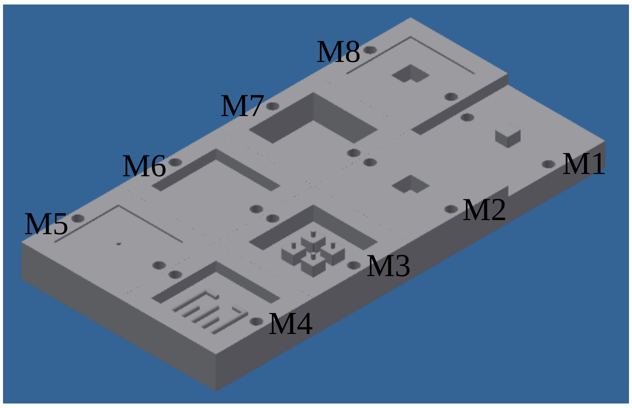


**Figure 3.7:** Mold designs with corresponding designation.

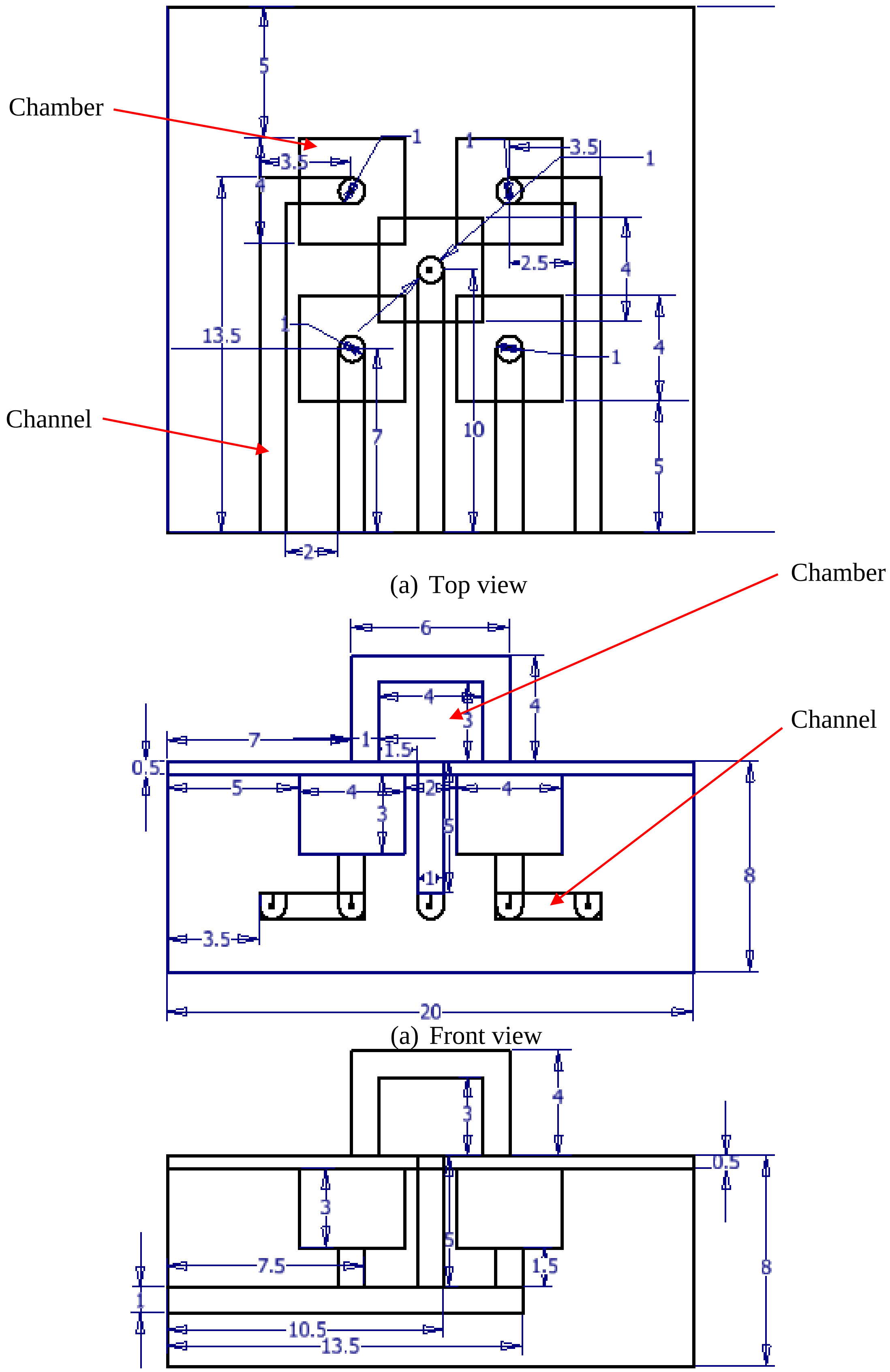


(a) Top view

(a) Front view

(c) Side view

**Figure 3.8:** Details dimension of the soft actuator.

### 3.4.2 Computer Aided Manufacturing (CAM)

In order to produce the block molds, rapid prototyping was implemented. Information from CAD was acquired where the Standard Triangle Language (STL) file of the drawing was used as an input to CAM. A polyester resin material was used as the block molds. After some preparation including cutting the polyester block according to the drawing dimension, mounting the end-mill bit with the chuck in its holder, placing the block in the workspace and configure the setting in CraftMILL software, the milling process started to produce the block molds.

**Figure 3.9:** Roland milling machine for rapid prototyping.

Figure 3.9 shows the Roland milling machine used to produce the molds. The milling process took about 8 – 10 hours to produce such a kind of block molds design. Details preparation and configuration procedure to operate CraftMILL and Roland milling machine is provided in Appendix A. Figure 3.10 shows the block molds produced from rapid prototyping and after cutting into individual block mold.

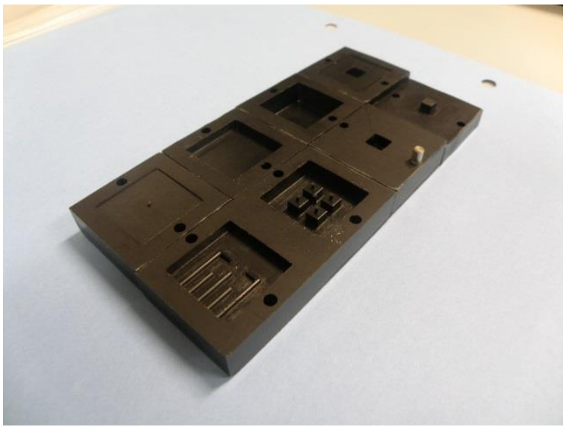

**Figure 3.10:** Fabricated block molds.

### 3.4.3 Silicone mixing

The fabrication of flexible leg involves several processes as depicted in Figure 3.11. The details of each of the process will be explained in the next following chapter.

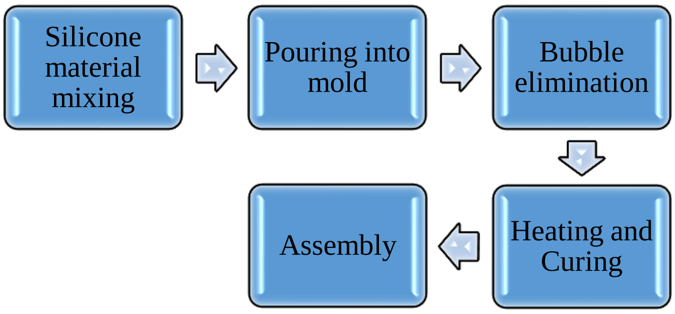


**Figure 3.11:** Flow process of flexible leg fabrication

Two-component Room Temperature Vulcanizing (RTV) rubber silicone from Shin Etsu was used for the silicone fabrication (KE1603 (A/B)). The mixing ratio of 1:1 was applied based on manufacturer specification for high transparency of the prototype. Nevertheless, the amount of each component depends on estimation of the size of the prototype. Figure 3.12 shows the mixing process of 2 components using digital weight scale.

**Figure 3.12:** Mixing 2 components of silicone rubber material.

To ensure a proper mixing between the 2 components, the mixture was put into conditioning vacuum mixer. Figure 3.13 shows the conditioning vacuum mixer and the machine was used twice during the process. The first usage was to assure a proper mixing as in this process, while in second usage it was used for eliminating bubbles in the mixture which will be elaborated in next bubble elimination subchapter. The operational procedure for the machine for both processes can be referred in Appendix B.


**Figure 3.13:** Conditioning vacuum mixer.

### 3.4.4 Pouring

After the mixture was taken out from the conditioning vacuum mixer, it is ready to be poured into the block mold. Spatula was used to transfer the compound from the container to the block mold. The amount of the compound should not be too much or too less as can be seen from Figure 3.14.

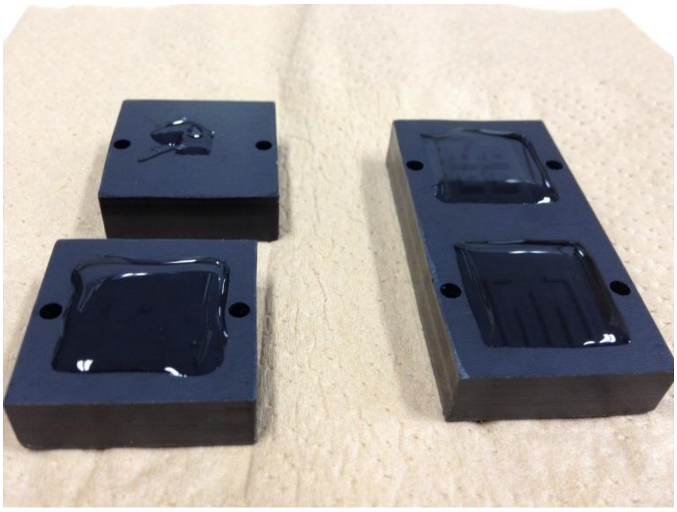

**Figure 3.14:** Proper amount of compound poured into block molds.

### 3.4.5 Air bubble elimination

Once the compound had been poured into the block mold, idle time has been allowed to let the high viscosity compound settled down and fulfilled every part of the block mold. Meanwhile, small bubble air were formed from the pouring session. For elimination of the bubble air, 2 ways were applied. Firstly, a toothpick was used to eliminate any visible bubble air in the compound inside the block mold. However, invisible bubble need to be eliminated using vacuum from conditioning vacuum mixer as in Figure 3.13.

The existence of bubble air in the compound will result in a hole-like sphere in the flexible leg. This defection subsequently will affect the behaviour of the flexible leg when pressure is applied during operation. Thus, it has to be eliminated where possible.

### 3.4.6 Heating and curing

The next process of fabrication is to cure the compound in order to produce 4 layers that constructed the flexible leg. The curing process started with mating the block mold with its cover using drill press vise. A paper wiper from Crecia was used to secure an excessive compound from the compression as can be seen in Figure 3.15.

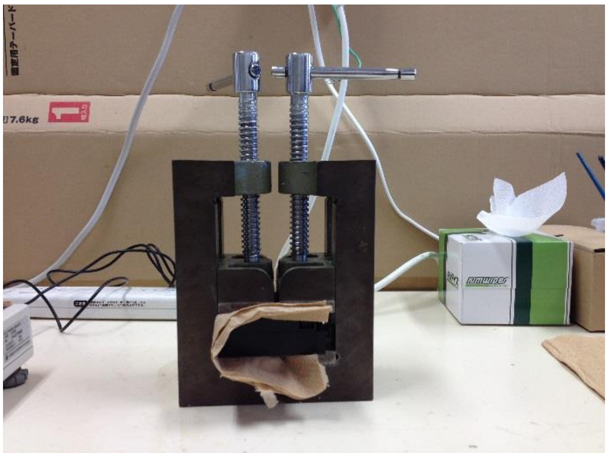

**Figure 3.15:** Pressing the mold before heating.

All block molds for constructing 4 layers with associate drill press vises for compression were put into oven for heating to cure the silicone rubber compound. The heating process took about 30 minutes at 80°C. Figure 3.16 show the natural convection oven used to heat the silicone compound. Afterwards, all the block molds were removed from the oven and the cured 4 layers of silicone compounds were pulled out from the block molds respectively using ethanol to facilitate the process.

**Figure 3.16:** Natural convection oven for curing.

### 3.4.7 Assembly

After it was cured, the layer assembly took place by applying the silicone to the surface layer and heating it again in the oven. The process was repeated to complete the rubber leg layer by layer.

The fabrication of the top chamber as the first layer was achieved by mating M1 with M2. The second layer was produced using M5 mated with a flat surface. A similar method was used to produce layers 3 and 4 with M3 and M4, respectively. To assemble each layer, M6 was used to bond layer 3 and layer 4 by applying silicone to the surface and mating the mold. The assembly was then transferred to M7. Assembling the top chamber and second layer involved mating M2 and M5. Next, the assembly was transferred to M8. Finally the two top layers and two bottom layers were bonded by mating M7 and M8, which resulted in a complete prototype structure.

Finally, a tube was connected to each of the chambers until a suitable tube diameter was achieved that matched the fitting size, as shown in Figure 3.17. Figures 3.18(a) and (b) shows the rubber leg prototype and its cross section, respectively with ball bearing of 0.7 mm in diameter as reference scale. The dimensions of the cross-sectional diagram indicate that the fabrication of the prototype successfully achieved dimensions similar to those of the CAD drawing.

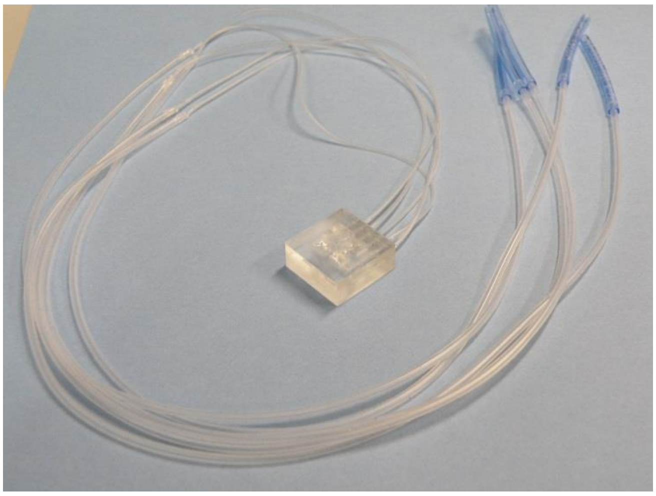

**Figure 3.17:** Complete prototype of flexible leg.

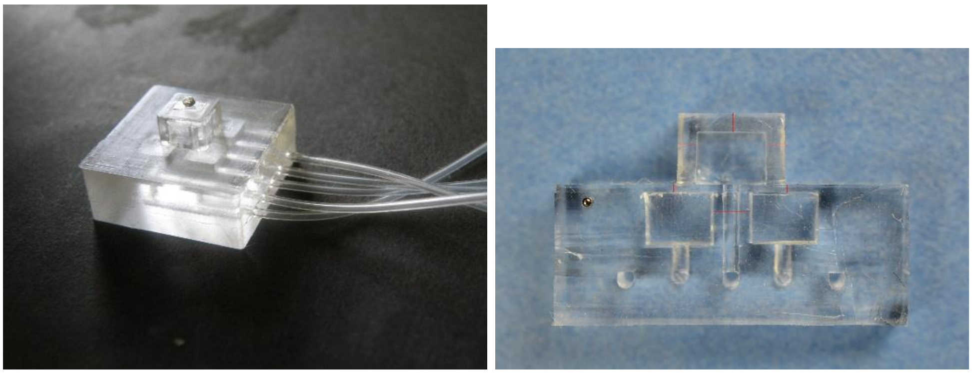

(a) (b)

**Figure 3.18:** (a) Flexible leg and (b) cross section of prototype.

## 3.5 Experiments

A simple experimental setup was designed to evaluate the deformation of the flexible leg. It consisted of a compressor that provided compressed air, an air compressor regulator to regulate the constant compressed air supply, an air compressor filter regulator to adjust the compressed air supply, and a camera to record the deformation.

The objective of the experiment was to record the deformations of the flexible leg for compressed air pressures ranging from 0 to 150 kPa. The pressure was incremented in 10 kPa steps at 15 s intervals, followed by capturing an image to ensure constant deformation of the flexible leg. Photographs of the deformation were taken under three conditions: vertical displacement, sideways displacement, and diagonal displacement. The following subsections describe the procedure of the experiment with these three conditions. Note that a small ball bearing with a diameter of 0.7 mm was used for image calibration purposes, as well as a reference point for the deflection.

The experiment was conducted twice for each deformation condition. In the vertical displacement, images were recorded from the side and front to confirm that symmetrical fabrication was achieved in the prototype. Meanwhile, in the side and diagonal displacements, images were recorded in the bending direction, which was to the left or right. The fabrication of a very symmetrical prototype will result in approximately the same values, despite the opposite directions of the bending displacements. Therefore, in term of the results, the opposite direction was disregarded because of the symmetry that resulted from the precise fabrication.

In addition, force gauge was used to measure the force generated in sideway and diagonal deflection as can be seen in Figure 3.19.


**Figure 3.19:** Force measurement.

### 3.5.1 Vertical displacement

Figure 3.20 shows the deformation of the flexible leg at 150 kPa. This was achieved by simultaneously pressurizing all five chambers (C1, C2, C3, C4, and C5). This produced a displacement along the reference axis, which is represented by the straight line in the *y* direction. The reference axis was determined to be the initial position of the tip of the ball bearing when no pressure was applied to any of the chambers.

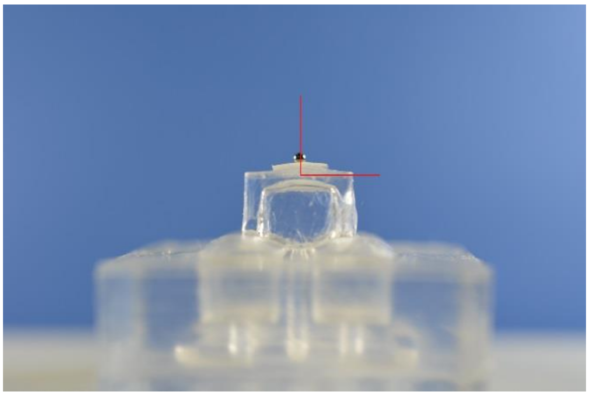

**Figure 3.20:** Vertical deformation at 150 kPa.

### 3.5.2 Sideways displacement

The sideways deformation of the flexible leg at 150 kPa can be seen in Fig. 3.21. This was achieved by pressurizing the top chamber C1 and two of the bottom chambers, C4 and C5, concurrently. The right-side displacement can be seen by the deflection of the ball bearing from the reference axis in both the *y* and *x* directions.

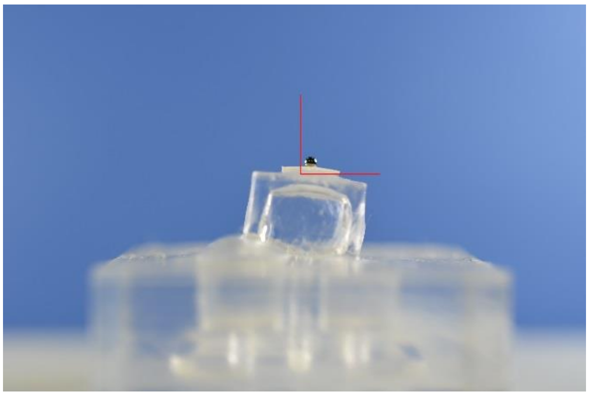

**Figure 3.21:** Sideway deformation at 150 kPa.

### 3.5.3 Diagonal displacement

Figure 3.22 shows the deformation of the flexible leg at 150 kPa. This deformation was achieved by concurrently pressurizing the top chamber C1 and three bottom chambers, C2, C4, and C5. The diagonal displacement can be seen by the deflection of the ball bearing from the reference axis in the *y* and *x*/*z* directions.

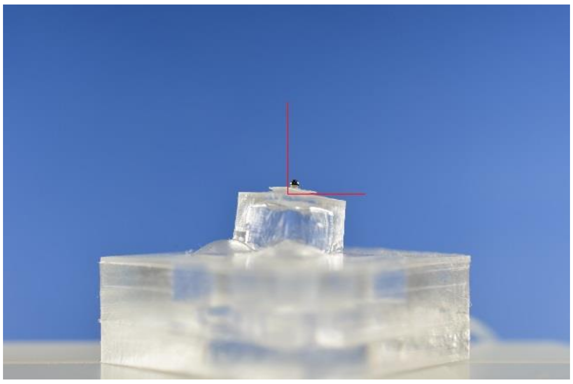

**Figure 3.22:** Diagonal deformation at 150 kPa.

## 3.6 Results and discussion

### 3.6.1 Vertical displacement

The displacement of the reference point in the *y* direction was measured and recorded, as can be seen in Figure 3.23. The maximum displacement of 1.31 mm was recorded at150 kPa, where as in simulation, the maximum displacement of 1.38 mm was recorded at 120 kPa. The difference between the simulation and experimental results was evident, especially above 70 kPa of applied pressure. The disparity indicates that in simulation, the nonlinearity of the actuator occurred at 100 kPa. In fact, the actuator behave with linear response during the experiment up to 150 kPa. Nevertheless, we confirmed that a symmetrical prototype was fabricated based on similar results in the front and side view recorded images.

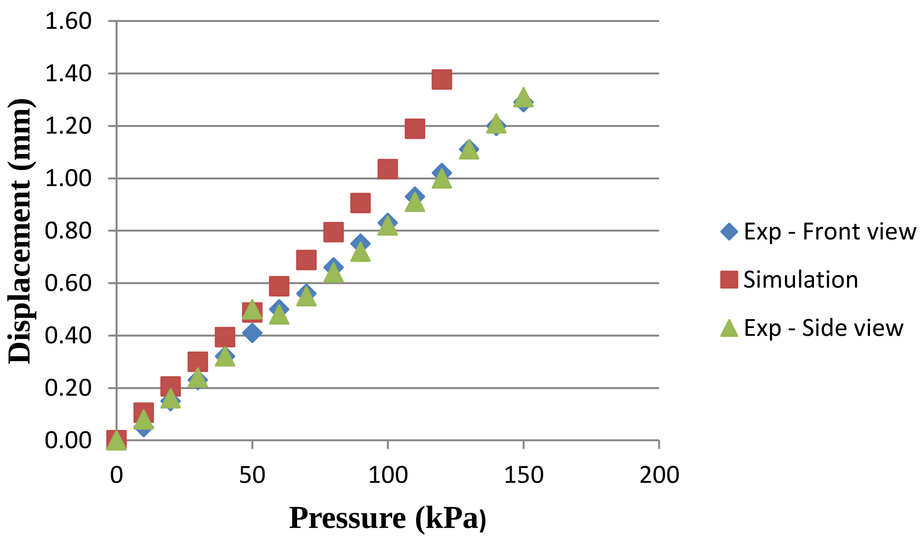


**Figure 3.23:** Displacement (mm) vs. pressure (kPa).

### 3.6.2 Sideway displacement

The displacements of the reference point in two dimensions were measured and recorded. Trigonometry was used to convert the two-dimensional displacement into the magnitude and deflection angle, as can be seen in Figure 3.24 and Figure 3.25, respectively.

For the left bending magnitude displacement, the maximum value of 1.24 mm was recorded at 150 kPa. However, a slight variance was recorded in the right bending, which had a value of only 1.07 mm at 150 kPa. The force generated from this deflection was measured at 0.344 N.

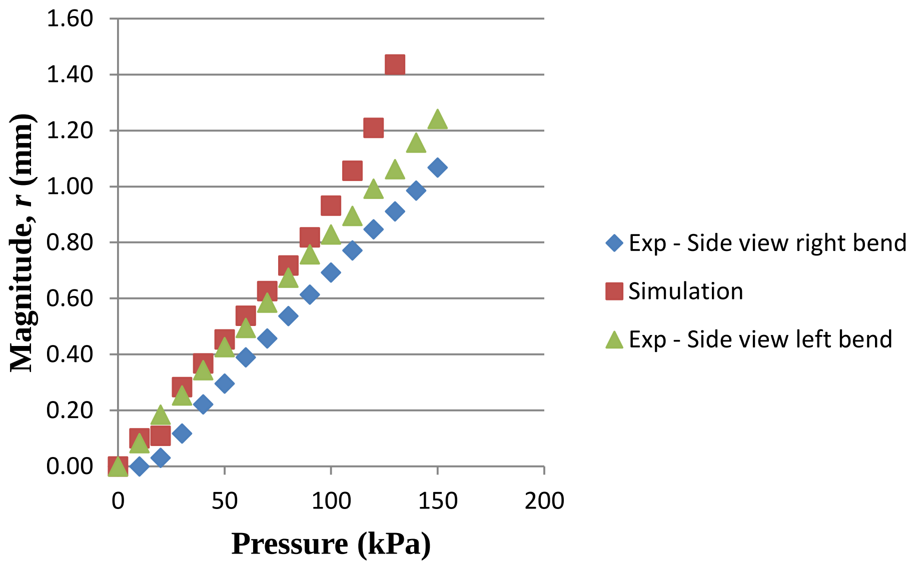


**Figure 3.24:** Magnitude, *r* (mm) vs. pressure (kPa).

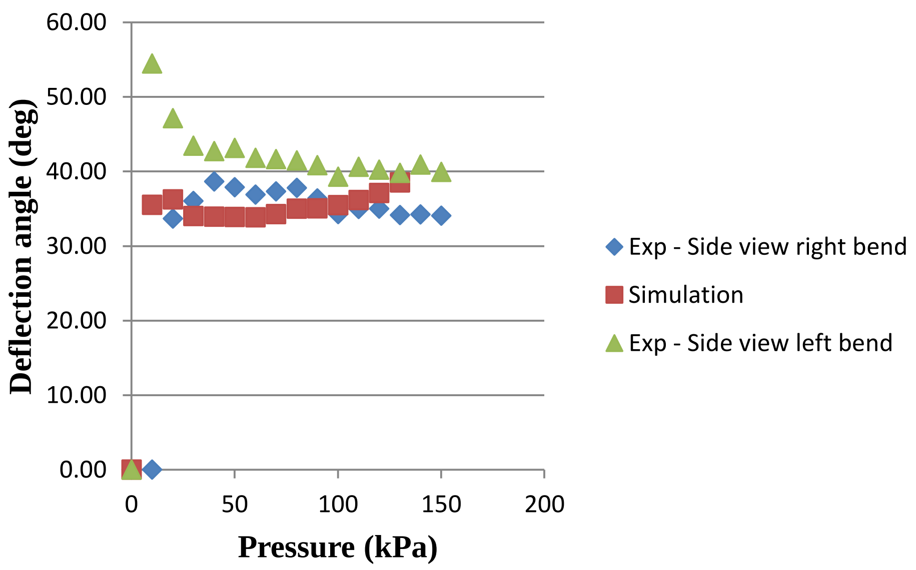


**Figure 3.25:** Deflection angle (°) vs. pressure (kPa).

We conclude that this small disagreement may have arisen for several reasons such as a small silicone build up in the bonding between the top layer and the bottom layer. This hypothesis was confirmed by an investigation that involved cutting a cross section of the prototype. Another factor that may have contributed to the dissimilarity was the misalignment of the camera while capturing images. Nonetheless, the difference between the simulation results and the left bending displacement was slight, which suggested an agreement with the experiment.

Meanwhile, mixed findings were achieved in the deflection angle analysis owing to the different forms of the simulation and experimental results. Therefore, we concluded that the operating pressure for the sideways deformation should be above 60 kPa owing to the constant range of deflection produced in both results. Equal deflection angle ranges were recorded in the simulation and right bending of approximately 35° −39°, although a higher deflection angle range was found for the left bending at 39° −42°.

### 3.6.3 Diagonal displacement

The displacement of the reference point in three dimensions was measured and recorded. Trigonometry was used to convert the three-dimensional displacement into the magnitude and deflection angle, as can be seen in Figure 3.26 and 3.27, respectively.

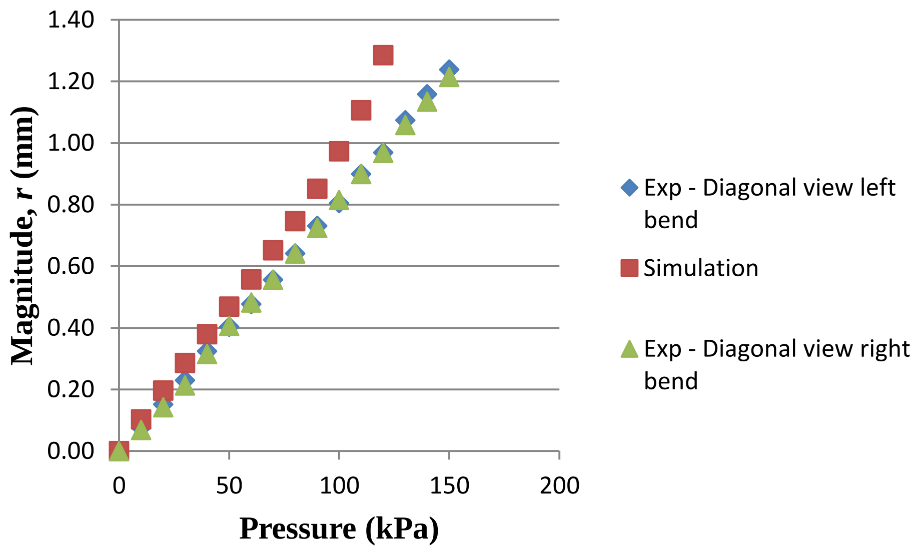


**Figure 3.26:** Magnitude, *r* (mm) vs. pressure (kPa).

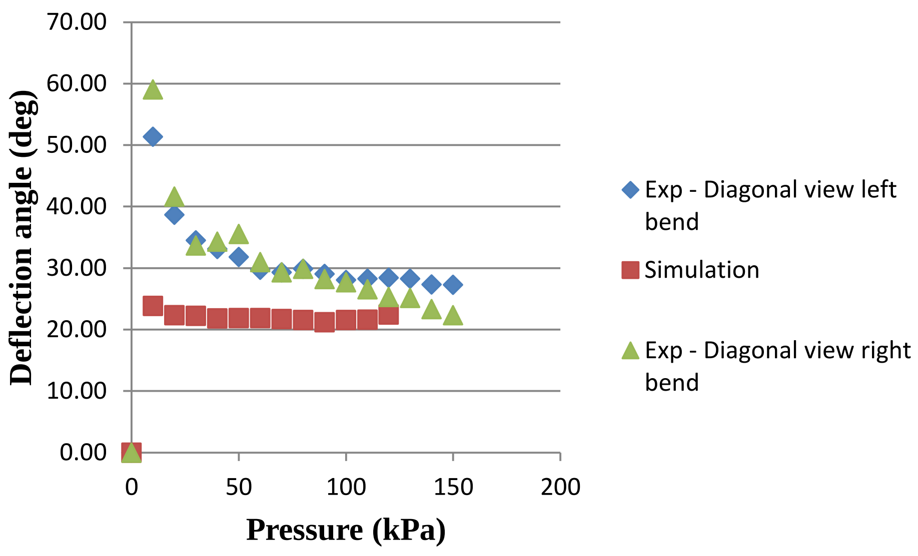


**Figure 3.27:** Deflection angle (°) vs. pressure (kPa).

The magnitude displacement results from the deflections on the right and left sides showed a strong similarity. Maximum displacements of 1.22 mm and 1.24 mm were recorded for the right and left bending, respectively, at 150 kPa. We assumed that the fabricated prototype had good symmetry in this direction. In addition, the simulation results likewise showed some agreement and can be used for future analysis. The force generated by this deflection was measured at 0.264 N.

However, the results for the deflection angle showed considerable differences between the experimental and simulation results. Therefore, we concluded that the operating pressure for the sideways deformation should be 60 kPa, similar to the previous displacement, owing to the constant range of deflections produced by the experimental results. The left bending deflection angle was recorded within a range of 27° −32°, whereas the right bending range was recorded at 22° −31°. The simulation deflection angle had a range of 21° −23°, which was smaller than both experimental ranges. Nevertheless, we presumed that the larger results in comparison with the simulation results were an advantage because of the larger stride that could be achieved for locomotion as a result of the large range of deflection angles.

## 3.7 Summary

In this chapter, the development of new mechanism soft actuator is presented to the readers. Through the process, we establish the omnidirectional soft actuator with linear, rotation and oscillatory motion as an active ball joint, using pneumatic pressure. The experiment results agreed well with simulation thus validated the works in developing the actuator.

# Chapter 4

## Development of Omnidirectional Locomotion Soft Robot

### 4.1 Introduction

This chapter describes the development of soft robot that includes the design, operating principle, fabrication process and the control system. Then, the experiments are explicitly explained to establish the operation of the system and the characteristics of the soft robot based on input parameters applied to the system. Finally, the results is presented as an evidence and components influencing the system are identified.

### 4.2 Design and Operation

Basically, the design of the soft robot is based on our previous pneumatic soft actuator. Therefore, all the dimensions are preserved as well as the mechanism and operating principle of the actuator. The soft robot is constructed from the combination of eight soft actuators that serve as the robot leg and the following subchapters explain the structure and operation of the soft robot.

#### 4.2.1 Structure of soft robot

The soft robot design can be seen as in Figure 4.1. It consists of eight soft actuators or referred as octopedal where the arrangement of the legs are in symmetrical, surrounding the bottom of the robot with no leg at the centre. The centre leg will render unnecessary analysis and controlling, especially during rotational motion. The dimension of the robot is set at 60 mm × 60 mm × 12 mm while the size of the leg is 6 mm × 6 mm × 4 mm, giving enough space for the pneumatic pillow to settle on top of the robot. In fact, a total number of forty chambers are occupying the soft robot with 1 mm air channel connecting the chambers to the tubes that will be connected to the valve and pressure supply. Figure 4.2 shows the details dimension of the robot construction in (a) side view and (b) top view. Note that all dimensions are in mm.

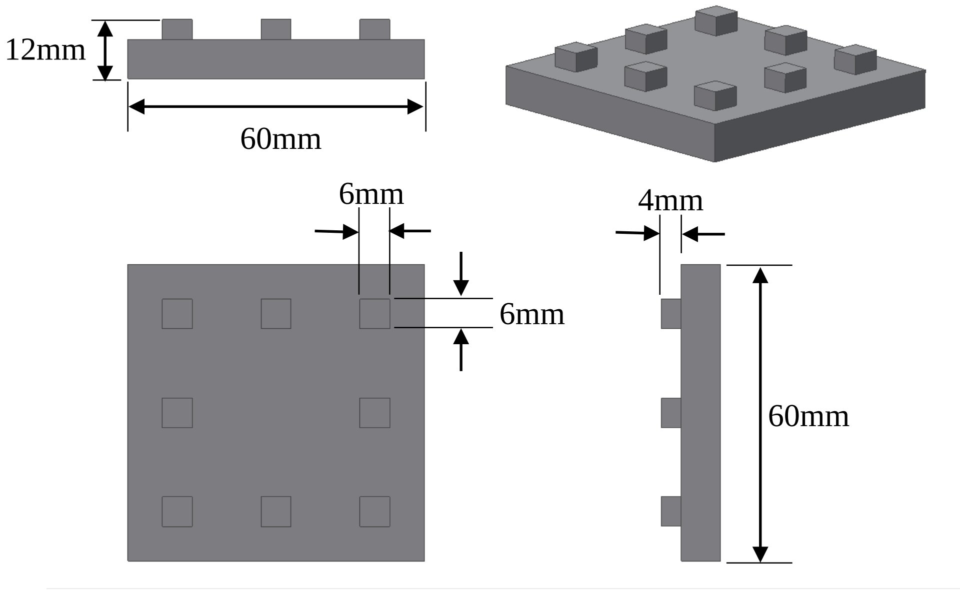


**Figure 4.1:** Soft robot design and dimension.

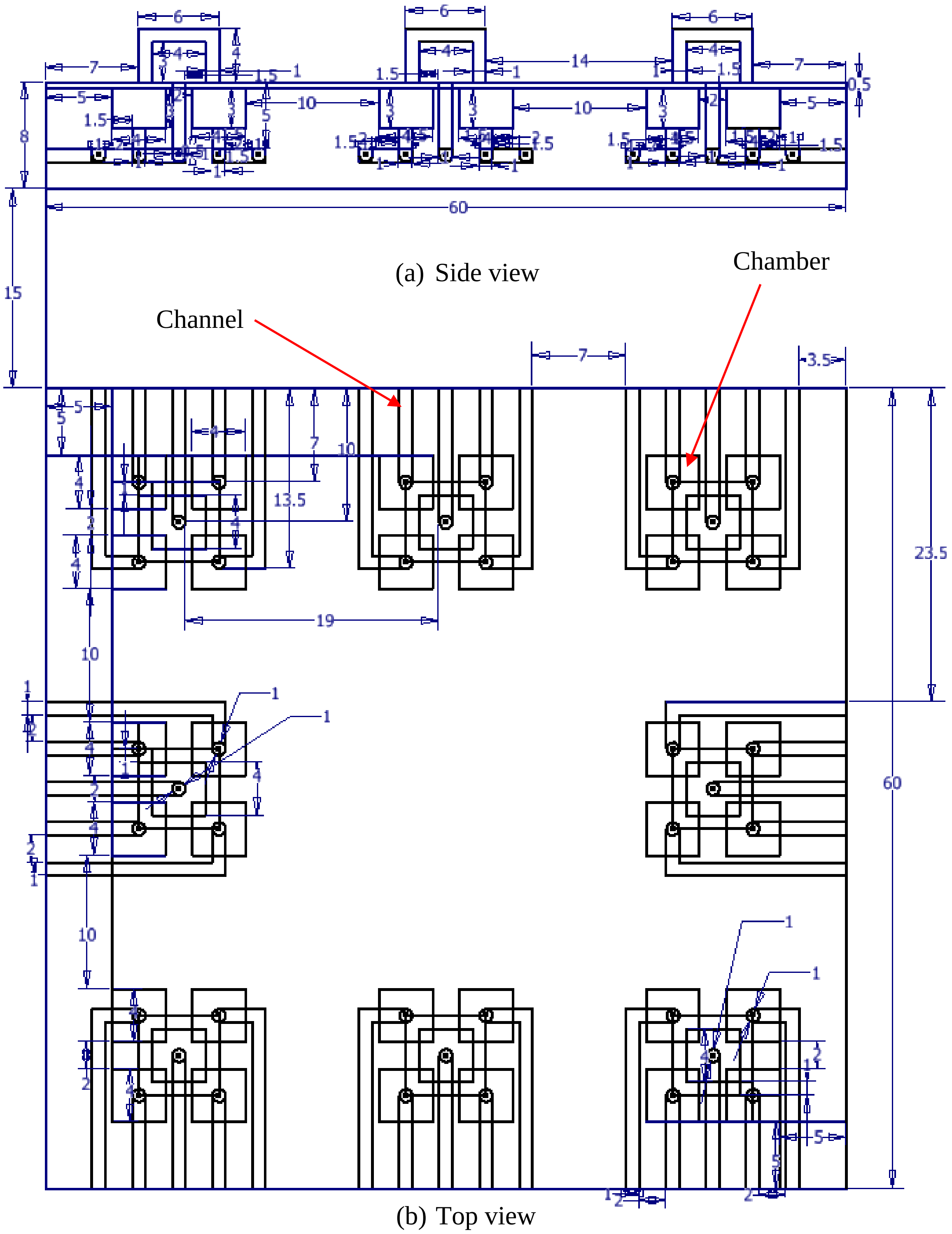


**Figure 4.2:** Details dimension of soft robot in (a) side view and (b) top view.

### 4.2.2 Soft robot operation

Figure 4.3 shows the proposed operation of the soft robot during fluoroscopy examination. The robot will carry the pneumatic pillow on top of it as shown in Figure 4.3 (a). Initially, the robot will be placed under patient's stomach as in Figure 4.3 (b). When the examination requires compression to the stomach, the pneumatic pillow will be activated and push the abdomen upwards as in Figure 4.3 (c). At this condition, no pressure is applied to the robot and the elasticity of the robot prevent it from bursting. In case of examining in different location of the stomach, the patient will be asked to lift up his/her body for a few seconds to allow the robot move to the target location controlled by radiologist in a separate room as in Figure 4.3 (d). This process will be repeated for a different target location to cover a thoroughly investigation of patient's stomach. For efficient application, the speed of the robot is targeted at human swing motion.

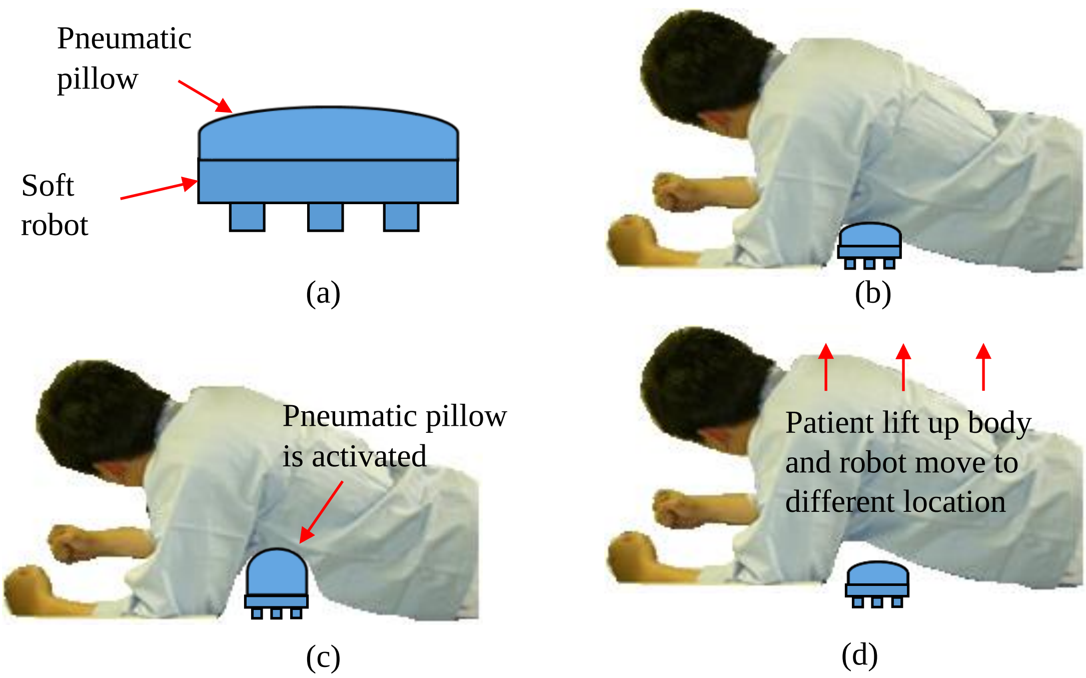


**Figure 4.3:** Proposed soft robot operation in stomach fluoroscopy examination.

In addition, the overview of the proposed complete system can be seen as in Figure 4.4. The remote control system of the soft robot can be achieved through separation between robot operational and robot control system. In the operator room, the robot control system is located where the operator will control the robot locomotion direction and speed via command prompt window from the computer interface. Meanwhile, the soft robot and pneumatic supply system are located in the examination room where the fluoroscopy test is conducted to the patient.

Therefore, there is no need for the radiologist to intervene during the examination and instruction to the patient can be done using microphone.

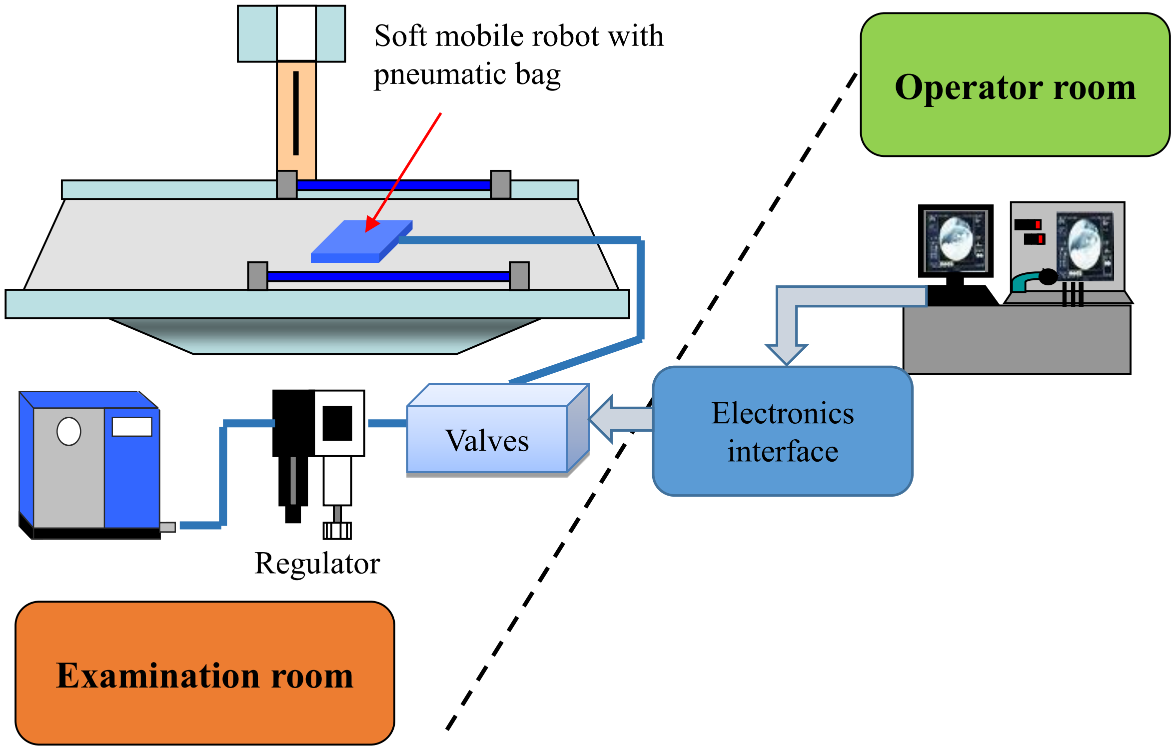


**Figure 4.4:** Overview of proposed complete system.

## 4.3 Soft Robot Development

Once the design of the robot is achieved, it is important to plan for the locomotion of the robot. It involves with identifying the leg motion and how the legs are synchronize to ensure locomotion ability and stability in any direction. In addition, the corresponding chamber for each gait need to distinguish to prevent valve activation mistake when operating the robot.

### 4.3.1 Gait locomotion and locomotion pattern

Before deciding the locomotion pattern, gait locomotion generated by the leg has to be identified. This includes recognizing the corresponding pressurized chamber for a certain gait locomotion. Table 4.1 shows the gait locomotion with corresponding pressurized chambers. In general, the gait locomotion has six sequences to generate a propelling force to move the body, namely Initial, Lifting, Forward Swing, Striking, Propulsive and Backward Swing. Similar gait locomotion is obtained in diagonal locomotion. However, instead of two pressurized chambers are applied at the base to deflect the leg in linear locomotion, three pressurized chambers are applied to deflect the leg in diagonal locomotion as well as in rotational locomotion.

**Table 4.1:** Gait locomotion and corresponding pressurized chamber.

<table>
<tr><th>Gait sequence</th><th>Side view</th><th>Top view</th><th>Chamber condition</th></tr>
<tr><td>1. Initial</td><td>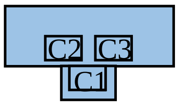</td><td>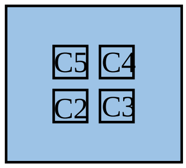</td><td>C1 – Depressurized<br>C2 – Depressurized<br>C3 – Depressurized<br>C4 – Depressurized<br>C5 – Depressurized</td></tr>
<tr><td>2. Lifting</td><td>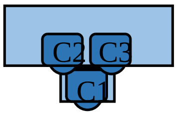</td><td>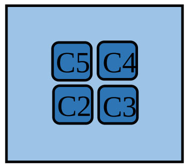</td><td>C1 – Pressurized (dark colour)<br>C2 – Pressurized (dark colour)<br>C3 – Pressurized (dark colour)<br>C4 – Pressurized (dark colour)<br>C5 – Pressurized (dark colour)</td></tr>
<tr><td>3. Forward swing</td><td>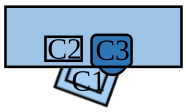</td><td>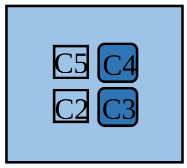</td><td>C1 – Depressurized<br>C2 – Depressurized<br>C3 – Pressurized (dark colour)<br>C4 – Pressurized (dark colour)<br>C5 – Depressurized</td></tr>
<tr><td>4. Striking</td><td>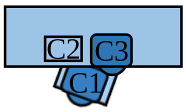</td><td>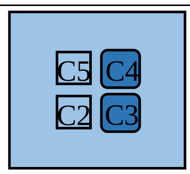</td><td>C1 – Pressurized (dark colour)<br>C2 – Depressurized<br>C3 – Pressurized (dark colour)<br>C4 – Pressurized (dark colour)<br>C5 – Depressurized</td></tr>
<tr><td>5. Propulsive</td><td></td><td>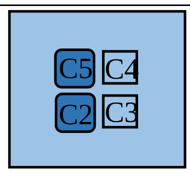</td><td>C1 – Pressurized (dark colour)<br>C2 – Pressurized (dark colour)<br>C3 – Depressurized<br>C4 – Depressurized<br>C5 – Pressurized (dark colour)</td></tr>
<tr><td>6. Backward swing</td><td>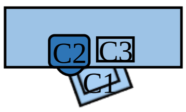</td><td>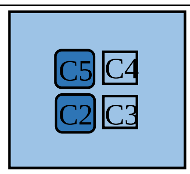</td><td>C1 – Depressurized<br>C2 – Pressurized (dark colour)<br>C3 – Depressurized<br>C4 – Depressurized<br>C5 – Pressurized (dark colour)</td></tr>
</table>

Afterwards, in order to generate gait locomotion from such legs arrangement, the legs are categorized into two groups consisting of four legs in one group. The legs situated at the four corners represented one group and referred as Corner Group (GC) while the other four legs situated between the two corner legs are identified as Middle Group (MG). As the motion of one leg is dictated by five chambers, a total number of forty chambers needed to be controlled in order to determine the locomotion direction of the soft robot.

Figure 4.5 shows locomotion pattern of the soft robot from a side view. In Figure 4.5 (a), the CG performed Backward Swing and at the same time MG initiated Striking gait. Then, the CG shifted to Forward Swing while MG executed Propulsive gait as in Figure 4.5 (b). In Figure 4.5 (c), the CG applied Striking gait as MG employed Backward Swing. In the final state as in Figure 4.5 (d), CG executed Propulsive gait while MG changed to Forward Swing. These four stages of locomotion gait both for CG and MG generated one cycle of locomotion pattern. As depicted in the Figure 4.5, the robot move to the left side of the figure. The phase different between CG and MG is determined at 180° in order to ensure constant contact between the robot leg and ground surface as well as to enable the legs to support the robot platform while performing gait locomotion. For that reason, static stability locomotion is obtained by four supporting legs at a time thus maintaining the stability of the robot while carrying a heavy and tall load. Notice that dark color chamber in the figure represents pressurized chamber to generate the locomotion pattern.

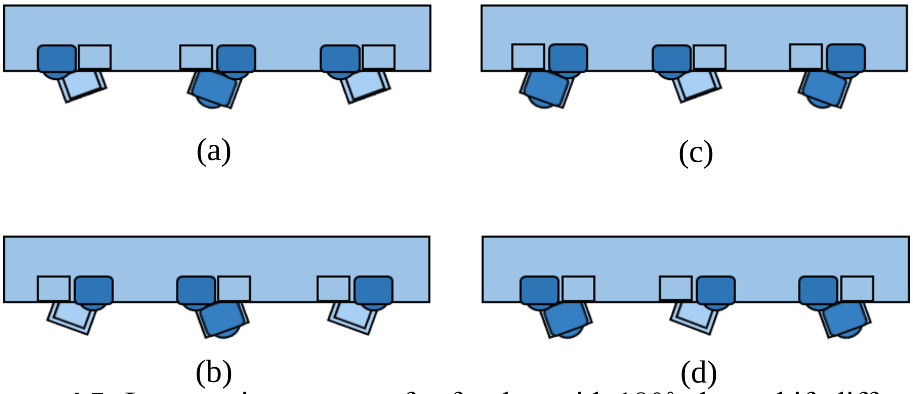


**Figure 4.5:** Locomotion pattern of soft robot with 180˚ phase shift different.

### 4.3.2 Fabrication Process

In general, the material and fabrication process of the soft robot is similar as in fabrication of soft actuator. The combination of the legs is done by fabricating the robot layer by layer instead of connecting each single unit of the leg together. By this fabrication method, fabrication time and cost can be reduced by avoiding fabrication of several single leg mold, and/or fabricating the single leg one by one, followed by connecting them together which consumes a lot of time and energy. Based on the design of the soft robot as in Figure 4.2, the design of the mold for shaping the robot is constructed as can be seen in Figure 4.6. The mold is constructed together with the assembly mold so that proper bonding can be assure to prevent leakage between the layers.

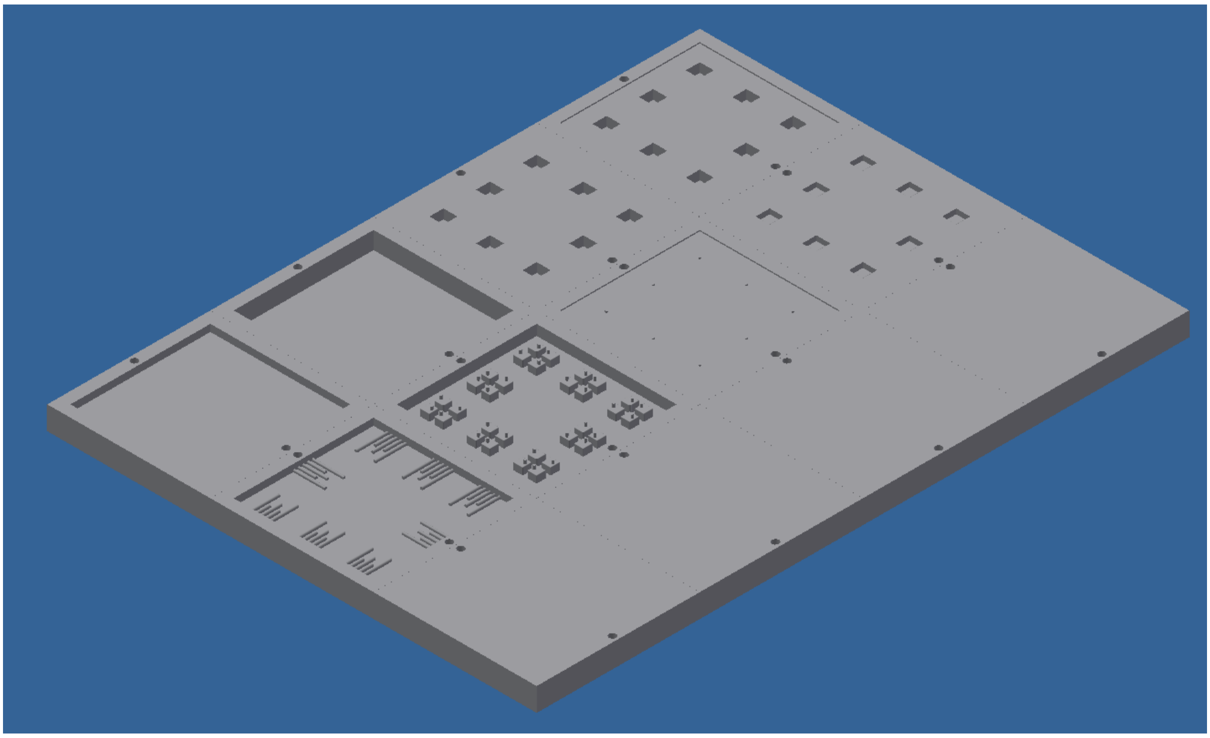

**Figure 4.6:** Mold drawing for the soft robot with the assembly mold.

From Standard Triangle Language (STL) file obtained in CAD, rapid prototyping of the mold was produced by CAM. Once the mold blocks are produced, delicate works of soft robot fabrication began that involved handling of silicone fluids, ensuring exact silicone mixture, eliminating bubbles, and curing the silicone. Assembling and connecting the prototype with corresponding tube are performed, which are similar to the fabrication process described in soft actuator fabrication. Figure 4.7 shows the prototype of soft robot with connecting tube that will be attached to the valves.

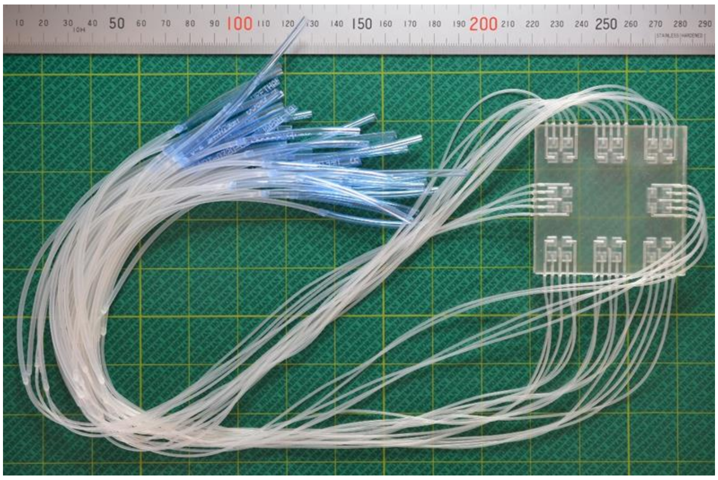

**Figure 4.7:** Fabricated prototype of soft robot.

## 4.4 Control System Development

In order to control forty chambers of the soft robot to initiate the omnidirectional locomotion, several hardware and software are involved. It consists of forty units of three-port-valve, DIO interface and a desktop computer. In software part, we used Microsoft Visual Studio (MVS) 2005 as human-machine interface to determine the locomotion direction, traveling speed and locomotion distance of the robot via command prompt window. The next following section will explain explicitly the hardware and software involve for the configuration of the soft robot control system.

### 4.4.1 Hardware development

4.4.1.1 Pneumatic systems

The pneumatic systems consist of compressor and pressure regulator. The compressor supply a pneumatic pressure which controlled by pressure regulator, CKD F1000 from CKDPneumatic

4.4.1.2 Valves

Forty vavles are required to control the pressure supplied to 40 chambers. The activation of vavle will generate a gait locomtoion. A 3-port direct acting solenoid valve normally close (NC) are used as Figure 4.8. The specification of the valve is as follow:

| | |
|---|---|
| Brand: | Koganei |
| Order codes: | YM10T stn.1-10 030E1-PLL-DC24V |
| Quantity: | 4 unit |
| Maximum operating frequency: | 5 Hz. |
| Operating voltage: | 24 VDC. |


**Figure 4.8:** Valve type.

4.4.1.3 Darlington circuit

Due to the low voltage from Digital Input Output (DIO) card at 3 – 5 VDC, a Darlington Sink Driver is required as a relay to increase the output current from DIO in order to activate the valves that operate in 24 VDC. A total number of eight 7-channel DIP-16 pin TD62003AP are used as in Figure 4.9 and circuit board with connecting terminal are produced.

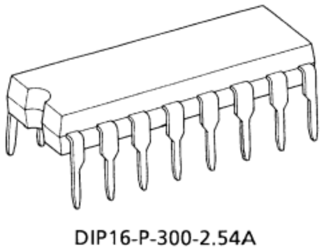


**Figure 4.9:** 7-channel Darlington Sink Driver.

4.4.1.4 DIO card and connections

In order to control the valves from the PC, a DIO card is required. The instruction from the PC will trigger the DIO card to generate a digital output in the range of 3 – 5 VDC. In our case, no input will be used. For that purpose, PCI-2746C DIO card from Interface is used as in Figure 4.10. The card have 48 DIO pins installed in Peripheral Component Interconnect (PCI) slot of the PC board. The configuration for the hardware is done automatically.

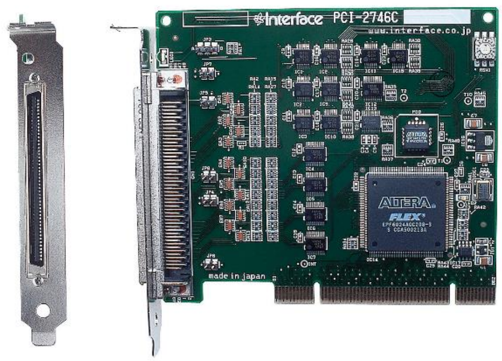


**Figure 4.10:** DIO card PCI-2746C from Interface.

Between the DIO card and the Darlington's Sink Driver, a connection cable and terminal are used. Complete connection between the terminal, Darlington's Sink Driver circuit and valves can be seen as in Figure 4.11.

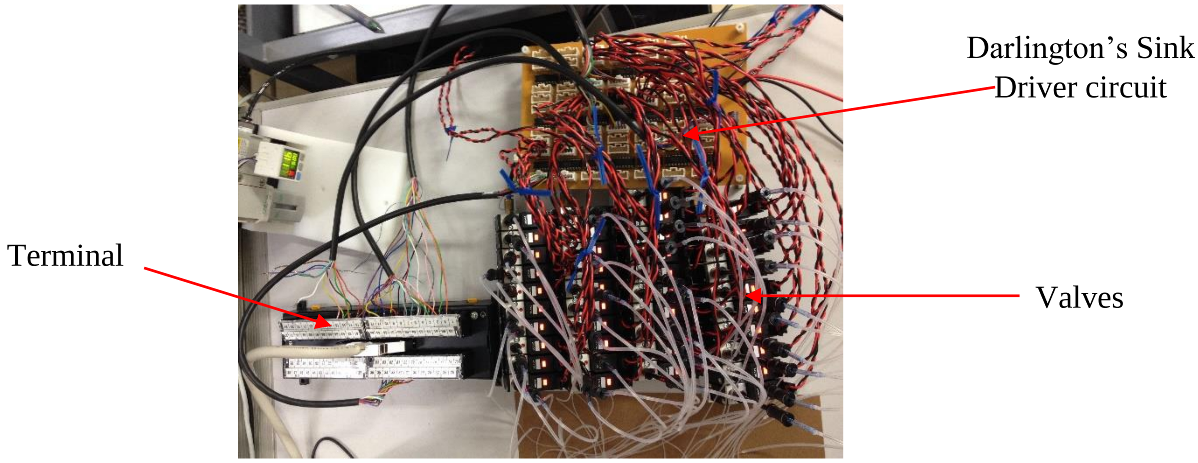


**Figure 4.11:** Connection between DIO's terminal, Darlington's Sink Driver circuit and valves.

One of the confusing task to complete the hardware control system part is to assign the output pin from the DIO with the corresponding chamber. One of the approach is by numbering the 40 chambers with respect to the position of the chamber as presented in Figure 4.12.

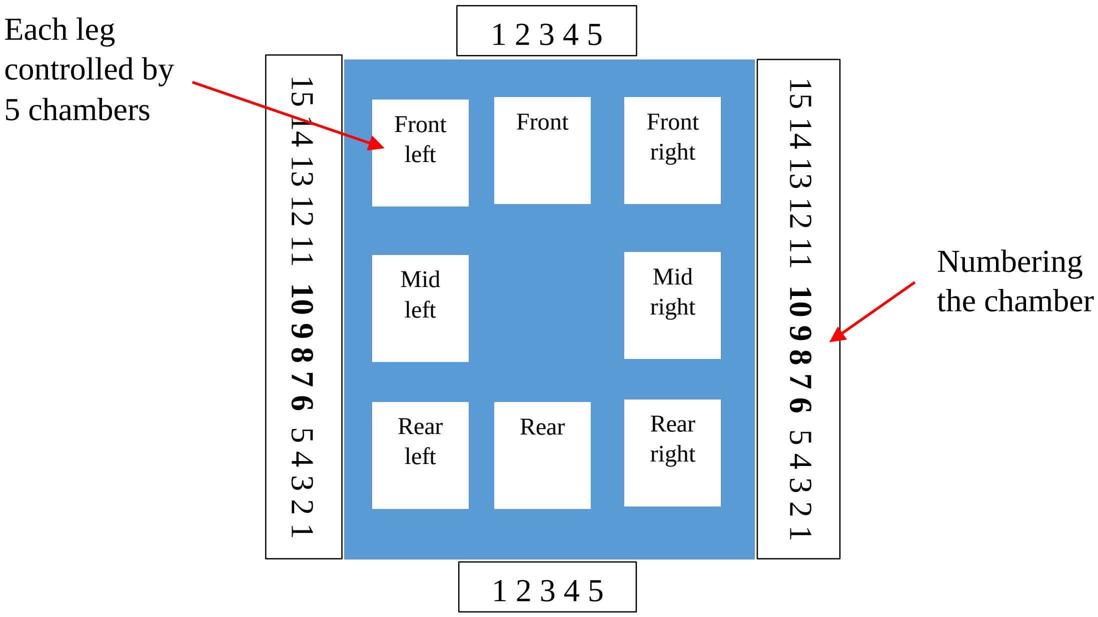


**Figure 4.12:** Chamber numbering based on chamber position.

Next, we identified the connection of the chamber to the valves. The valves are assigned to respected chambers by numbering the valves with corresponding chamber as can be seen in Figure 4.13.

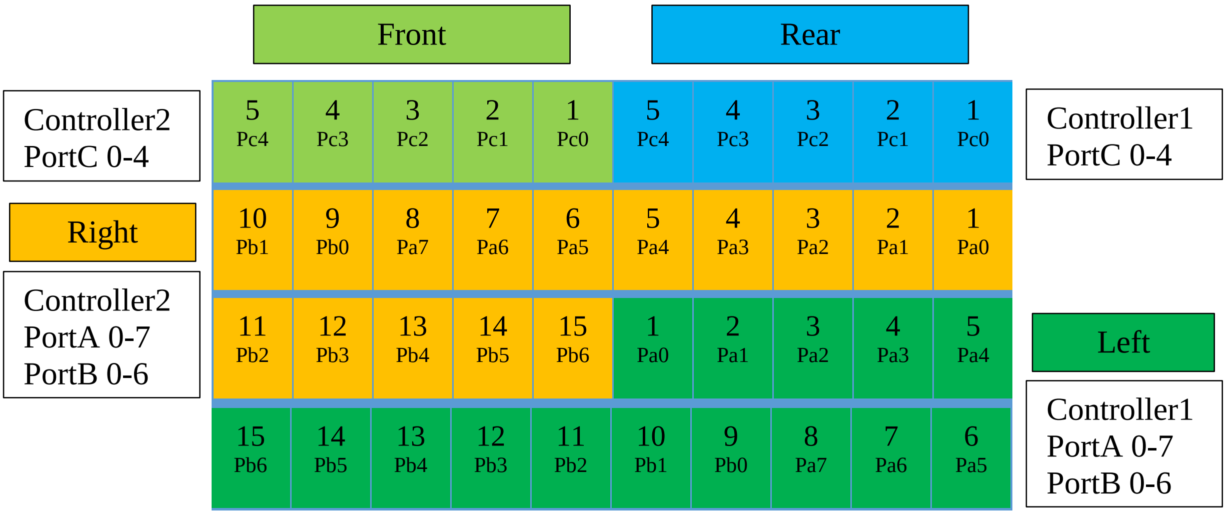


**Figure 4.13:** Valves assigning with corresponding chambers using colour coding to differentiate the chamber position.

Finally, we assigned the connection between the valves and the terminal by referring to pin assignment from the PCI-2746C user's manual. The simplification of the connection and pin assignment can be referred to Table 4.2.

**Table 4.2** Pin assignment with corresponding chamber.

| Grouping | Channel | Pin | Valve |
|---|---|---|---|
| Front leg | 1PC0 – 1PC4 | 31 - 35 | 1 -5 |
| Rear leg | 2PC0 – 2PC4 | 79 - 83 | 6 - 10 |
| Left leg | 1PA0 – 1PB6 | 3 -17 | 11 -25 |
| Right leg | 2PA0 – 2PB6 | 51 - 65 | 26 - 40 |

After the connection is established, the experimental setup is tested to confirm the correct connection. Then, the soft robot is connected to the valves with pneumatic supply to observe the workability of the system configuration.

### 4.4.2 Software development

4.4.2.1 Microsoft Visual Studio (MVS) 2005

For interfacing between the operator and the soft robot, human-machine interface is developed using MVS 2005. The interface will allow the operator to control the movement of the robot in term of locomotion direction, speed and distance. These input parameters are entered to the system via command prompt window.

#### 4.4.2.2 C Programming

In order to develop the human-machine interface, a programming is needed. However, before the programming is developed, 2 components are required. The first component is the representation of each gait locomotion for activation of chamber in binary value. For example, in Striking gait locomotion, three chambers are pressurized and for that representation which chambers are activated is determined by the hexadecimal value. The second component is the locomotion pattern. The synchronization between the two groups of leg is also represented by the hexadecimal number for valves activation.

*Analysis of gait locomotion in omnidirectional and chamber activation.*

Based on the gait locomotion and corresponding pressurized chambers, a digital representation of each gait is established. The representation analysis for binary value is performed in omnidirectional locomotion consists of 10 direction, namely Forward, Backward, Sideway Right, Sideway Left, Diagonal Northeast, Diagonal Northwest, Diagonal Southeast, Diagonal Southwest, Rotational Clockwise and Rotational Anti-Clockwise. Figure 4.14 shows the analysis for forward and backward analysis to identify the digital representation of each leg.

Once the binary value for chamber conditions are obtained, the arrangement of locomotion pattern is performed. In this process, the binary condition of the chamber are filled according to Output terminal that represent the robot leg with appropriate cycle. Table 4.3 shows an example of Forward locomotion sequence based on chamber binary condition. The complete arrangement of binary value for the 7 bit output terminal will provide a hexadecimal value which is important during writing the programming code in order to trigger the output value.

| | | | 4 | 3 | 2 | 1 | 0 | Hex | Side view | | |
|---|---|---|---|---|---|---|---|---|---|---|---|
| RL | 1 | No press | 0 | 0 | 0 | 0 | 0 | 00 | | | |
| C1PC | 2 | Press | 1 | 1 | 1 | 1 | 1 | 1F | 1/ 5 | 2/ 4 | Rear Leg |
| | 3 | No press fwd swing | 0 | 1 | 0 | 1 | 0 | 0A | 3 | | |
| | 4 | Press fwd swing | 0 | 1 | 1 | 1 | 0 | 0E | | | |
| | 5 | No press bwd swing | 1 | 0 | 0 | 0 | 1 | 11 | | | |
| | 6 | Press bwd swing | 1 | 0 | 1 | 0 | 1 | 15 | | | |

| | | | 4 | 3 | 2 | 1 | 0 | Hex | Side view | | |
|---|---|---|---|---|---|---|---|---|---|---|---|
| FL | 1 | No press | 0 | 0 | 0 | 0 | 0 | 00 | | | |
| C2PC | 2 | Press | 1 | 1 | 1 | 1 | 1 | 1F | 2/ 4 | 1/ 5 | Front leg |
| | 3 | No press fwd swing | 1 | 0 | 0 | 0 | 1 | 11 | 3 | | |
| | 4 | Press fwd swing | 1 | 0 | 1 | 0 | 1 | 15 | | | |
| | 5 | No press bwd swing | 0 | 1 | 0 | 1 | 0 | 0A | | | |
| | 6 | Press bwd swing | 0 | 1 | 1 | 1 | 0 | 0E | | | |

| | | | 4 | 3 | 2 | 1 | 0 | Side view | | |
|---|---|---|---|---|---|---|---|---|---|---|
| RRL | 1 | No press | 0 | 0 | 0 | 0 | 0 | | | |
| C1PA | 2 | Press | 1 | 1 | 1 | 1 | 1 | 4/ 5 | 2/ 1 | Rear left leg |
| | 3 | No press fwd swing | 0 | 0 | 0 | 1 | 1 | 3 | | |
| | 4 | Press fwd swing | 0 | 0 | 1 | 1 | 1 | | | |
| | 5 | No press bwd swing | 1 | 1 | 0 | 0 | 0 | | | |
| | 6 | Press bwd swing | 1 | 1 | 1 | 0 | 0 | | | |

| | | | 1 | 0 | 7 | 6 | 5 | Side view | | |
|---|---|---|---|---|---|---|---|---|---|---|
| MRL | 1 | No press | 0 | 0 | 0 | 0 | 0 | | | |
| C1PAB | 2 | Press | 1 | 1 | 1 | 1 | 1 | 9/ 10 | 6/ 7 | Middle left leg |
| | 3 | No press fwd swing | 0 | 0 | 0 | 1 | 1 | 8 | | |
| | 4 | Press fwd swing | 0 | 0 | 1 | 1 | 1 | | | |
| | 5 | No press bwd swing | 1 | 1 | 0 | 0 | 0 | | | |
| | 6 | Press bwd swing | 1 | 1 | 1 | 0 | 0 | | | |

| | | | 6 | 5 | 4 | 3 | 2 | Side view | | |
|---|---|---|---|---|---|---|---|---|---|---|
| FRL | 1 | No press | 0 | 0 | 0 | 0 | 0 | | | |
| C1PB | 2 | Press | 1 | 1 | 1 | 1 | 1 | 14/ 15 | 11/ 12 | Front left leg |
| | 3 | No press fwd swing | 0 | 0 | 0 | 1 | 1 | 13 | | |
| | 4 | Press fwd swing | 0 | 0 | 1 | 1 | 1 | | | |
| | 5 | No press bwd swing | 1 | 1 | 0 | 0 | 0 | | | |
| | 6 | Press bwd swing | 1 | 1 | 1 | 0 | 0 | | | |

| | | | 4 | 3 | 2 | 1 | 0 | Side view | | |
|---|---|---|---|---|---|---|---|---|---|---|
| RLL | 1 | No press | 0 | 0 | 0 | 0 | 0 | | | |
| C2PA | 2 | Press | 1 | 1 | 1 | 1 | 1 | 4/ 5 | 1/ 2 | Rear right leg |
| | 3 | No press fwd swing | 0 | 0 | 0 | 1 | 1 | 3 | | |
| | 4 | Press fwd swing | 0 | 0 | 1 | 1 | 1 | | | |
| | 5 | No press bwd swing | 1 | 1 | 0 | 0 | 0 | | | |
| | 6 | Press bwd swing | 1 | 1 | 1 | 0 | 0 | | | |

| | | | 1 | 0 | 7 | 6 | 5 | Side view | | |
|---|---|---|---|---|---|---|---|---|---|---|
| MLL | 1 | No press | 0 | 0 | 0 | 0 | 0 | | | |
| C2PAB | 2 | Press | 1 | 1 | 1 | 1 | 1 | 9/ 10 | 6/7 | Middle right leg |
| | 3 | No press fwd swing | 0 | 0 | 0 | 1 | 1 | 8 | | |
| | 4 | Press fwd swing | 0 | 0 | 1 | 1 | 1 | | | |
| | 5 | No press bwd swing | 1 | 1 | 0 | 0 | 0 | | | |
| | 6 | Press bwd swing | 1 | 1 | 1 | 0 | 0 | | | |

| | | | 6 | 5 | 4 | 3 | 2 | Side view | | |
|---|---|---|---|---|---|---|---|---|---|---|
| FLL | 1 | No press | 0 | 0 | 0 | 0 | 0 | | | |
| C2PB | 2 | Press | 1 | 1 | 1 | 1 | 1 | 14/ 15 | 11/ 12 | Front right leg |
| | 3 | No press fwd swing | 0 | 0 | 0 | 1 | 1 | 13 | | |
| | 4 | Press fwd swing | 0 | 0 | 1 | 1 | 1 | | | |
| | 5 | No press bwd swing | 1 | 1 | 0 | 0 | 0 | | | |
| | 6 | Press bwd swing | 1 | 1 | 1 | 0 | 0 | | | |

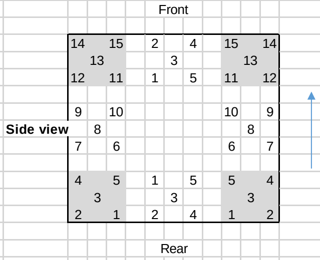


FORWARD & BACKWARD ANALYSIS

**Figure 4.14** Chamber condition and binary value representation.

.

**Table 4.3:** Forward locomotion sequence

| | | | | | | | | | | | | | | | |
|---|---|---|---|---|---|---|---|---|---|---|---|---|---|---|---|
| **Forward walking 4 cycle - Pattern A** | | | | | | | | | | | | | | | |
| **Cycle 1** | | | | **Cycle 2** | | | | **Cycle 3** | | | | **Cycle 4** | | | |
| FL | 4 | RRL | 5 | FL | 6 | RRL | 3 | FL | 5 | RRL | 4 | FL | 3 | RRL | 6 |
| RL | 4 | FRL | 5 | RL | 6 | FRL | 3 | RL | 5 | FRL | 4 | RL | 3 | FRL | 6 |
| MRL | 4 | RLL | 5 | MRL | 6 | RLL | 3 | MRL | 5 | RLL | 4 | MRL | 3 | RLL | 6 |
| MLL | 4 | FLL | 5 | MLL | 6 | FLL | 3 | MLL | 5 | FLL | 4 | MLL | 3 | FLL | 6 |
| | | | | | | | | | | | | | | | |
| **Cycle** | **7** | **6** | **5** | **4** | **3** | **2** | **1** | **0** | **hex** | | | **Cycle 1** | | | |
| c1pa | 1 | 1 | 1 | 1 | 1 | 0 | 0 | 0 | F8 | RRL | | FL | 4 | RRL | 5 |
| c1pb | 0 | 1 | 1 | 0 | 0 | 0 | 0 | 0 | 60 | FRL | | RL | 4 | FRL | 5 |
| c1pc | 0 | 0 | 0 | 0 | 1 | 1 | 1 | 0 | 0E | RL | | MRL | 4 | RLL | 5 |
| c2pa | 1 | 1 | 1 | 1 | 1 | 0 | 0 | 0 | F8 | RLL | | MLL | 4 | FLL | 5 |
| c2pb | 0 | 1 | 1 | 0 | 0 | 0 | 0 | 0 | 60 | FLL | | | | | |
| c2pc | 0 | 0 | 0 | 1 | 0 | 1 | 0 | 1 | 15 | FL | | | | | |
| **Cycle** | **7** | **6** | **5** | **4** | **3** | **2** | **1** | **0** | **hex** | | | **Cycle 2** | | | |
| c1pa | 1 | 0 | 0 | 0 | 0 | 0 | 1 | 1 | 83 | RRL | | FL | 6 | RRL | 3 |
| c1pb | 0 | 0 | 0 | 0 | 1 | 1 | 1 | 1 | 0F | FRL | | RL | 6 | FRL | 3 |
| c1pc | 0 | 0 | 0 | 1 | 0 | 1 | 0 | 1 | 15 | RL | | MRL | 6 | RLL | 3 |
| c2pa | 1 | 0 | 0 | 0 | 0 | 0 | 1 | 1 | 83 | RLL | | MLL | 6 | FLL | 3 |
| c2pb | 0 | 0 | 0 | 0 | 1 | 1 | 1 | 1 | 0F | FLL | | | | | |
| c2pc | 0 | 0 | 0 | 0 | 1 | 1 | 1 | 0 | 0E | FL | | | | | |
| **Cycle** | **7** | **6** | **5** | **4** | **3** | **2** | **1** | **0** | **hex** | | | **Cycle 3** | | | |
| c1pa | 0 | 0 | 0 | 0 | 0 | 1 | 1 | 1 | 07 | RRL | | FL | 5 | RRL | 4 |
| c1pb | 0 | 0 | 0 | 1 | 1 | 1 | 1 | 1 | 1F | FRL | | RL | 5 | FRL | 4 |
| c1pc | 0 | 0 | 0 | 1 | 0 | 0 | 0 | 1 | 11 | RL | | MRL | 5 | RLL | 4 |
| c2pa | 0 | 0 | 0 | 0 | 0 | 1 | 1 | 1 | 07 | RLL | | MLL | 5 | FLL | 4 |
| c2pb | 0 | 0 | 0 | 1 | 1 | 1 | 1 | 1 | 1F | FLL | | | | | |
| c2pc | 0 | 0 | 0 | | | | | | 0A | FL | | | | | |
| **Cycle** | **7** | **6** | **5** | **4** | **3** | **2** | **1** | **0** | **hex** | | | **Cycle 4** | | | |
| c1pa | 0 | 1 | 1 | 1 | 1 | 1 | 0 | 0 | 7C | RRL | | FL | 3 | RRL | 6 |
| c1pb | 0 | 1 | 1 | 1 | 0 | 0 | 0 | 0 | 70 | FRL | | RL | 3 | FRL | 6 |
| c1pc | 0 | 0 | 0 | 0 | 1 | 0 | 1 | 0 | 0A | RL | | MRL | 3 | RLL | 6 |
| c2pa | 0 | 1 | 1 | 1 | 1 | 1 | 0 | 0 | 7C | RLL | | MLL | 3 | FLL | 6 |
| c2pb | 0 | 1 | 1 | 1 | 0 | 0 | 0 | 0 | 70 | FLL | | | | | |
| c2pc | 0 | 0 | 0 | 1 | 0 | 0 | 0 | 1 | 11 | FL | | | | | |

*Programming code for omnidirectional locomotion.*

The final part is to simplify the hexadecimal value in order to facilitate the development of programming code. In addiiton, it serves as critical value for locomotion direction of the soft robot and small error can lead to improper robot locomotion. Table 4.4 shows the obtained hexadecimal value for 10 locomotion directions. These hexadecimal values are used to develop the programming code. Operator is able to select which locomotion direction the robot is to be performed. Besides, the operator have to enter the cycle time - which represent how fast the robot will perform the cycle, and number of cycle which represents the distance of the robot locomotion.

Nevertheless, for the opposite direction, it is easily achieve by exchanging two cycle between the prior obtained cycles. Practically, by substituting cycle 2 in Forward direction with cycle 4 in Backward direction and cycle 4 in Forward direction with cycle 2 in Backward direction, the analysis of Backward direction can easily achieve without analysis of chamber condition binary assignment.

**Table 4.4** Simplified hexadecimal value for programming development.

| | | | | | | | | | | |
|---|---|---|---|---|---|---|---|---|---|---|
| **FORWARD WALKING** | | | | | | **BACKWARD WALKING** | | | | |
| | Cycle 1 | Cycle 2 | Cycle 3 | Cycle 4 | | | Cycle 1 | Cycle 2 | Cycle 3 | Cycle 4 |
| C1PA | F8 | 83 | 07 | 7C | | C1PA | F8 | 7C | 07 | 83 |
| C1PB | 60 | 0F | 1F | 70 | | C1PB | 60 | 70 | 1F | 0F |
| C1PC | 0E | 15 | 11 | 0A | | C1PC | 0E | 0A | 11 | 15 |
| C2PA | F8 | 83 | 07 | 7C | | C2PA | F8 | 7C | 07 | 83 |
| C2PB | 60 | 0F | 1F | 70 | | C2PB | 60 | 70 | 1F | 0F |
| C2PC | 15 | 0E | 0A | 11 | | C2PC | 15 | 11 | 0A | 0E |
| | | | | | | | | | | |
| **RIGHT SIDE WALKING** | | | | | | **LEFT SIDE WALKING** | | | | |
| | Cycle 1 | Cycle 2 | Cycle 3 | Cycle 4 | | | Cycle 1 | Cycle 2 | Cycle 3 | Cycle 4 |
| C1PA | D1 | AA | 2E | 55 | | C1PA | D1 | 55 | 2E | AA |
| C1PB | 45 | 2A | 3A | 55 | | C1PB | 45 | 55 | 3A | 2A |
| C1PC | 03 | 18 | 1C | 07 | | C1PC | 03 | 07 | 1C | 18 |
| C2PA | AA | D1 | 55 | 2E | | C2PA | AA | 2E | 55 | D1 |
| C2PB | 2A | 45 | 55 | 3A | | C2PB | 2A | 3A | 55 | 45 |
| C2PC | 03 | 18 | 1C | 07 | | C2PC | 03 | 07 | 1C | 18 |
| | | | | | | | | | | |
| **NORTHEAST** | | | | | | **SOUTHWEST** | | | | |
| | Cycle 1 | Cycle 2 | Cycle 3 | Cycle 4 | | | Cycle 1 | Cycle 2 | Cycle 3 | Cycle 4 |
| C1PA | F9 | AB | 2F | 7D | | C1PA | F9 | 7D | 2F | AB |
| C1PB | 65 | 2F | 3F | 75 | | C1PB | 65 | 75 | 3F | 2F |
| C1PC | 0F | 1D | 19 | 0B | | C1PC | 0F | 0B | 19 | 1D |
| C2PA | FA | D3 | 57 | 7E | | C2PA | FA | 7E | 57 | D3 |
| C2PB | 6A | 4F | 5F | 7A | | C2PB | 6A | 7A | 5F | 4F |
| C2PC | 17 | 1E | 1A | 13 | | C2PC | 17 | 13 | 1A | 1E |
| | | | | | | | | | | |
| **NORTHWEST** | | | | | | **SOUTHEAST** | | | | |
| | Cycle 1 | Cycle 2 | Cycle 3 | Cycle 4 | | | Cycle 1 | Cycle 2 | Cycle 3 | Cycle 4 |
| C1PA | D3 | 57 | 7E | FA | | C1PA | D3 | FA | 7E | 57 |
| C1PB | 4F | 5F | 7A | 6A | | C1PB | 4F | 6A | 7A | 5F |
| C1PC | 17 | 13 | 1A | 1E | | C1PC | 17 | 1E | 1A | 13 |
| C2PA | AB | 2F | 7D | F9 | | C2PA | AB | F9 | 7D | 2F |
| C2PB | 2F | 3F | 75 | 65 | | C2PB | 2F | 65 | 75 | 3F |
| C2PC | 0F | 0B | 19 | 1D | | C2PC | 0F | 1D | 19 | 0B |
| | | | | | | | | | | |
| **CLOCKWISE ROTATION** | | | | | | **ANTICLOCKWISE ROTATION** | | | | |
| | Cycle 1 | Cycle 2 | Cycle 3 | Cycle 4 | | | Cycle 1 | Cycle 2 | Cycle 3 | Cycle 4 |
| C1PA | D3 | 57 | 7E | FA | | C1PA | D3 | FA | 7E | 57 |
| C1PB | 2F | 3F | 76 | 66 | | C1PB | 2F | 66 | 76 | 3F |
| C1PC | 0F | 0B | 19 | 1D | | C1PC | 0F | 1D | 19 | 0B |
| C2PA | FA | 7E | 37 | B3 | | C2PA | FA | B3 | 37 | 7E |
| C2PB | 65 | 75 | 3F | 2F | | C2PB | 65 | 2F | 3F | 75 |
| C2PC | 1E | 1A | 13 | 17 | | C2PC | 1E | 17 | 13 | 1A |

Figure 4.15 shows the human-machine interface for operating the robot using Microsoft Visual Studio via command prompt window.

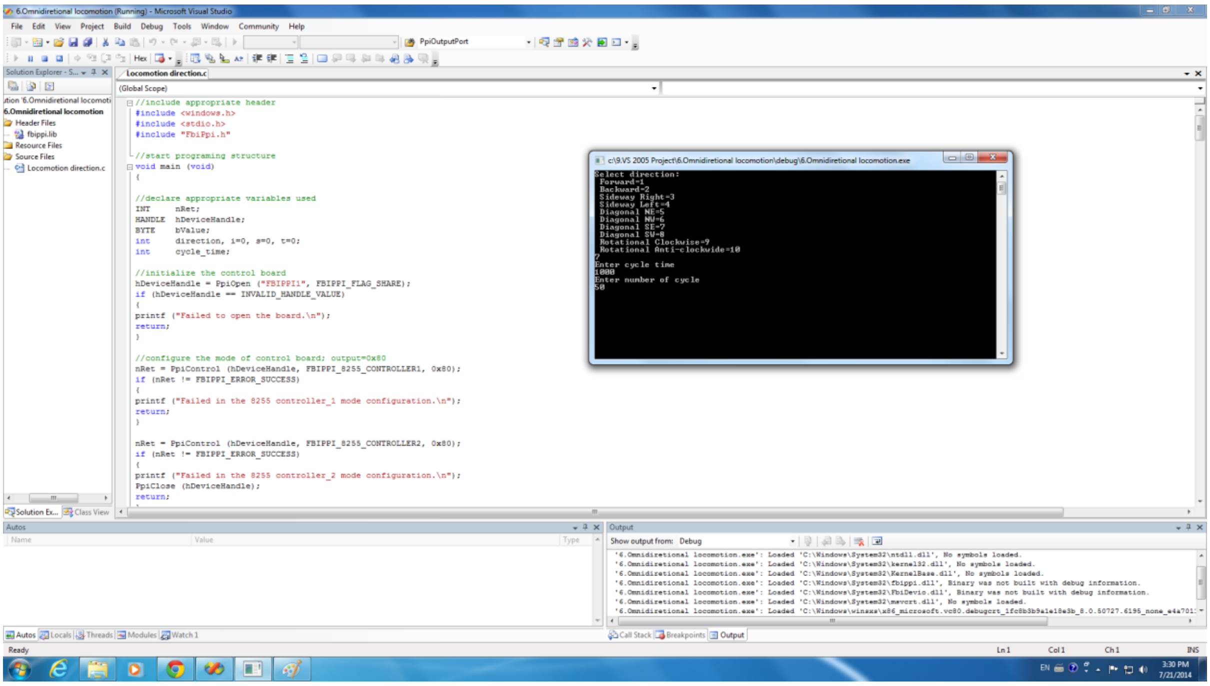


**Figure 4.15:** Command prompt window for operating the soft robot.

Figure 4.16 shows the system configuration and experimental setup for investigating the robot characteristics based on input parameters. A digital camera is used to record the robot response after input parameters are applied to the system.

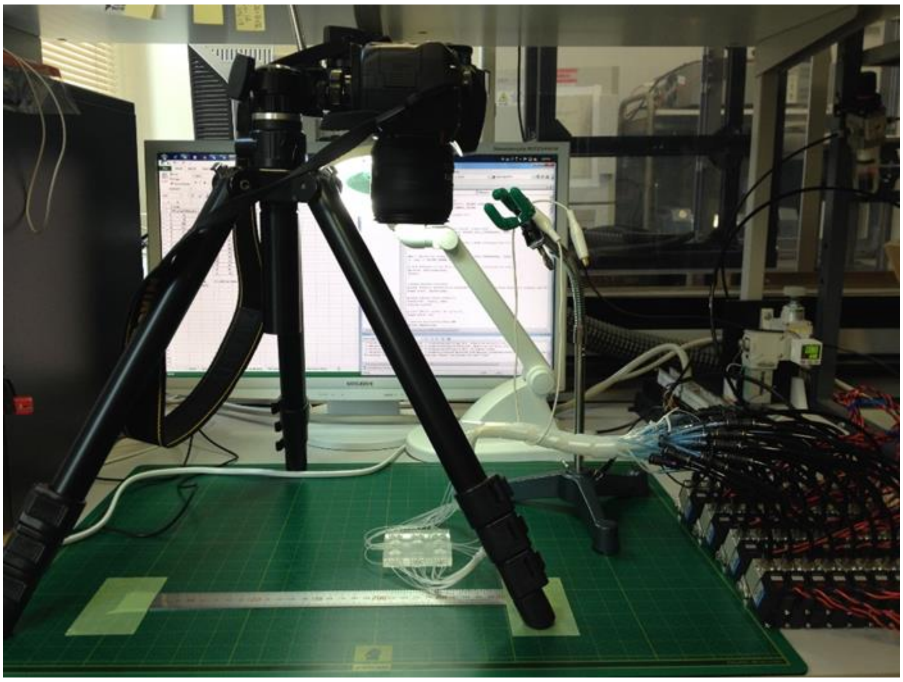

**Figure 4.16:** System configuration.

## 4.5 Experiments

The purpose of the experiment is to establish the omnidirectional locomotion of the soft robot and its locomotion characteristics based on several input parameters. Four experiments were conducted as the following subchapters. Each of the experiments were conducted in three times and an average results were calculated.

The operating pressure was set at 90 kPa for safety reason instead of optimum pressure of 150 kPa obtained from the previous works. For system operation, user have to input three parameters; first – the locomotion direction, represented by number 1 to 10 for 10 directions of locomotion namely forward, backward, sideway right, sideway left, northeast, northwest, southeast, southwest, clockwise and anti-clockwise directions, second – the cycle time which determines the frequency of the locomotion, and third – the number of cycle that dictates the operating time subsequently defines the distance of locomotion.

### 4.5.1 Omnidirectional locomotion

The omnidirectional locomotion of the soft robot comprises of straightway motion, diagonal motion and rotational motion. In straightway motion, the robot can move in forward, backward, sideway right and sideway left as in Figure 4.17 (a). Meanwhile, in diagonal motion the movement includes northeast, northwest, southeast and southwest direction as in Figure 4.16 (b). In rotational motion, the robot rotates in clockwise and anti-clockwise direction as Figure 4.16 (c). From these 10 locomotion directions, the operator entered the value from 1 to 10 that represents 10 direction of locomotion via command prompt window in MVS environment. Then, the locomotion direction was observed to confirm the corresponding direction was achieved.

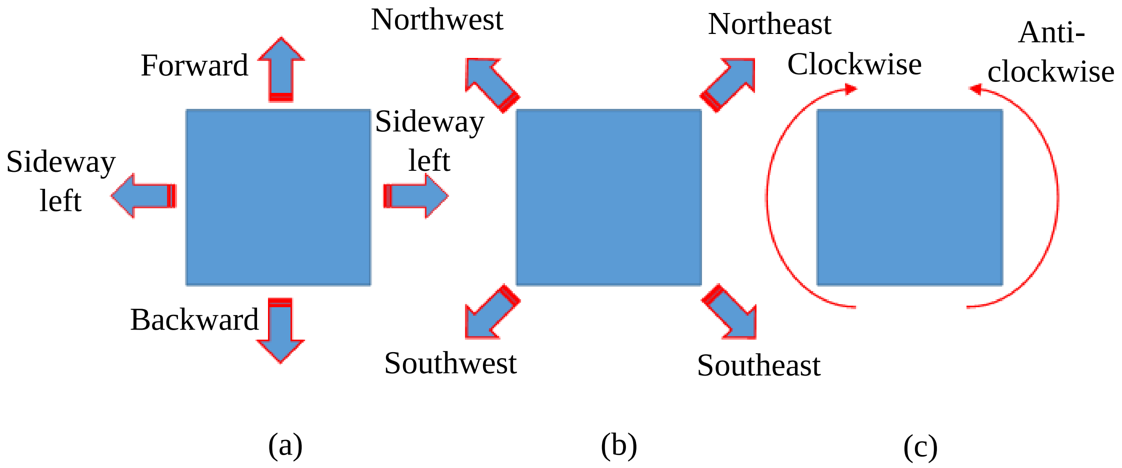


**Figure 4.17:** Omnidirectional locomotion.

### 4.5.2 Operating frequency and locomotion speed

The experiment was designed to establish the relation between locomotion speed and operating frequency for robot locomotion. The operating frequency depends on maximum operating frequency of pneumatic valve used. In this experiment, a pneumatic valve with maximum operating frequency of 5 Hz was used.

Experiment was conducted by varying the operating frequency from 0 to 5 Hz with 0.5 Hz step and robot movement were recorded. The procedure was repeated for all 10 directions and calculation was performed to obtain the traveling speed.

### 4.5.3 Traction force

The experiment was intended to achieve traction force generated by the soft robot. The experimental setup can be seen as in Figure 4.18 where the traction force was generated horizontally. Digital force gauge was used to measure the traction force where the robot was connected to the force gauge by using plastic cable sticking with double-sided tape. The experiment was conducted in forward, northeast and clockwise direction.

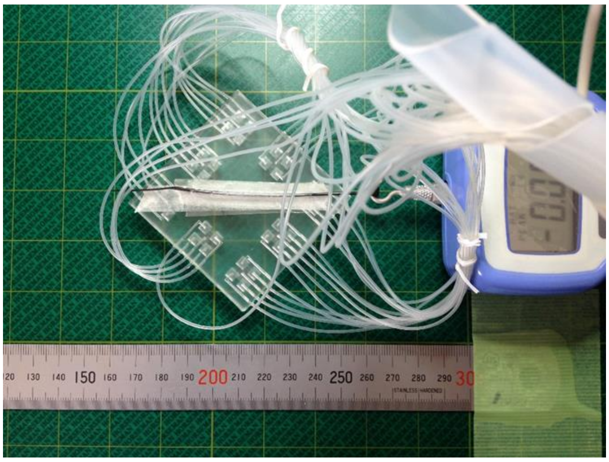

**Figure 4.18:** Traction force experimental setup.

### 4.5.4 Payload

In order to attach a pushing mechanism on top of the soft robot as an assisting medical device in fluoroscopy examination, it is necessary to distinguish the maximum payload the robot can carry. The experiment was conducted in forward, northeast and clockwise direction with different payload range from 99.54 g to 367.76 g. Figure 4.19 shows the experimental setup for forward direction with black plastic acetal as payload at 99.54 g weight located on top of the robot.

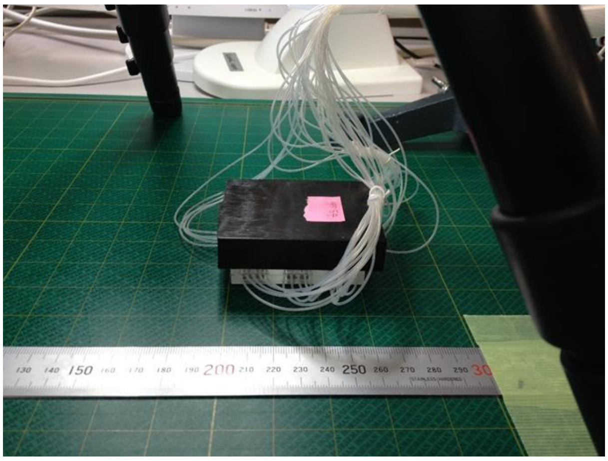

**Figure 4.19:** Payload experimental setup.

## 4.6 Results and Discussion

### 4.6.1 Omnidirectional locomotion

Figure 4.19 shows the omnidirectional locomotion of the soft robot. The red arrow and the red dot in the figure indicates the locomotion direction and front side of the robot respectively. This is to facilitate the recognition of the movement of the robot since the robot was symmetrical in shape. In order to maintain the position of the robot in starting point, a black holder was used where the robot was placed precisely at the corner side of the holder.

Figure 4.20 (a), (b) and (c) show the results of robot locomotion in straightway, diagonal and rotational direction respectively after corresponding input direction was entered by the operator. The robot worked well in other directions thus demonstrating an omnidirectional locomotion ability.

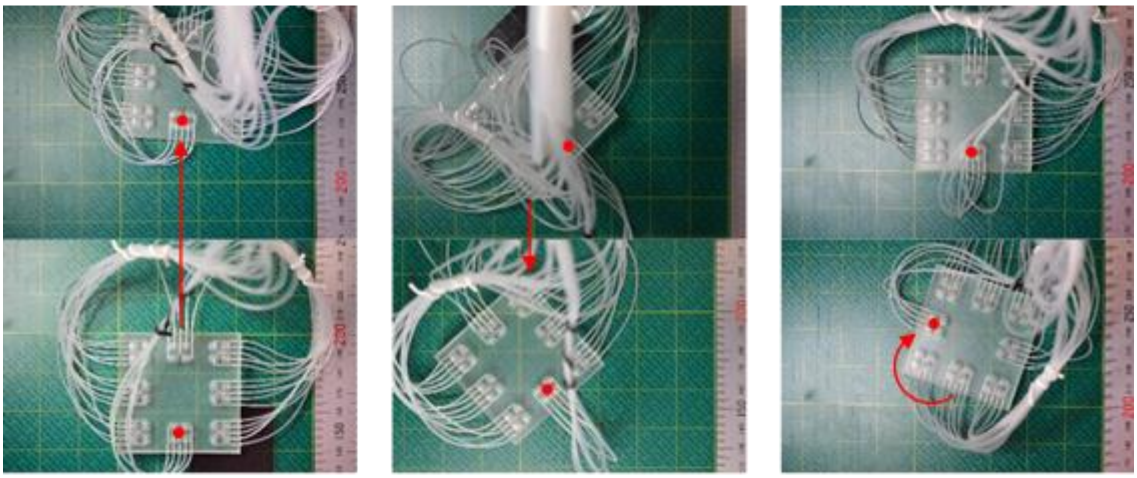

(a) (b) (c)

**Figure 4.20:** Locomotion ability in (a) straightway, (b) diagonal, and (c) rotational.

### 4.6.2 Locomotion speed

In straightway locomotion, the results of the locomotion speed versus operating frequency can be seen as in Figure 4.21. The locomotion speed was increased with the increased of the frequency for all directions. Maximum speed was recorded in forward direction at 6.90 mm/s while for backward direction was at 6.40 mm/s. In sideway right and sideway left, the maximum speed was recorded at 5.40 mm/s and 5.00 mm/s, respectively.

Although the results should be almost identical in all straightway locomotion, the discrepancy between sideways and forward/backward direction was due to some resistance from thirty tubes located at both side of the soft robot. The tubes created some resistance to the robot in the sense that extra force was required to overcome the thirty tubes when moving in sideway. Nevertheless, this restriction can be resolved by embedding the tubes inside the robot which required some modification in robot design.

Figure 4.22 shows the experimental results for locomotion speed in diagonal motion, namely northeast, northwest, southeast and southwest direction. The maximum traveling speed for all directions were almost the same at 5.10 mm /s. Notice that there was no discrepancy in the results suggesting that equal resistance was experienced in all diagonal directions.

Similar results was obtained in rotational motion as in Figure 4.23. The maximum angular speed were recorded at 0.18 rad/s for both clockwise and anti-clockwise directions. Again, an equal resistance was experienced in both rotational directions.

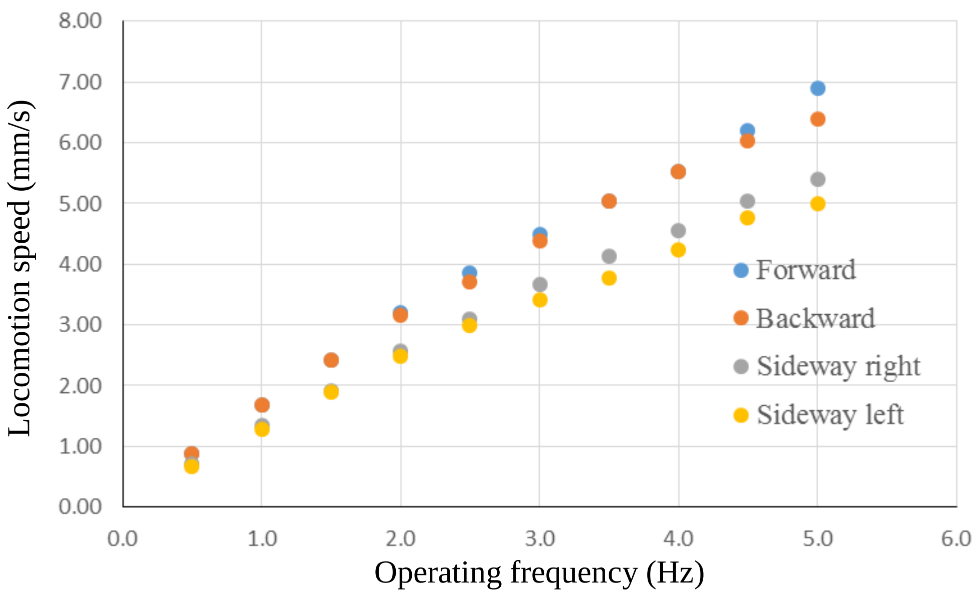


**Figure 4.21:** Locomotion speed in straightway direction.

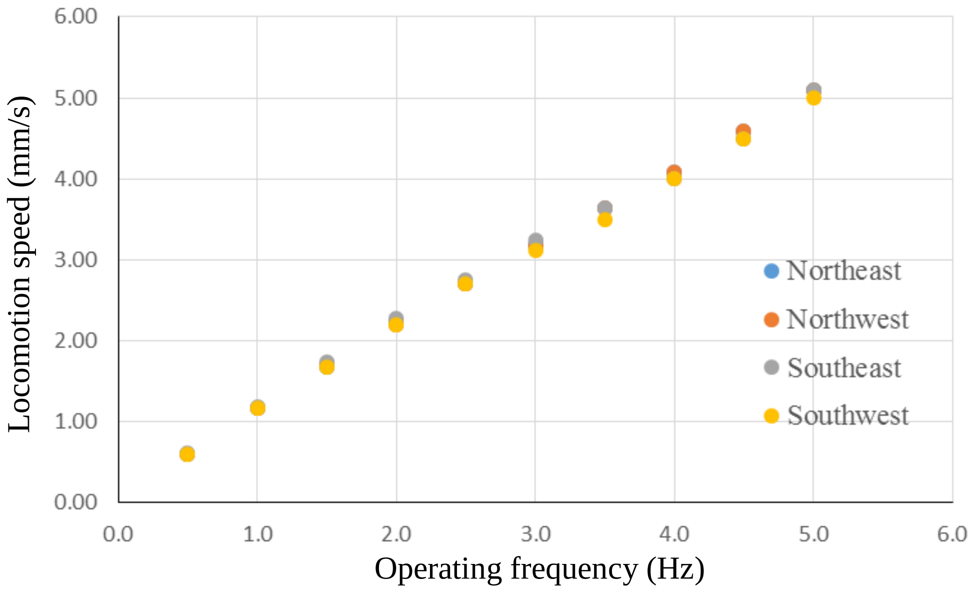


**Figure 4.22:** Locomotion speed in diagonal direction.

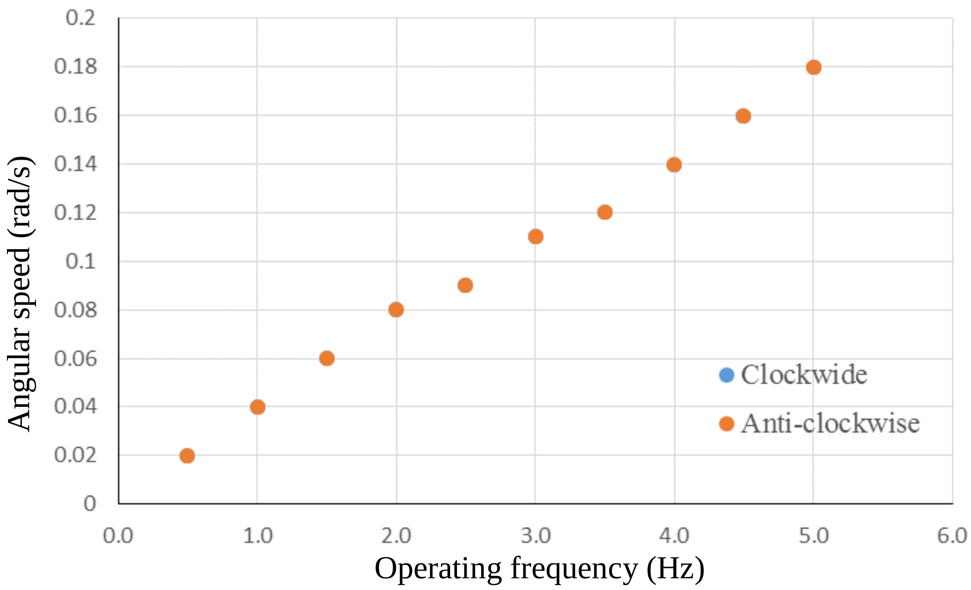


**Figure 4.23:** Locomotion speed in rotational direction.

### 4.6.3 Traction force

The experiment results showed that the traction force was measured at 0.37 N, 0.55 N and 0.31 N in average for forward, diagonal and rotational direction, respectively. This information provided us that the robot generated strong force in diagonal direction. Furthermore, the robot ability to climb a slope during the fluoroscopy examination can be calculated when the exam table was tilted at several angle. However, the ability was also subject to surface roughness which at this moment was not in our consideration.

### 4.6.4 Maximum payload

Figure 4.24 shows the results of locomotion speed with payload applied to the soft robot in forward and diagonal direction. The locomotion speed was decreased significantly with the increased of the payload before the robot came into stalling position when the payload was at 368 g in diagonal locomotion.

Meanwhile, in rotational direction the locomotion speed was reduced similarly as in previous locomotion direction as can be seen in Figure 4.25. The robot also came into stalling position when the payload achieved at 368 g.

Nevertheless, from the linear approximation of these results, the characteristics of soft robot locomotion can only be maintain at payload below 70 g. Thus we decided that the maximum payload for the robot is at 70 g.

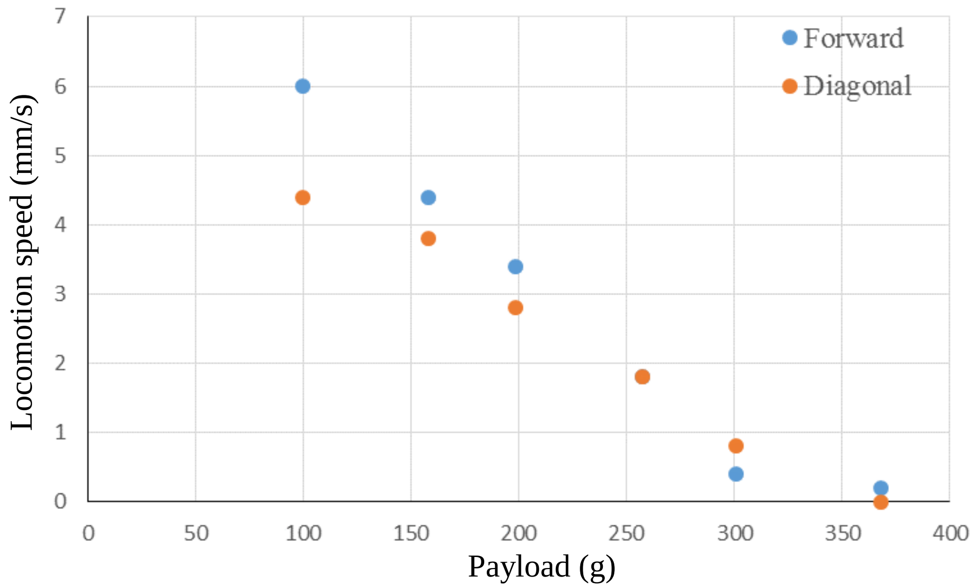


**Figure 4.24:** Locomotion speed with payload in linear direction.

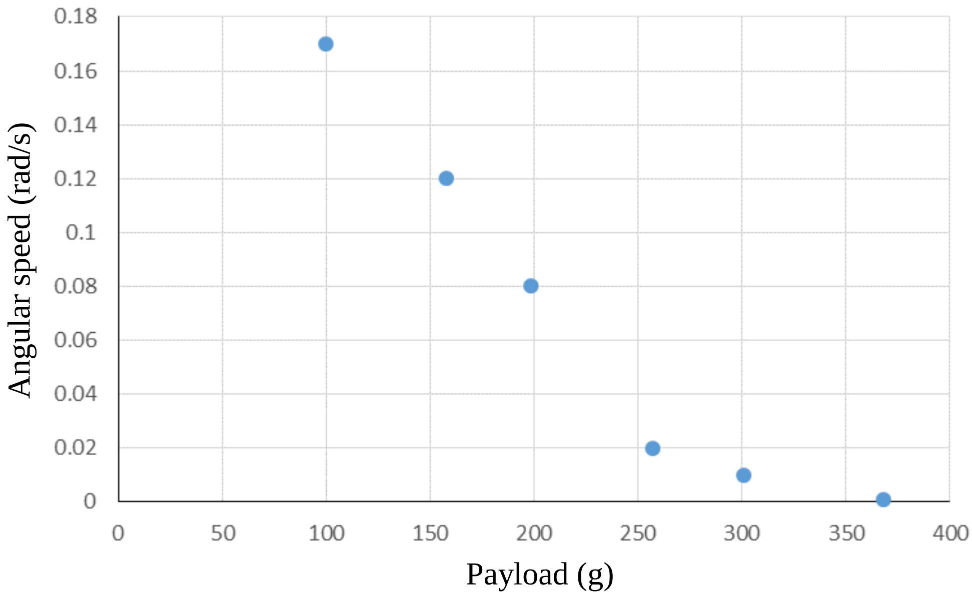


**Figure 4.25:** Locomotion speed with payload in rotational direction.

## 4.7 Summary

In this chapter, the development of soft robot was presented. It began with the design and operation of the soft robot followed by the locomotion planning and fabrication process. Then, the control system development was explained explicitly, covering the hardware and software components. Finally, the experiments was described and the results were presented to establish the omnidirectional locomotion ability and characteristics.

# Chapter 5

## Soft Robot and Pneumatic Pillow Integration for Medical Assisting Device

### 5.1 Introduction

This chapter discusses the adaptation of the soft robot and pneumatic pillow. It begins with the description of pneumatic pillow, developed in our laboratory previously to create the pushing mechanism. Then, the adaptation and simple experiment are demonstrated to prove the potential of the coalition to serve as medical assisting device. Finally the transparency of the soft robot is explained under an X-ray examination.

### 5.2 Pneumatic Pillow

The most identical development in producing pushing mechanism from pneumatic pressure was presented by Hayakawa [53 – 55]. Although the design was much convincing with sponge covered by silicone rubber referred as Sponge Core Soft Rubber Actuator for human friendly support device, the displacement was very small to give a sufficient pressure to the stomach for fluoroscopy examination. Figure 5.1 shows the actuator arranged in matrix. On the other hand, our pneumatic pillow referred as pneumatic bag actuator [62 – 63] expand up to 90 mm to give a significant pressure to the stomach during the test.

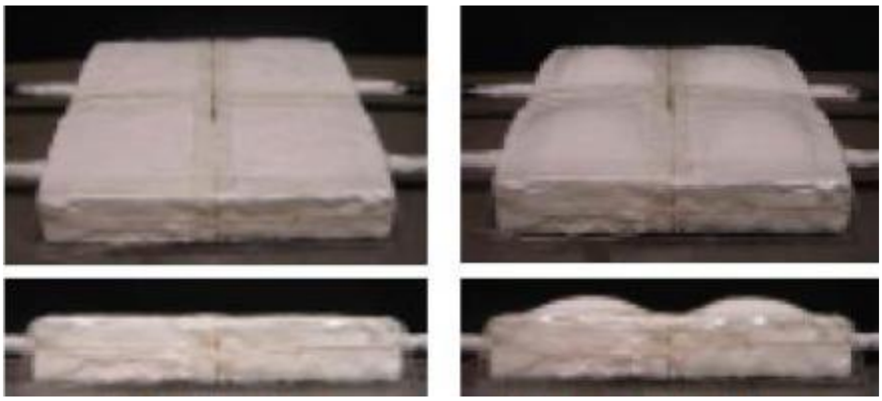

(a) (b)

**Figure 5.1:** Sponge Core Soft Rubber Actuator in matrix arrangement, (a) initial state, and (b) pressurized state [55].

### 5.2.1 Design and working principle

Figure 5.2 shows the design of our pneumatic bag actuator. It was constructed from resin film with 110 mm x 110 mm and covered with cloth. The actuator will inflate when 50 kPa pressure is supplied to the actuator. In order to increase the displacement, two actuators were stacked together with gusset part to prevent slippage between the actuator and not interfering when the actuators were deformed as Figure 5.3.

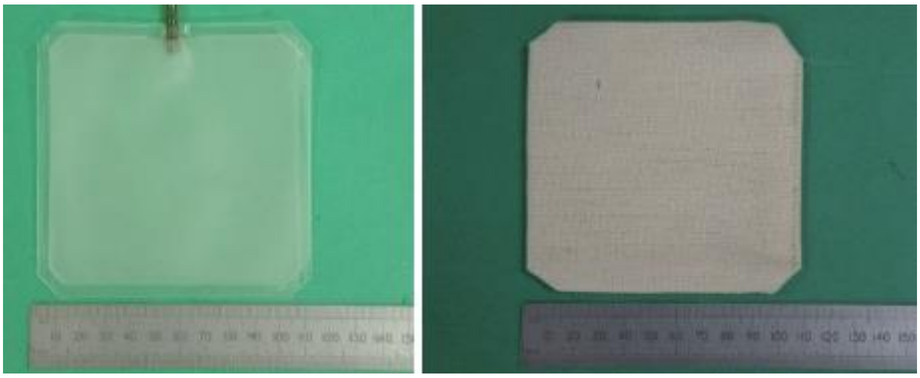

(a) (b)

**Figure 5.2:** Design of pneumatic bag actuator from (a) resin film, and (b) cloth cover [62].

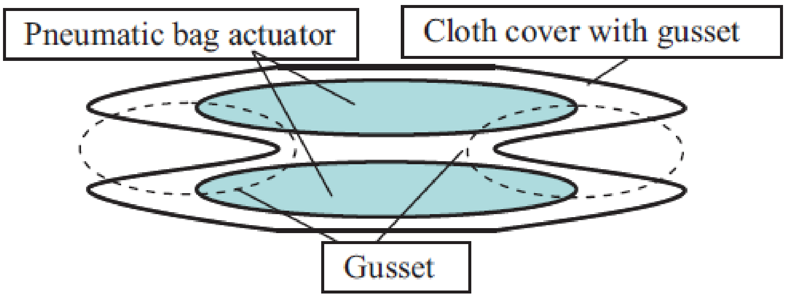


**Figure 5.3:** 2 actuators stacking with gusset [62].

### 5.2.2 Specification

Table 5.1 summarizes the specification of our pneumatic bag actuator. Figure 5.4 shows the displacement of single actuator while Figure 5.5 shows the displacement of two actuators.

**Table 5.1:** Pneumatic bag actuator specification.

| Number of actuator | Operating pressure (kPa) | Displacement (mm) |
|---|---|---|
| Single actuator | 50 | 65 |
| Double actuator | 50 | 45 (one actuator pressurized) |
| Double actuator | 50 | 90 (two actuator pressurized) |

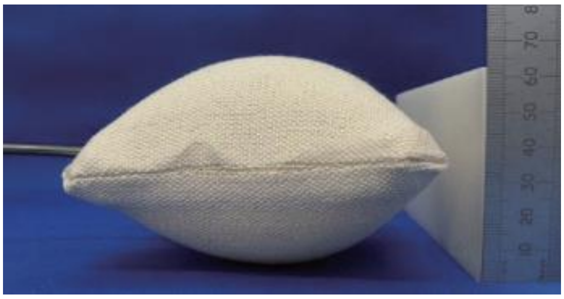

**Figure 5.4:** Pressurized single actuator [62].

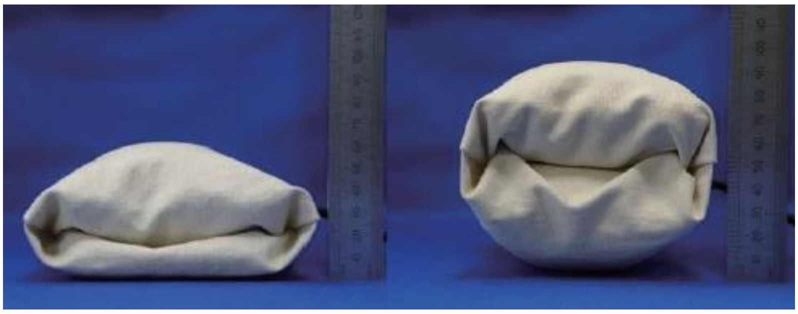

(a) (b)

**Figure 5.5:** Double actuator with (a) pressurized single actuator, and (b) pressurized both actuator [62].

## 5.3 Integration and Adaptability

For generating a significant amount of pressure to the stomach, double bag actuator was used as assisting medical device and referred as pneumatic pillow. The integration was evaluated by examining the ability of the soft robot to combine with the pneumatic pillow and transferred it to a certain distance while maintaining its stability during locomotion as well as when the pillow was pressurized. The pillow weight at 52.11 g and loaded on the top of the robot with double-sided tape and forward locomotion was performed. Then, the pillow was inflated into maximum height and the stability of the robot was observed.

## 5.4 X-ray compatibility

Although compression paddle has been used since 1955 [149] and to the paediatric patients [150], the side-effect from fluoroscopy examination can be very severe [151]. Therefore, the compatibility of the soft robot with an X-ray is very crucial to be established. A sample of soft material with different thickness and stiffness were fabricated with dimension and fabricated sample shown by Figure 5.6 and Figure 5.7, respectively. Two types of stiffness were produced with the same dimension and tested under X-ray to evaluate the transparency property.

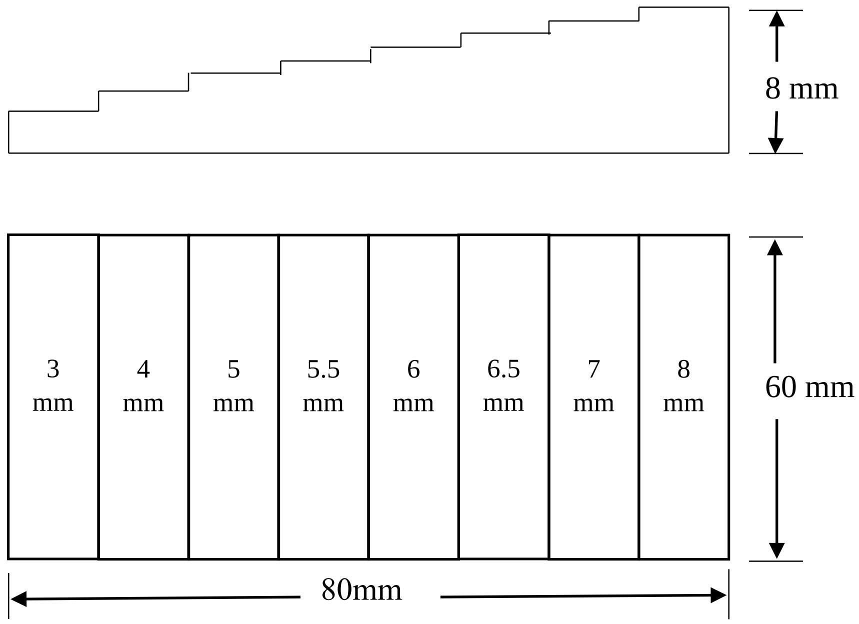


**Figure 5.6:** Dimension of soft material sample.

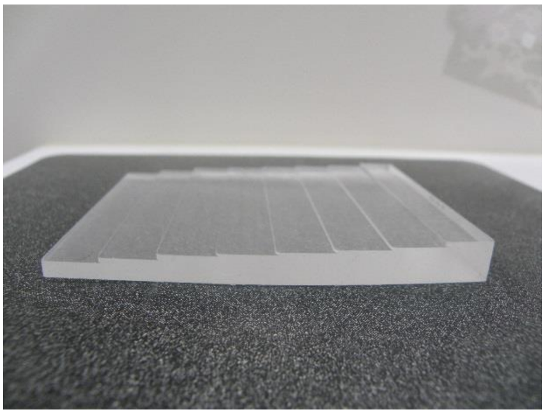

**Figure 5.7:** Fabricated sample.

## 5.5 Results and Discussion

### 5.5.1 Mobile stomach compression medical assisting device

From the simple experiment, the soft robot was able to transfer the pneumatic pillow in forward direction without any difficulty. In addition, the robot was able to maintain its stability even though the pillow was inflated to the maximum level which was 7 times higher than the robot height as in Figure 5.8. Since the weight of the pneumatic pillow was under maximum weight the soft robot can carry, the locomotion characteristics can maintain as for all directions. These results establish the adaptability and readiness of the soft robot to work together with the pneumatic pillow as mobile stomach compression medical assisting device.

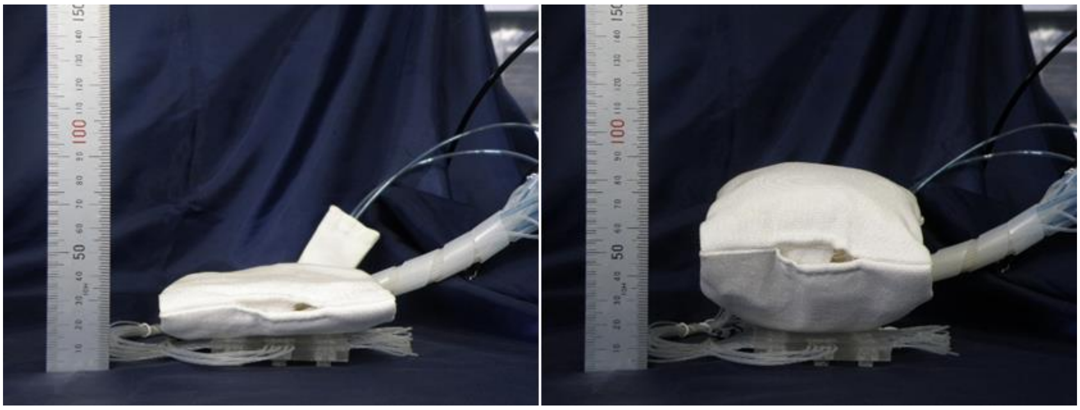

(a) (b)

**Figure 5.8:** (a) Initial position, and (b) pressurized mobile stomach compression medical assisting device.

### 5.5.2 X-ray traceability

The investigation under X-ray test provides us with a significant finding. From the examination, we found that different stiffness was not affecting the traceability of the soft materials. Nevertheless, the thickness and the design did influenced the output image of the X-ray as can be seen in Figure 5.9. The pneumatic pillow was almost not appear while the square-shaped sample with different thickness was apparent in slightly different contrast though can be neglected due to not critically affecting the image.

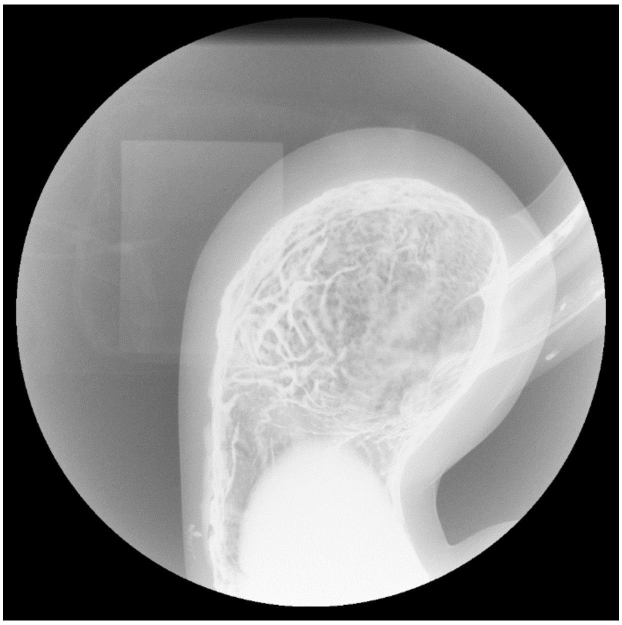

**Figure 5.9:** X-ray image of pneumatic pillow and soft material sample with different thickness.

Further modification on the sharp edge of the sample, by cutting it at certain angle results in undetected under the X-ray test. Figure 5.10 shows the sample edge was cut at certain angle. Then, both the soft robot and sample were located under an X-ray with phantom stomach to investigate the transparency and Figure 5.11 shows the results of X-ray image. As an evidence, the slanting edge sample was hardly noticeable in the image which is pointed by red arrow while the square-shaped soft robot was visible in the image.

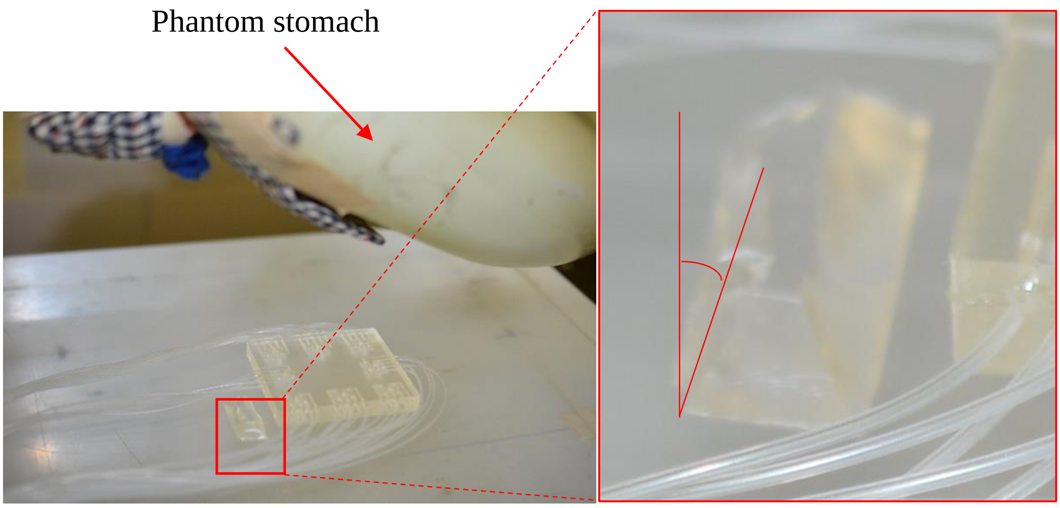


**Figure 5.10:** Sample with edge cut at certain angle.

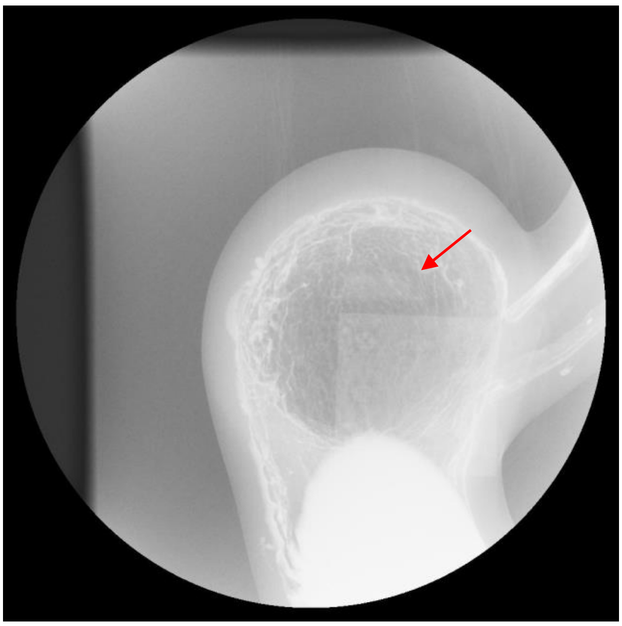

**Figure 5.11:** X-ray image of sample, which its edge was slanted.

## 5.6 Summary

In this chapter, the integration of soft robot and pneumatic pillow was presented. The information of pneumatic pillow was briefly described and several test on the combination of soft robot and pneumatic pillow was demonstrated. The results give us an important information where parameters that affecting the transparency of the soft robot were successfully identified.

# Chapter 6

## Conclusion and Future Works

### 6.1 Summary and Contribution

Generally, the research managed to produce a soft robot to transfer a pneumatic pillow as stomach compression device in fluoroscopy examination. Normal practise of applying compression paddle and/or folded towel to compress patient's stomach manually cause uncomfortable and bothersome to the patient. As the test involves extreme environment where an X-ray is used for cancer cell detection, soft robot with transparent property and compliance for human interaction suit the purpose as an assisting medical device and replace the conventional practise.

In addition, we are able to fulfil all the objectives of the research as stated previously in Chapter 1. We successfully produce a new soft actuator with omnidirectional mechanism from silicone rubber for safe and human compliance interaction. Based on the actuator, we are able to develop soft robot with omnidirectional locomotion operated pneumatically for clean and quiet application. The control system for the robot is established and the characteristics of the robot is successfully quantified. Furthermore, the incorporation of soft robot and pneumatic pillow is achieved confirming the ability of the coalition to perform as medical assisting device.

Several contributions has been achieved from the investigation. Firstly, the invention of new mechanism soft actuator functions as the legs for the soft robot. It provides the robot with an ability to produce combination of motion; namely linear, rotation and oscillatory motion from a short structure operated pneumatically. Compared to previous investigations from researchers that results in single motion, the mechanism results in novel idea and never been established to the best of our knowledge. In addition, fast response from the actuator makes it sensible for the application compared to the rest of the mechanisms.

Secondly, the unique arrangement of the soft actuator as the robot legs enable the robot to perform omnidirectional locomotion, eliminating complex mechanism for the robot to change its direction as demonstrated by researches before. Moreover, grouping of the eight legs into two different groups from such an arrangement ensure a static stability locomotion for smooth and small transition of robot's body. This allows the robot to be positioned at specific location within millimetre range of locomotion distance that is required for positioning the compressing device during the stomach investigation. The stable locomotion is crucial especially when the pneumatic pillow carried by the robot can inflate seven times higher than the robot height.

Finally, from the X-ray examination, it was obtained that the soft robot stiffness did not affect the detection level of an X-ray. Instead, the thickness of the robot and its shape did influence the traceability of the robot under X-ray. The reason for this occurrence is due to the X-ray intensity where sudden change such as sharp edge will be detected on the image. The discovery is crucial as not only having transparent property will assure X-ray penetration, the design of soft material also another element that should be considered. Hence, next following paragraph will describe some improvement to be done for next stage of the research.

## 6.2 Future Works

Current robot design is square in shape and every edges are 90° sharp. Under the X-ray, the soft robot is detectable and appear in image. To prevent such condition, the design of the robot should be in curve edges or slanting so that the X-ray intensity can gradually penetrate the robot without significant contrast, which can be detected in the X-ray image. Unfortunately, this is only applicable to the body of the robot. To apply curve edges to the leg required complete new analysis of the soft actuator hence this investigation will no longer validate in term of characteristics and performance of the soft actuator and the soft robot as well.

Another issue pertaining the design and fabrication of the robot; during assembly where the robot is assembled layer by layer, the bonding material is applied manually using toothpick. Unequal distribution of fluid results poor bonding and leaking after intensive operation of the soft robot. Therefore, a method such as roller might results in a uniform distribution of fluid during assemble the robot layer.

In term of robot performance, although the locomotion speed is adequate for positioning the robot, faster traveling ability will match human hand gesture. This can be achieved by using higher operating frequency of valve. Current maximum operating frequency of the valve is 5 Hz. As established from our experimental results, the locomotion speed is proportional to operating frequency. Even though the locomotion speed can be increased by using bigger size of robot, it thickness will results in detection in the X-ray film image.

Furthermore, one obvious missing part in the system is the feedback from the robot. Since the system is an open loop, operator have to intuitively estimate the position of the robot from the captured video image. A closed loop system will accurately positioned the robot hence expedite the examination process. A sensor could be possibly used without impairing the compliance property of the robot.

Finally, the employment of joystick for controlling the locomotion direction of the robot is very useful for system operation. Current exercise of inputting number in window prompt command that represents the direction, locomotion speed and distance is merely prove of concept for robot operation. Engaging the joystick will add value to the system for commercialization.

# References


[1] F. Iida and C. Laschi, "Soft robotics: challenges and perspectives," *Procedia Computer Science*, vol. 7, pp. 99-102, 2001.

[2] B. A. Trimmer, A. E. Takesian, and B. M. Sweet, "Caterpillar locomotion: a new model for soft-bodied climbing and burrowing robots," in *Int. Symp. On Technology and the Mine Problem*, Monterey, CA, 2006, pp. 1-10.

[3] B. Trimmer and J. Issberner, "Kinematics of soft-bodied, legged locomotion in manduca sexta larvae," *Biol. Bull.* vol. 212, pp. 130-142, 2007.

[4] B. A. Trimmer, "New challenges in biorobotics: incorporating soft tissue into control systems," *Applied Bionics and Biomechanics*, vol. 5, no. 3, pp. 119-126, 2008.

[5] J. Rieffel, B. Trimmer, and H. Lipson, "Mechanism as mind: what tensegrities and caterpillars can teach us about sot robotics," *Artificial Life*, vol. 11, pp. 506-512, 2008.

[6] A. Albu-Schaffer, and O. Eiberger, "Soft robotics," *IEEE Robotics and Automation Mag.*, pp. 20-30, 2008.

[7] C. Laschi, B. Mazzolai, V. Mattoli, M. Cianchetti, and P. Dario, "Design and development of a soft actuator for a robot inspired by the octopus arm," in *Experimental Robotics*, Springer Berlin Heidelberg, 2009, pp. 25-33.

[8] H. Lin, and B. A. Trimmer, "The substrate as a skeleton: ground forces from a soft-bodied legged animal," *The Journal of Experimental Biology*, vol. 213, pp. 1133-1142, 2010.

[9] B. A. Trimmer, H. Lin, A. Baryshyan, G. G. Leisk, and D. L. Kaplan, "Towards a biomorphic soft robot: design constraints and solutions," in *IEEE RAS/EMBS Intl. Conf. on Biomedical Robotics and Biomechatronics*, pp. 599-605, June 2012.

[10] C. Laschi, M. Cianchetti, B. Mazzolai, L. Margheri, M. Follador, and P. Dario, "Soft robot arm inspired by the octopus," *Advanced Robotics*, vol. 26, pp. 709-727, 2012.

[11] F. Renda, M. Giorelli, M. Calisti, M. Cianchetti, and C. Laschi, "Dynamic model of a multibending soft robot arm driven by cables," *IEEE Trans. on Robotics*, vol. 30, no. 5, pp. 1109-1122, October 2014.

[12] D. Rus, and M. T. Tolley, "Design, fabrication and control of soft robots," *Nature*, vol. 521, issue 7553, pp. 467-475, May 2015.

[13] M. D. Volder, and D. Reynaerts, "Pneumatic and hydraulic microactuators: a review," *J. of Micromech. Microeng*., vol. 20, pp. 043001-043018, 2010.

[14] T. Fukuda, H. Hosokai, and M. Uemura, "Rubber gas actuator driven by hydrogen storage alloy for in-pipe inspection mobile robot with flexible structure," in *Proc. IEEE Int. Conf. on Robotics and Automation*, pp. 1847-1852, 1989.

[15] T. Noritsugu, and T. Tanaka, "Application of rubber artificial muscle manipulator as a rehabilitation robot," *IEEE/ASME on Mechatronics*, vol. 2, no. 4, pp. 259-267, Dec. 1997.

[16] D. G. Caldwell, N. Tsagarakis, D. Badihi, and G. A. M. Cerda, "Pneumatic muscle actuator technology a light weight power system for a humanoid robot," in *Proc. of IEEE Intl. Conf. on Robotics and Automation*, pp. 3053-3058, May 1998.

[17] Q. Yang, L. Zhang, G. Bao, and J. Ruan, "Research on novel flexible pneumatic actuator (FPA)," in *Proc. Of the 2004 IEEE Conf. on Robotics, Automation and Mechatronics*, vol. 1, pp. 385-389, 2004.

[18] T. Noritsugu, H. Yamamoto, D. Sasaki, and M. Takaiwa, "Wearable power assist device for hand grasping using pneumatic artificial rubber muscle," in *IEEE Int. Workshop on ROMAN*, pp. 420-425, 2004.

[19] D. Sasaki, T. Noritsugu, and M. Takaiwa, "Development of active support splint driven by pneumatic soft actuator (ASSIST)," in *Proc. of IEEE Intl. Conf. on Robotics*

*and Automation*, pp. 520-525, 2005.
[20] D. Sasaki, T. Noritsugu, and M. Takaiwa, "Development of pneumatic power assist splint "ASSIST" operated by human intention," *J. of Robotic and Mechatronics*, vol. 17, no. 5, pp. 568-574, 2005.
[21] K. Iwata, K. Suzumori, and S. Wakimoto, "A method of designing and fabricating Mckibben muscle driven by 7 Mpa hydraulics," *Int. J. of Automation Technology,* vol.6, no.4, pp. 482-487, 2012.
[22] G. Andrikopoulos, G. Nikolakopoulos, and S. Manesis, "Motion control of a novel robotic wrist exoskeleton via pneumatic muscle actuators," in *IEEE Conf. on Emerging Technologies and Factory Automation*, pp. 1-8, Sept. 2015.
[23] T. Noritsugu, D. Sasaki, and M. Takaiwa, "Application of artificial pneumatic rubber muscles to a human friendly robot," in *Proc. of IEEE Intl. Conf. on Robotics & Automation*, pp. 2188-2193, 2003.
[24] N. G. Tsagarakis, and D. G. Caldwell, "Development and control of a 'Soft-actuated' exoskeleton for use in physiotherapy and training," *Autonomous Robot*, vol. 15, pp. 21-33, 2003.
[25] Y. Park, J. Santos, K. G. Galloway, E. C. Goldfield, and R. J. Wood, "A soft wearable robotic device for active knee motions using flat pneumatic artificial muscle," in *IEEE Int. Conf. on Robotics and Automation (ICRA)*, pp. 4805-4810, 2014.
[26] J. Zhang, H. Wang, J. Tang, H. Guo, and J. Hong, "Modeling and design of a soft pneumatic finger for hand rehabilitation," in *Proc. of IEEE Intl. Conf. on Information and Automation*, pp. 2460-2465, 2015.
[27] S. Guo, F. Zhao, W. Wei, J. Guo, X. Zhao, and W. Zhang, "Soft actuator for hand rehabilitation," in *Proc. of IEEE Intl. Conf. on Mechatronics and Automation*, pp. 2197-2202, 2015.
[28] N. Yee and G. Coghill, "Modelling of a novel rotary pneumatic muscle," in *Proc. Australiasian Conf. on Robotics and Automation*, pp. 186-190, 27-29, Nov. 2002.
[29] S. Wakimoto, I. Kumagai, and S. Suzumori, "Development of large intestine endoscope changing its stiffness," in *Proc. of IEEE Intl. Conf. on Robotics and Biomimetics*, pp. 2320-2325, 2009.
[30] I. Kumagai, S. Wakimoto, and K. Suzumori, "Development of large intestine endoscope changing its stiffness-2$^{nd}$ report: Improvement of stiffness change device and insertion experiment," in *Proc. on IEEE Intl. Conf. on Robotics and Biomimetics*, pp. 241-246, 2010.
[31] S. Wakimoto, K. Suzumori, and J. Takeda, "Flexible artificial muscle by bundle of McKibben fiber actuators," in *IEEE/ASME Intl. Conf. on Advanced Intelligent Mechatronics (AIM2011)*, pp. 457-462, 2011.
[32] M. D. Volder, A.J.M. Moers, and D. Reynaerts, "Fabrication and control of miniature McKibben actuator," *Sensors and Actuators A*, vol. 166, pp. 111-116, 2011.
[33] S. Krishnan, T. Nagarajan, A. M. A. Rani, and T. V. V. L. N. Rao, "Silk pneumatic artificial muscle (SPAM) construction for bio-medical engineering application," *IEEE Business, Engineering & Industrial Applications Colloquium (BEIAC)*, pp. 302-306, 2012.
[34] A. A. M. Faudzi, M. R. M. Razif, I. N. A. M. Nordin, and K. Suzumori, "Development of bending soft actuator with different braided angles," in *IEEE/ASME Intl. Conf. on Advanced Intelligent Mechatronics (AIM)*, pp. 1093-1098, 2012.
[35] T. Driver, and X. Shen, "Sleeve muscle actuator: concept and prototype demonstration," *Journal of Bionic Engineering*, vol. 10, pp. 222-230, 2013.
[36] E. H. Skorina, M. Luo, S. Ozel, F. Chen, W. Tao, and C. D. Onal, "Feedforward augmented sliding mode motion control of antagonistic soft pneumatic actuators," in

*IEEE Intl. Conf. on Robotics and Automation (ICRA)*, pp. 2544-2549, 2015.

[37] M. Luo, E. H. Skorina, W. Tao, F. Chen, and C. D. Onal, "Optimized design of a rigid kinematic module for antagonistic soft actuation," in *IEEE Intl. Conf. on Technologies for Practical Robot Applications (TePRA)*, pp. 1-6, 2015.

[38] P. Polygerinos, Z. Wang, J. T. B. Overvelde, *et al.*, "Modeling of soft fiber-reinforced bending actuators," *IEEE Transactions on Robotics*, vol. 31, no. 3, pp.778-789, June 2015.

[39] M. Memarian, R. Gorbet, and D. Kulic, "Modelling and experimental analysis of a novel design for soft pneumatic artificial muscles," in *IEEE/RSJ Intl. Conf. on Intelligent Robots and Systems (IROS)*, pp. 1718-1724, 2015.

[40] M. Memarian, R. Gorbet, and D. Kulic, "Control of soft pneumatic finger-like actuators for affective motion generation," in *IEEE/RSJ Intl. Conf. on Intelligent Robots and Systems (IROS)*, pp. 1691-1697, 2015

[41] N. Giri, and I. Walker, "Continuum robots and underactuated grasping," in *IFToMM/ ASME Intl. Workshop on Underactuated Grasping (UG2010)*, pp. 51-58, 2011.

[42] K. Suzumori, S. Wakimoto, K. Miyoshi, and K. Iwata, "Long bending rubber mechanism combined contracting and extending fluidic actuators," in *IEEE/RSJ Intl. Conf. on Intelligent Robots and Systems (IROS)*, pp. 4454-4459, 2013.

[43] K. Suzumori, S. Iikura, and H. Tanaka, "Flexible microactuator for miniature robots," *Proc. MEMS*, pp. 204-209, 1991.

[44] K. Suzumori, S. Iikura, and H. Tanaka, "Development of flexible microactuator and its applications to robotic mechanisms," in *Proc. of IEEE Intl. Conf. on Robotics and Automation*, pp. 1622-1627, 1991.

[45] K. Suzumori, S. Iikura, and H. Tanaka, "Applying a flexible microactuator to robotic mechanisms," *IEEE Control Systems*, vol. 12, issue 1, pp. 21-27, 1992.

[46] K. Suzumori, A. Koga, and R. Haneda, "Microfabrication of integrated FMAs using stereo lithography," in *Proc. IEEE Workshop on MEMS*, pp. 136-141, 1994.

[47] K. Suzumori, T. Maeda, H. Watanabe, and T. Hisada, "Fiberless flexible microactuator designed by finite-element method," *IEEE/ASME Transactions on Mechatronics*, vol. 2, no. 4, pp. 281-286, Dec 1997.

[48] N. Fujiwara, S. Sawano, and S. Konishi, "Linear expansion and contraction or paired pneumatic balloon bending actuators toward telescopic motion," in *IEEE Intl. Conf. on Micro Electro Mechanical Systems MEMS*, pp. 435-438, 2009.

[49] T. Chishiro, T. Ono, and S. Konishi, "Pantograph mechanism for conversion from swelling into contraction motion of pneumatic balloon actuator," in *IEEE Int. Conf. on MEMS*, pp. 532-535, 2013.

[50] S. Honda, Y. Tsujimura, and S. Konishi, "Design and characterization of contraction motion actuator converted from swelling pneumatic balloon actuator for large deformation and force," in *Intl. Conf. on Solid-state Sensors, Actuators and Microsystems (TRANDUCERS)*, pp. 2140-2143, 2015.

[51] F. Z. Low, R. C. H. Yeow, H. K. Yap, "Study on the use of soft ankle-foot exoskeleton for alternative mechanical prophylaxis of deep vein thrombosis," in *IEEE Intl. Conf. on Rehabilitation Robotics (ICORR)*, pp. 589-593, 2015.

[52] G. Chen, M. T. Pham, and T. Redarce, "Development and kinematic analysis of a silicone-rubber bending tip for colonoscopy," in *Proc. IEEE/RSJ Int. Conf. on Intelligent Robots and Systems*, pp. 168-173, 2006.

[53] Y. Hayakawa, K. Morishita, and M. Aichi, "Control performance of a pneumatic silicon outer fence mold actuator," in *SICE Annual Conf.*, pp. 498-501, 2003.

[54] Y. Hayakawa, and K. Morishita, "Development of a silicone outerfence mold actuator with human compatibility," in *Proc. IEEE Intl. Conf. on Robotics and Automation*, pp.

4059-4064, 2004.
[55] Y. Hayakawa and S. R. Pandian, “Development of a hybrid element by using sponge core soft rubber actuator,” in *Proc. IEEE Intl. Conf. on Robotics and Automation*, pp. 538-543, 2005.
[56] H. J. Kwon, S. W. Lee, and S. S. Lee, “Braille dot display module with a PDMS membrane driven by a thermopneumatic actuator,” *Sensors and Actuators A*, vol. 154, pp. 238-246, 2009.
[57] Y. Hongbin, Z. Guangya, S. S. Kumar, C. F. Siong, and W. Shouhua, “Lens integrated with self-aligned variable aperture using pneumatic actuation method,” *Sensors and Actuators A*, vol. 159, pp. 105-110, 2010.
[58] Y. Han, and C. Liu, “Pneumatically actuated active polymer pen lithography,” *Sensors and Actuators A*, vol. 167, pp. 433-437, 2011.
[59] B. Gorissen, M. D. Volder, A. D. Greef, and D. Reynaerts, “Theoretical and experiment analysis of pneumatic balloon microactuators,” *Sensors and Actuators A*, vol. 168, pp. 58-65, 2011.
[60] X. Wu, S. H. Kim, H. Zhu, C. H. Ji, and M. G. Allen, “A refreshable Braille cell based on pneumatic microbubble actuators,” *Journal on Microelectromechanical Systems*, vol. 21, no. 4, pp. 908-916, Aug 2012.
[61] A. Alogla, P. Scanlan, W. M. Shu, and R. L. Reuben, “A scalable syringe-actuated microgripper for biological manipulation,” *Sensor and Actuators A: Physical*, pp. 1-5, 2013.
[62] M. Iwamura, S. Wakimoto, K. Suzumori, H. Oka, and K. Sumi, “Fundamental tests of pneumatic soft devices for pushing abdomen in stomach X-ray examination,” in *Proc. IEEE Int. Conf. on Robotics and Biomimetics*, pp. 2649-2654, 2014.
[63] K. Shibuya, K. Sumi, T. Watanabe, K. Suzumori, and H. Oka, “Development and usefulness evaluation of a remote control pressured pillow for prone position,” *Japan Radiological Technologist J.*, vol. 61, no. 738, pp. 21-25, 2014.
[64] J. H. Low, P. M. Khin, and K. H. Yeow, “A pressure-redistributing insole using soft sensors and actuators,” in *IEEE Intl. Conf. on Robotics and Automation (ICRA)*, pp. 2926-2930, 2015.
[65] O. P. Ogunmolu, X. Gu, S. Jiang, and N. R. Gans, “A real-time, soft robotics patient positioning systems for maskless head-and-neck cancer radiotherapy: an initial investigation,” in *IEEE Intl. Conf. on Automation Science and Engineering (CASE)*, pp. 1539-1545, 2015.
[66] X. Lu, W. Xu, and X. Lee, “Concept and simulations of a soft robot mimicking human tongue,” in *Proc. of Int. Conf. on Automation, Robotics and Applications*, pp. 332-336, 2015.
[67] S. Konishi, F. Kawai, and P. Cusin, “Thin flexible end-effector using pneumatic balloon actuator,” *Sensor and Actuators A*, vol. 89, pp. 28-35, 2001.
[68] J. He, L. Xu, X. Song, M. Luo, and J. Chu, “The driving mechanism research of six unit soft robots,” in *IEEE Conf. on Robotics, Automation and Mechatronics*, pp. 79-83, 2013.
[69] O. C. Jeong, and S. Konishi, “Fabrication and drive test of pneumatic PDMS micro pump,” *Sensor and Actuators A*, vol. 165, pp. 86-93, 2011.
[70] B. T. Chia, H. H. Lio, and Y. J. Yang, “A novel thermos-pneumatic peristaltic micropump with low temperature elevation on working fluid,” *Sensor and Actuators A*, vol. 89, pp. 28-35, 2001.
[71] Z. Deng, M. Stommel, and W. Xu, “A novel soft machine table for manipulation of delicate objects inspired by caterpillar locomotion,” *IEEE/ ASME Transactions on Mechatronics*, vol. PP, issue 99, pp. 1-9, 2016.

[72] M. Stommel, and W. Xu, “Optimal, efficient sequential control of a soft-bodied, peristaltic sorting table,” *IEEE/ ASME Transactions on Automation Science and Engineering*, vol. PP, issue 99, pp. 1-10, 2015.
[73] M. Stommel, and W. L. Xu, “Qualitative control of soft robotic peristaltic sorting tables,” in *IEEE Intl. Conf. on Mechatronics*, pp. 82-87, 2015.
[74] S. Dirven, W. Xu, and L. K. Cheng, “Sinusoidal peristaltic waves in soft actuator for mimicry of esophageal swallowing,” *IEEE/ASME Transactions on Mechatronics*, vol. 20, no. 3, pp. 1331-1337, 2015.
[75] N. Saga, J. Nagase, and T. Saikawa, “Development of a tendon driven system using a pneumatic balloon,” in *Proc. of IEEE Int. Conf. on Mechatronics and Automation*, pp. 1087-1092, 2005.
[76] J. Nagase, and N. Saga, “Design of tendon-driven robot hand using pneumatic balloon actuators,” in *World Automation Congress*, pp. 1-6, 2010.
[77] J. Nagase, and N. Saga, “Two tendon-driven systems using pneumatic balloons,” *Advanced Robotics*, vol. 25, pp. 1349-1361, 2011.
[78] N. Saga N. Saito, and J. Nagase, “Ankle rehabilitation device to prevent contracture using a pneumatic balloon actuator,” *Int. J. of Automation Technology*, vol. 5, no. 4, pp. 538-543, 2011.
[79] M. Yoda, and S. Konishi, “Acoustic impedance control through structural tuning by pneumatic balloon actuators,” *Sensor and Actuators A*, vol. 95, pp. 222-226, 2002.
[80] D. Sasaki, T. Noritsugu, and M. Takaiwa, “Development of high contractile pneumatic artificial rubber muscle for power assist device,” *Journal of Robotics and Mechatronics*, vol. 24, no. 1, pp. 150-157, 2012.
[81] Y. Sun, C. M. Lim, H. H. Tan, and H. Ren, “Soft oral interventional rehabilitation robot based on low-profile soft pneumatic actuator,” in *IEEE Int. Conf. on Robotics and Automation (ICRA)*, pp. 2907-2912, 2015.
[82] S. Y. Chang, K. Takashima, S. Nishikawa *et al.*, “Design of small-size pouch motors for rat gait rehabilitation device,” in *IEEE Annual Int. Conf. on Engineering in Medicine and Biology Society (EMBC)*, pp. 4578-4581, 2015.
[83] S. Konishi, T. Kobayashi, H. Maeda, S. Asajima, and M. Makikawa, “Cuff actuator for adaptive holding condition around nerves,” *Sensor and Actuators B*, vol. 83, pp. 60-66, 2002.
[84] W. Choi, M. Akbarian, V. Rubtsov, and C. Kim, “Microhand with internal visual system,” *IEEE Trans. On Industrial Electronics*, vol. 56, no. 4, pp. 1005-1011, 2009.
[85] Y. Shapiro, A. Wolf, and K. Gabor, “Bi-bellows: pneumatic bending actuator,” *Sensor and Actuators A*, vol. 167, pp. 484-494, 2011.
[86] C. Meng, W. Xu, H. Li, and T. Wang, “A novel soft manipulator based on beehive structure,” in *IEEE/RSJ Int. Conf. on Intelligent Robot and System (IROS)*, pp. 2342-2347, 2015.
[87] V. Oguntosin, W. S. Harwin, S. Kawamura, S. J. Nasuto, and Y. Hayashi, “Development of a wearable assistive soft robotic device for elbow rehabilitation,” in *IEEE Int. Conf. on Rehabilitation Robotics (ICORR)*, pp. 747-752, 2015.
[88] L. B. Yehoshua, M. Ochoa, and B. Ziaie, “Rapid fabrication of 3D elastomeric structures via laser-machining and vacuum deformation,” in *Int. Conf. on Solid-state Sensors, Actuators and Microsystems (TRANSDUCERS)*, pp. 1299-1302, 2015.
[89] J. H. Low, M. H. Ang, and C. H. Yeow, “Customizable soft pneumatic finger actuators for hand orthotic and prosthetic applications,” in *IEEE Int. Conf. on Rehabilitation Robotics (ICORR)*, pp. 380-385, 2015.
[90] B. Gorissen, T. Chishiro, S. Shimomura, D. Reynaerts, M. D. Volder, and S. Konishi, “Flexible pneumatic twisting actuators and their application to tilting micromirros,”

*Sensors and Actuators A*, pp. 1-5, 2014.

[91] R. Niiyama, D. Rus, and S. Kim, "Pouch motors: printable/ inflatable soft actuators for robotics," in *IEEE Int. Conf. on Robotics and Automation (ICRA)*, pp. 6332-6337, 2014.

[92] H. Amase, Y. Nishioka, and T. Yasuda, "Mechanism and basic characteristics of a helical inflatable gripper," in *Proc. IEEE Int. Conf. on Mechatronics and Automation*, pp. 2559-2564, 2015.

[93] O. Ivlev, "Soft fluidic actuators of rotary type for safe physical human-machine interaction," in *IEEE Int. Conf. on Rehabilitation Robotics*, pp. 1-5, 2009.

[94] M. Jordon, D. Pietrusky, M. Mihajlov, and O. Ivlev, "Precise position and trajectory control of pneumatic soft-actuators for assistance robots and motion therapy device," in *IEEE Int. Conf. on Rehabilitation Robotics*, pp. 663-668, 2009.

[95] A. Wilkening, D. Baiden, and O. Ivlev, "Assistive control of motion therapy devices based on pneumatic soft-actuators with rotary elastic chambers," in *IEEE Int. Conf. on Rehabilitation Robotics*, pp. 1-6, 2011.

[96] D. Baiden, A. Wilkening, and O. Ivlev, "Safety and handling concept for assistive robotic devices with pneumatic rotary soft-actuators," in *IEEE/ASME Int. Conf. on Advanced Intelligent Mechatronics (AIM2011)*, pp. 754-759, 2011.

[97] A. Wilkening, H, Stoppler and O. Ivlev, "Adaptive assistive control of a soft elbow trainer with self-alignment using pneumatic banding joint," in *IEEE Int. Conf. on Rehabilitation Robotics (ICORR)*, pp. 729-734, 2015.

[98] S. Schulz, C. Pylatiuk, and G. Bretthauer, "A new ultralight anthromorphic hand," in *Proc. of the 2001 IEEE Intl. Conf. on Robotics and Automation (ICRA2001)*, vol. 3, pp. 2437-2441, 2001.

[99] K. Ogura, S. Wakimoto, K. Suzumori, and Y. Nishioka, "Micro pneumatic curling actuator – Nematode actuator –," in *Proc. IEEE Int. Conf. on Robotics and Biomimetics*, pp. 462-467, 2008.

[100] S. Wakimoto, K. Ogura, and K. Suzumori, "Miniature soft hand with curling rubber pneumatic actuators," in *IEEE Intl. Conf. on Robotics and Automation (ICRA09)*, pp. 556-561, 2009.

[101] S. Wakimoto, K. Suzumori, and K. Ogura, "Miniature pneumatic curling rubber actuator generating bidirectional motion with one air-supply tube," *Advanced Robotics*, vol. 25, pp. 1311-1330, 2011.

[102] Y Hwang, O. H. Paydar, and R. N. Candler, "Pneumatic microfinger with balloon fins for linear motion using 3D printed molds," *Sensors and Actuators A*, vol. 234, pp. 65-71, 2015.

[103] E. Steltz, A. Mozeika, N. Rodenberg, E. Brown, and H. M. Jaeger, "JSEL: Jamming skin enabled locomotion," in *IEEE/RSJ Intl. Conf. on Intelligent Robots and Systems*, pp. 5672-5677, 2009.

[104] E. Steltz, A. Mozeika, J. Rembisz, N. Corson and H. M. Jaeger, "Jamming as an enabling technology for soft robotics," in *Proc. Electroactive Polymer Actuator and Devices (EAPAD)*, vol. 7642, 2010.

[105] T. Ranzani, M. Cianchetti, G. Gerboni, I. D. Falco, and A. Menciassi, "A soft modular manipulator for minimally invasive surgery: design and characterization of a single module," *IEEE Transactions on Robotics*, vol. 32, no. 1, pp. 187-200, 2016.

[106] A. Jiang, G. Xynogalas, P. Dasgupta, K. Althoefer, and T. Nanayakkara, "Design of a variable stiffness flexible manipulator with composite granular jamming and membrane coupling," in *IEEE/ RSJ Intl. Conf. on Intelligent Robots and Systems*, pp. 2922-2927, 2012.

[107] E. T. Bean, O. Steiner and A. McDaid, "A soft robotic exoskeleton utilizing granular

jamming," in *IEEE Int. Conf. on Advanced Intelligent Mechatronics (AIM)*, pp. 165-170, 2015.
[108] I. Zubrycki, and G. Granosik, "Novel haptic glove-based interface using jamming principle," in *Proc. of Intl. Workshop on Robot Motion and Control*, pp. 46-51, 2015.
[109] A. D. Greef, P. Lambert, and A. Delchambre, "Towards flexible medical instruments: review of flexible fluidic actuators," *Precision Engineering*, vol. 33, pp. 311-321, 2009.
[110] Y. Cai, S. Bi, L. Zhang, and J. Gao, "Design of a robotic fish propelled by oscillating flexible pectoral foils," in *IEEE/RSJ Intl. Conf. on Intelligent Robots and Systems*, pp. 2138-2142, 2009.
[111] Y. Koizumi, M. Shibata, and S. Hirai, "Rolling tensegrity driven by pneumatic soft actuators," in *IEEE Int. Conf. on Robotics and Automation*, pp. 1988-1993, 2012.
[112] I. S. Godage, D. T. Branson, E. Guglielmino, and D. G. Caldwell, "Pneumatic muscle actuated continuum arms: modelling and experimental assessment," in *IEEE Int. Conf. on Robotics and Automation*, pp. 4980-4985, 2012.
[113] I. Godage, T. Nanayakkara, and D. Caldwell, "Locomotion with continuum limbs," in *Proc. IEEE/RSJ Int. Conf. on Intelligent Robots and Systems (IROS)*, pp. 293-298, 2012.
[114] K. Suzumori, "Elastic materials producing compliant robots," *J. of Robotics and Autonomous Systems*, vol. 18, no. 1-2, pp. 135-140, 1996.
[115] K. Suzumori, S. Endo, T. Kanda, N. Kato, and H. Suzuki, "A bending pneumatic rubber actuator realizing soft-bodied manta swimming robot," in *IEEE Int. Conf. on Robotics and Automation*, pp. 4975-4980, 2007.
[116] H. Takeshima, and T. Takayaa, "Six-braided tube in-pipe locomotive device," in *IEEE/RSJ Int. Conf. on Intelligent Robots and Systems (IROS)*, pp. 1125-1130, 2015.
[117] K. Suzumori and S. Asaad, "A novel pneumatic rubber actuator for mobile robot," in *Proc. IROS*, pp. 1001-1006, 1996.
[118] K. Suzumori, T. Hama, and T. Kanda, "New pneumatic rubber actuator to assist colonoscope insertion," in *Proc. IEEE Int. Conf. on Robotics and Automation*, pp. 1824-1829, 2006.
[119] H. Onoe, K. Suzumori, and T. Kanda, "Development of tetra chamber actuator," in *Proc. IEEE/RSJ Int. Conf. on Intelligent Robots and Systems (IROS)*, pp. 777-782, 2007.
[120] H. Onoe, K. Suzumori, and S. Wakimoto, "Optimum design of pneumatic multi-chamber rubber tube actuator generating traveling deformation waves for colonoscope insertion," in *Proc. IEEE/ASME Int. Conf. on Adv. Intelligent Mechatronics*, pp. 31-36, 2008.
[121] S. Wakimoto, and K. Suzumori, "Fabrication and basic experiment of pneumatic multi-chamber rubber tube actuator for assisting colonoscope insertion," in *IEEE Int. Conf. on Robotics and Automation*, pp. 3260-3265, 2010.
[122] K. Ozaki, S. Wakimoto, K. Suzumori, and Y. Yamamoto, "Novel design of rubber tube actuator improving mountability and drivability for assisting colonoscope insertion," in *IEEE Int. Conf. on Robotics and Automation*, pp. 3263-3268, 2011.
[123] G. D. Weymouth, V. Subramaniam, and M. S. Triantafyllou, "Ultra-fast escape maneuver of an octopus-inspired robot," *Bioinspir. Biomim.*, vol. 10, pp. 1-8, 2015.
[124] F. Ni, D, Rojas, K. Tang, L. Cai, and T Asfour, "A jumping robot using soft pneumatic actuator" in *IEEE Int. Conf. on Robotics and Automation (ICRA)*, pp. 3154-3159, 2015.
[125] C. M. Best, J. P. Wilson, and M. D. Killpack, "Control of a pneumatically actuated, fully inflatable, fabric-based, humanoid robot," in *IEEE-RAS Int. Conf. on Humanoid Robots (Humanoids)*, pp. 1133-1140, 2015.

[126] T. Noritsugu, M. Kubota, and S. Yoshimatsu, "Development of pneumatic rotary soft actuator made of silicone rubber," *J. Robot Mechatron.*, vol. 13, no. 1, pp. 17-22, 2001.

[127] F. Ilievski, A. D. Mazzeo, R. F. Shepherd, X. Chen, and G. M. Whitesides, "Soft robotics for chemists," *Angew. Chem,* pp. 1890-1895, 2011.

[128] R. Shepherd, F. Ilievski, W. Choi, S. Morin, A. Stokes, A. Mazzeo, *et al.*, "Multigait soft robot," in *Proc. Of National Academy of Science of the United States of America,* pp. 20400-20403, 2011.

[129] J. Florez, B. Shih, Y. Bai and J. Paik, "Soft pneumatic actuators for legged locomotion," in *Proc. IEEE Int. Conf. on Robotics and Biomimetics,* pp. 27-34, 2014.

[130] R. F. Shepherd, A. A. Stokes, J. Freake, *et al.*, "Using explosion to power a soft robot," *Angew. Chem,* vol. 125, pp. 2964-2968, 2013.

[131] M. Tolley, R. F. Shepherd, M. Karpelson, *et al.*, "An untethered jumping soft robot", in *IEEE/RSJ Int. Conf. on Intelligent Robots and Systems (IROS 2014)*, pp. 561-566, 2014.

[132] C. Onal, X. Chen, G. Whitesides and D. Rus, "Soft mobile robot with on-board chemical pressure generation," in *Int. Symp. on Robotics Research,* pp. 1-16, 2011.

[133] C. Onal, and D. Rus, "A modular approach to soft robots," in *IEEE RAS/EMBS Int. Conf. on Biomedical Robotics and Biomechatronics*, pp. 1038-1045, 2012.

[134] M. Luo, W. Tao, F. Chen, T. K. Khuu, S. Ozel, and C. D. Onal, "Design improvement and dynamic characterization on fluidic elastomer actuators for a soft robotic snake," in *IEEE Int. Conf. on Technologies for Practical Robot Applications (TePRA),* pp. 1-6, 2014.

[135] A. Slatkin, and J. Burdick, "The development of robotic endoscope," in *Proc. IEEE/RSJ Int. Conf. on Intelligent Robots and System,* pp 162-171, 1995.

[136] M. Carrozza, L. Lencioni, B. Magnani, and P. Dario, "A microrobot for colonoscopy," in *Proc. of Int. Symp. on Micromachine and Human Science,* pp. 223-228, 1996.

[137] A. Menciassi, J. Park, S. Lee, S. Gorini, P. Dario and J. Park, "Robotic solutions and mechanism for semi-autonomous endoscope," in *Proc. IEEE/RSJ Int. Conf. on Intelligent Robots and Systems (IROS),* pp. 1379-1384, 2002.

[138] L. Phee, D. Accoto, A. Menciasso, C. Stefanini, M. Carrozza, and P. Dario, "Analsyis and development of locomotion devices for the gastrointestinal tract," *IEEE Tran. On Biomedical Eng.*, vol. 49, no. 6, pp. 613-616, 2002.

[139] P. Dario, P. Ciarletta, and A. Menciassi, "Modeling and experimental validation of the locomotion of endoscopic robots in the colon," *The International Journal of Robotics Research*, vol. 23, no. 4-5, pp. 549-556, 2004.

[140] K. Adachi, M. Yokojima, Y. Hidaka, and T. Nakamura, "Development of endoscopic robot and experiment in the large intestine of dead swine," *IEEE Intl. Conf, on Robotics and Biomimetics*, pp. 467-472, 2011.

[141] T. Yanagida, K. Adachi, and T. Nakamura, "Development of bellow-type artificial rubber muscle and application to peristaltic crawling endoscopic robot," *J. of Robotics and Mechatronics*, vol. 25, no. 4, pp. 748-754, 2013.

[142] K. Suzumori, M. Mihara, and S. Wakimoto, "Beautiful flexible microactuator changing its structural color with variable pitch grating", in *IEEE Intl. Conf. on Robotics and Automation,* pp. 2771-2776, 2011.

[143] S. Morin, R. Shepherd, S. Kwok, A. Stokes, A. Nemiroski, and G. Whitesides, "Camouflage and display for soft machine," *Science Magazine,* vol. 337, no. 828, pp. 828-832, 2012.

[144] R. A. Beasley, "Medical robots: current systems and research directions," *Journal of Robotics,* vol. 2012, doi:10.1155/2012/401613.

[145] R. V. Martinez, A. C. Glavan, C. Keplinger, A. I. Oyetibo, and G. M. Whitesides,

"Soft actuators and robots that are resistant to mechanical damage", *Adv. Funct. Mater. J.*, vol. 24, pp. 3003-3010, 2004.
[146] A. Matsuda, T. Matsuda, K. Katanoda, T. Sobue, H. Nishimoto, and The Japan Cancer Surveillance Research Group, "Cancer incidence and incidence rates in Japan in 2007: A study of 21 population-based cancer registries for the Monitoring of Cancer Incidence in Japan (MCIJ) project," *Jpn. J. Clin. Oncol.*, vol. 43, no. 3, pp. 329–336, 2013.
[147] A. Jemal, F. Bray, M. M. Center, J. Ferlat, E. Ward, and D. Forman, "Global cancer statistics", *CA Cancer J. Clin*, vol. 61, no. 2, pp. 69-90, 2011.
[148] K. J. Lee, M. Inoue, T. Otani, M. Iwasaki, S. Sasazuki, and S. Tsugane, "Gastric cancer screening and subsequent risk of gastric cancer: A large-scale population-based cohort study, with a 13-year follow-up in Japan," *Int. J. Cancer*, vol. 118, pp.2315–2321, 2005.
[149] R. P. Barden, "A compression device for use in gastrointestinal examinations, when the patient lies prone," *Am. J. Roentgenol Radium Ther. Nucl. Med.* , vol. 2, no. 74, pp. 330-332, Aug. 1955.
[150] M. B. Nogrady, J. S. Dunbar, "On the use of the pneumatic compression paddle for improved visualization of the upper urinary tract in pediatric patients," *AJR*, vol. 103, No. 1, pp. 218-222, 1968.
[151] T. B. Shope, "Radiation-induced skin injuries from fluoroscopy," *Imaging & Therapeutic Technology*, vol. 16, No. 5, pp. 1195-1199, 1996.

# Publications

## Article Accepted/ Submitted in Refereed International Journal

1. New Pneumatic Rubber Leg Mechanism for Omnidirectional Locomotion

   Mohamed Najib Ribuan, Koichi Suzumori, and Shuichi Wakimoto

   International Journal of Automation Technology, Vol. 8 No. 2, February 10, 2014.

2. Locomotion Characteristics of Soft Mobile Robot Platform for Upper Gastrointestinal (UGI) Fluoroscopic Examination

   Mohamed Najib Ribuan, Shuichi Wakimoto, Koichi Suzumori, and Takefumi Kanda
   IEEE/ SICE International Symposium on System Integration (SII), Meijo University, Nagoya, Dec. 11-13, 2015, pp. 175-180.

3. Omnidirectional Soft Robot Platform from Flexible Actuators for Medical Assisting Device
   Mohamed Najib Ribuan, Shuichi Wakimoto, Koichi Suzumori, and Takefumi Kanda
   International Journal of Automation Technology (submitted)

## International Conferences/ Symposium

1. Pneumatic Soft Robot Base with Omnidirectional Locomotion

   Mohamed Najib Ribuan, Koichi Suzumori, Shuichi Wakimoto, and Takefumi Kanda

   Proceedings of the 9$^{th}$ JFPS International Symposium on Fluid Power, Matsue, Oct. 28-31, 2014, pp. 171-176.

2. Design and Locomotion of Eight-legged Soft Mobile Robot

   Mohamed Najib Ribuan, Shuichi Wakimoto, Koichi Suzumori, and Takefumi Kanda

   Proceedings of the 6$^{th}$ International Conference on Advanced Mechatronics (ICAM2015), Tokyo, Dec. 5-8, 2015, pp. 128-129.

## APPENDIX A

**Information regards end-mill.**

1. End-mill can be divided into 3-type:

a. Square

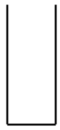

PLEM2LB6 -> diameter 6

b. Ball End Mill (BEM)

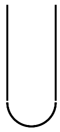

BEM2LB1.5-> diameter 3

c. Radius
(square+ball)

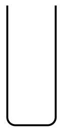

**Preparation before configure CraftMILL software and Roland machine.**

1. Save copy as the CAD drawing to *.stl file and click option to select the unit and high resolution then copy it to thumb drive.
2. Cut the raw material (polyester) – subject, according to the drawing plus the appropriate margin.
3. Clean the subject and the holder with ethanol and tissue.
4. Apply double sided tape to the object and stick the subject to the holder.
5. Apply weight (using vise) to the subject to ensure strong bonding between the subject and the holder.
6. Remove the vise after 10-15 minutes or after finish setting the CraftMill.

**Placing the subject in Roland**

1. Position the screw to the holder as following figure.

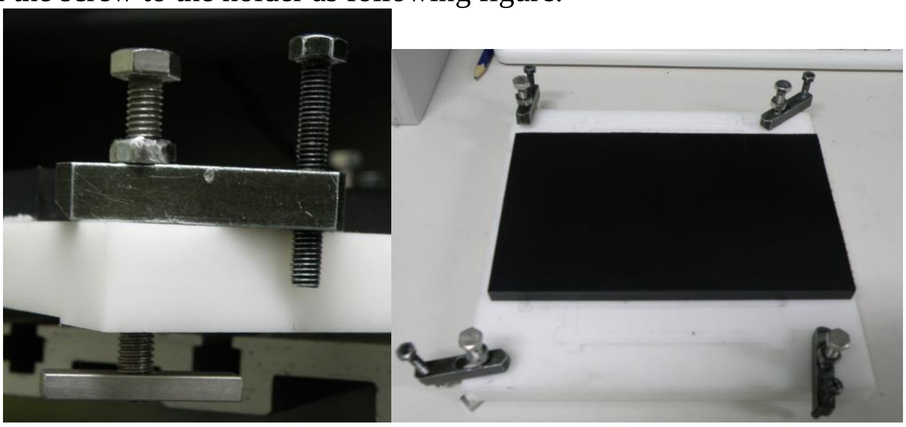

2. Slot the screw into Roland machine and make sure the bar is parallel to the holder as following figure.

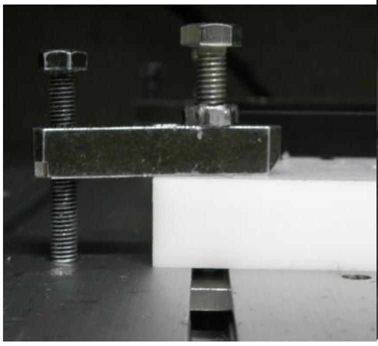

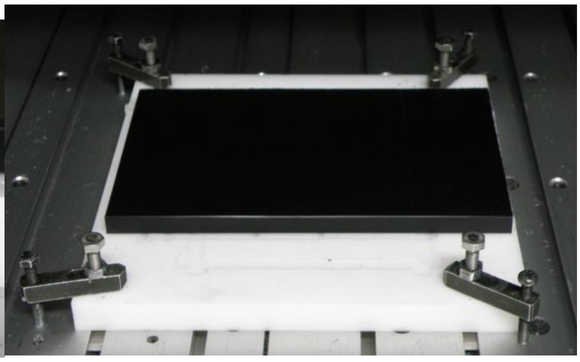

3. Tighten the screw and ensure its not moving by trying to move it with your hand.

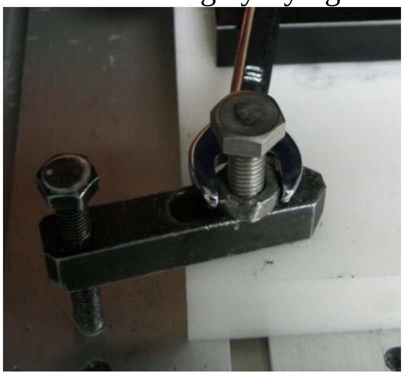

**Assembling the tools**

1. Pick you selected end-mill from the end-mill box.
2. Pick the chuck and suitable collet that fit your end-mill.

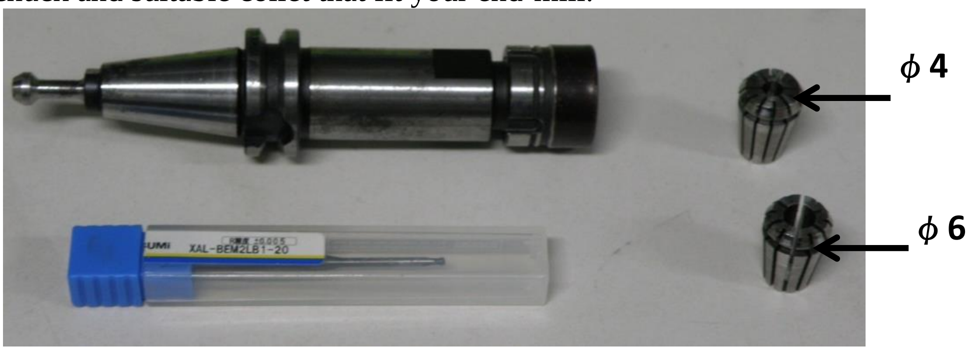


3. Put the chuck into the chuck holder and tightening the screw to lock it. Remove the chuck head and insert the collet into the chuck head as following figure.

4. Assemble the chuck head with its body by tightening it with your hand and make sure the collet is at the centre before you can insert the end-mill as following figure.

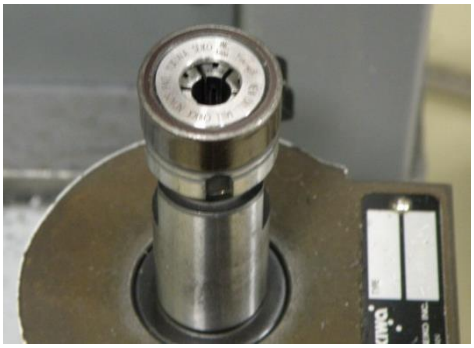

5. Ensure the height of the end-mill match the limit as the following figure and tighten the chuck head using the tool.

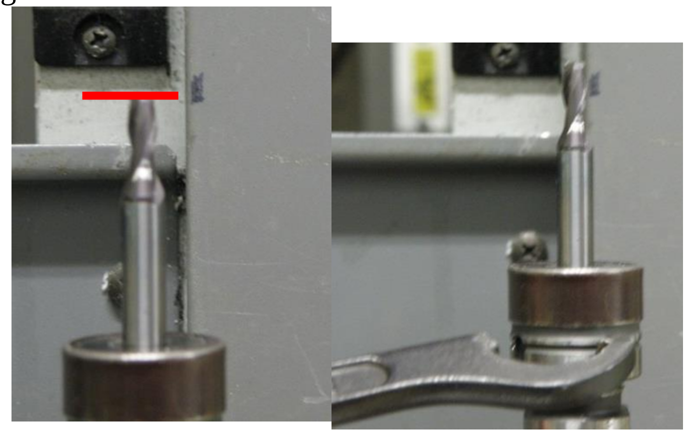

6. Place the tools into the Roland’s tools holder as following figure. Make sure to hold only the center of the chuck, not the cone shape as it can dirt and spoil the assembly.

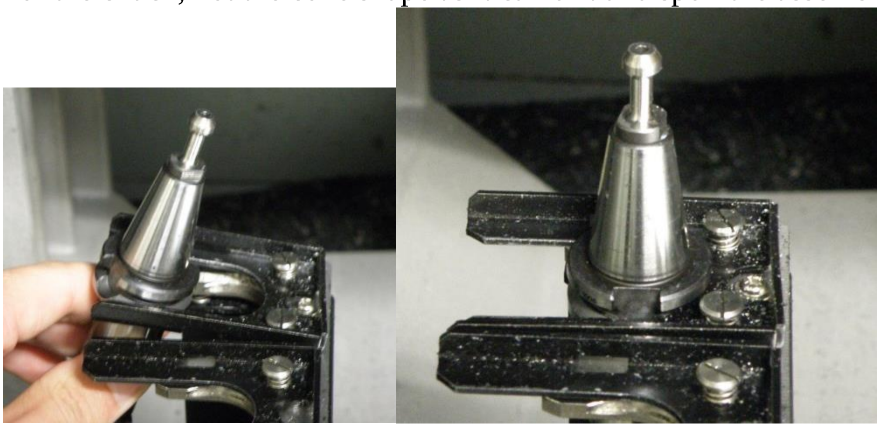

**Calibrate and configure the tools**

1. Switch on the compressor
2. Switch on the Roland machine.
3. Press Enter → the platform will move backward for calibration
4. Bring the platform near to the tools holder → put the sensor as following figure

5. Press Enter to display Menu.
6. Turn the dial into no 13 → press Enter → turn the dial into 13-2 → press Enter → enter the number of the tools accordingly by turning the dial and press Enter as follow

| | | | | |
|---|---|---|---|---|
| Location | 1 | 2 | 3 | 4 |
| Mill | 1 | 2 | 3 | 4 |

7. Press Enter → the gripper will pick the tool and perform calibration for each tool → press –Z to increase speed until near to the sensor and release the –Z button → it will slowly touch the sensor until `beep` sound and return the tools to the holder then continue calibrating the next tool until finish and stop.
8. Remove the sensor from holder → turn the dial to no. 13-1 → press Enter → press Enter → turn the dial to select no. 1 → press Enter
9. By pressing the X, Y and Z button, locate the tool no. 1 at the starting point as figure.

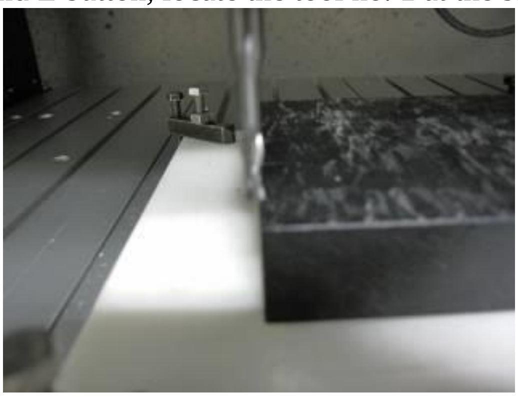

10. Press XY/A → turn the dial to 7 → press Enter to set the location as XY origin.
11. Put the sensor at the center of the subject → press the +Z to bring the tool upwards → → by pressing X and Y button, locate the tool on the top of the sensor →
12. Press Enter → turn the dial to 11 → press Enter → turn the dial to 11-1 → press Enter → press & hold –Z button until the end mill touch the sensor.

**For more than 4 end-mill**

13. Remove all the previous tools and replace the end-mill with the next end-mill (5, 6…)
14. Repeat Step 4, 5, 6 (enter 1, 2…. The same, not 5, 6…) followed by Step 7.
15. Repeat Step 11 and 12.
16. Click Execution icon in CraftMILL → uncheck the 1-4 tools → change the no. for end-mill no. 5 to no.1 in all the column → select Kurando → click OK → click (E)

**Note:** Roland machine only understand tools no. from 1 to 4 and CraftMILL understand 1 to greater than 4. Hence, adjusting the no. 5, 6, 7… to 1, 2, 3… in CraftMILL in important for Roland to execute the instruction.

**Configure CraftMILL.**

1. Double click CraftMILL icon 

on the desktop.

2. Select the second selection → click OK

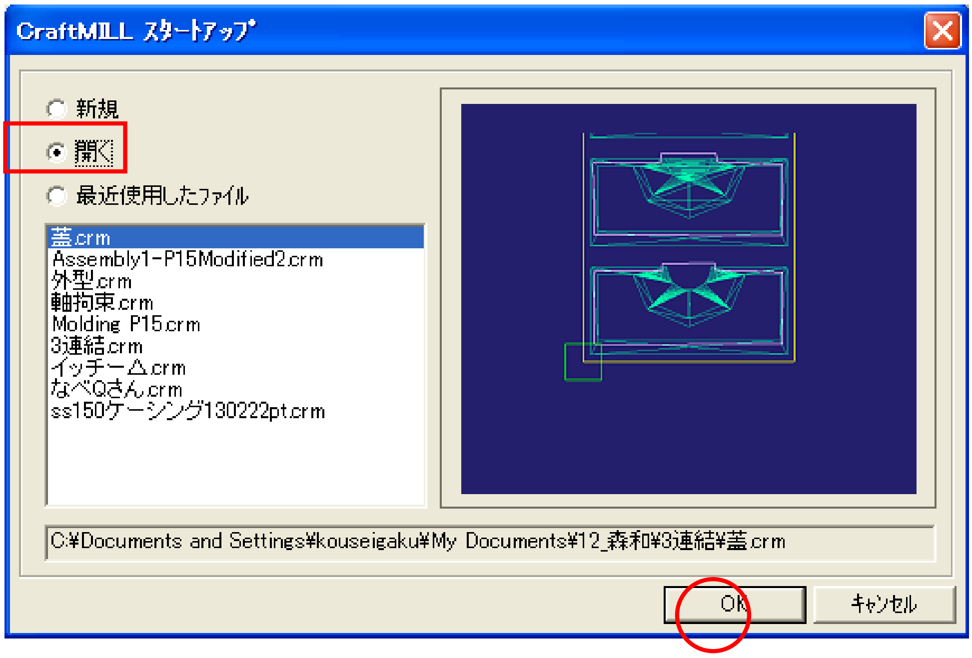


3. Select display *.stl file → select the folder → click the target*.stl file → click OK

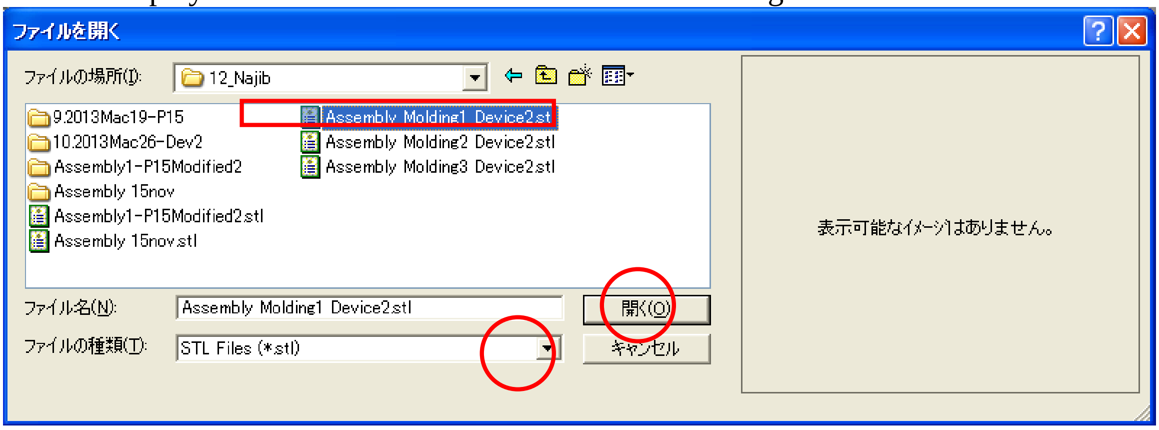


4. Select the folder you want to save your work→ click the folder → click OK → click OK

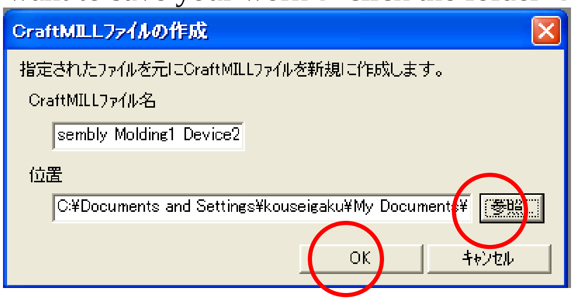

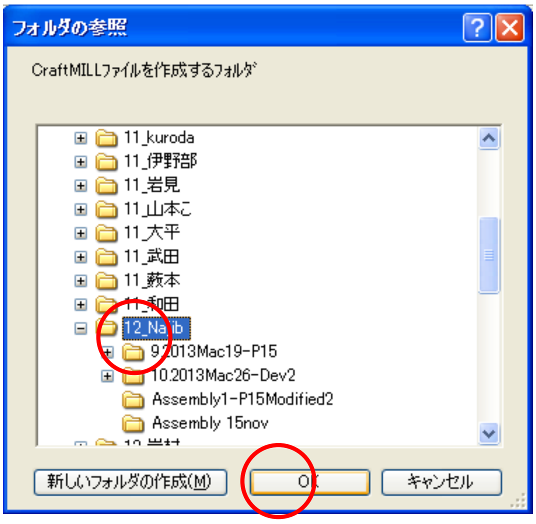


5. Click the (G) tab → select (A) → align the position of subject by adjusting the 3 options → use icon on the left side to confirm the arrangement

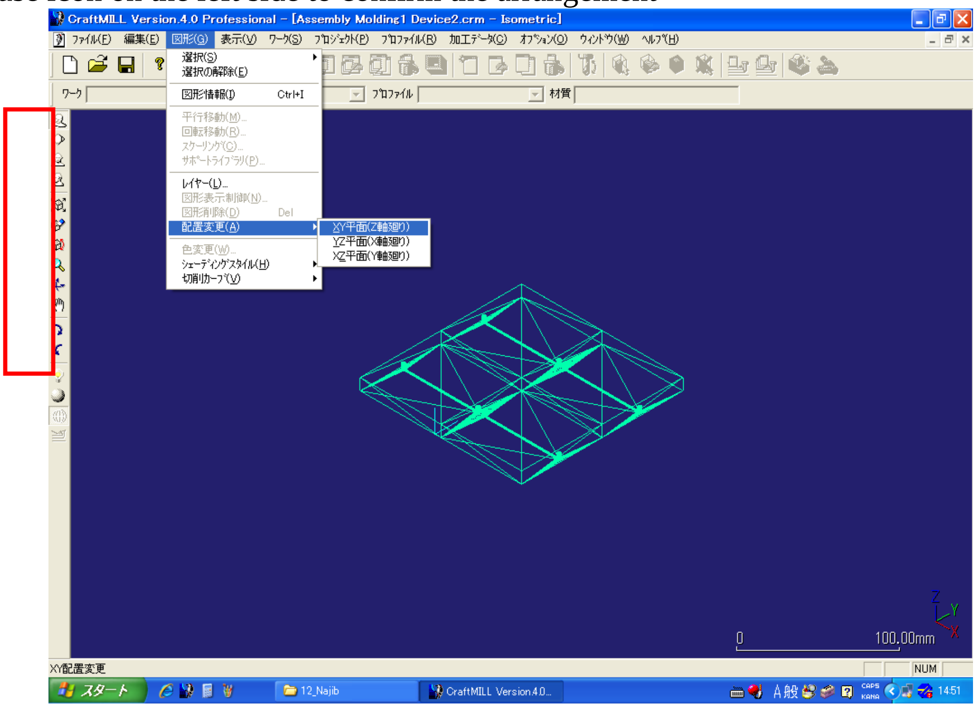


6. Click New Work icon → enter the margin (M) values at the bottom cluster. The values are corresponding to your subject where usually 2mm margin is used for Y & X axis for right and left side →enter the exact value of subject thickness in Z axis → click OK.

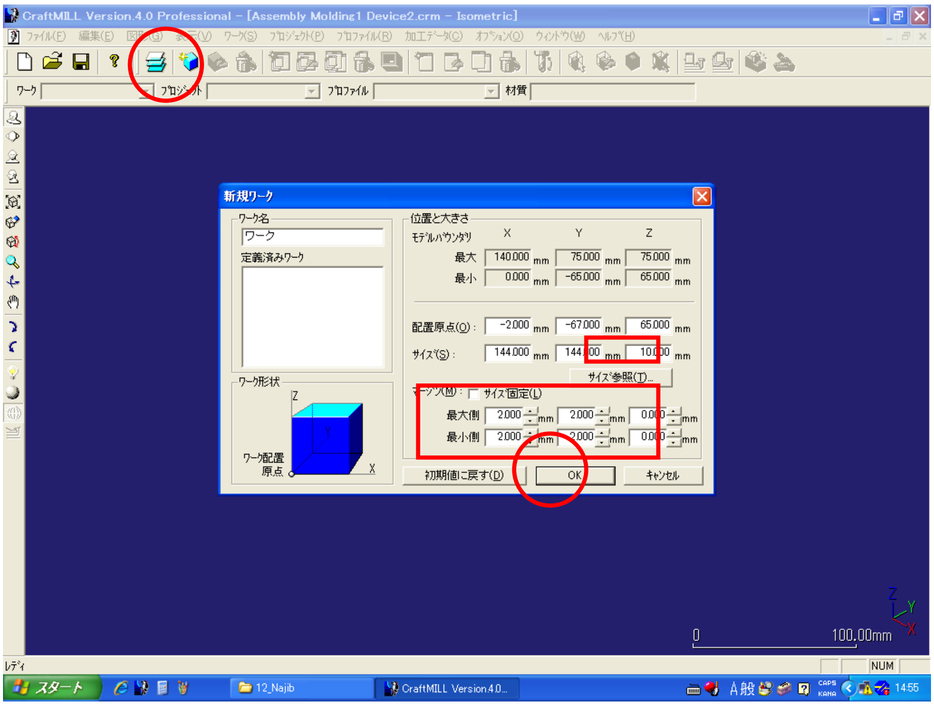


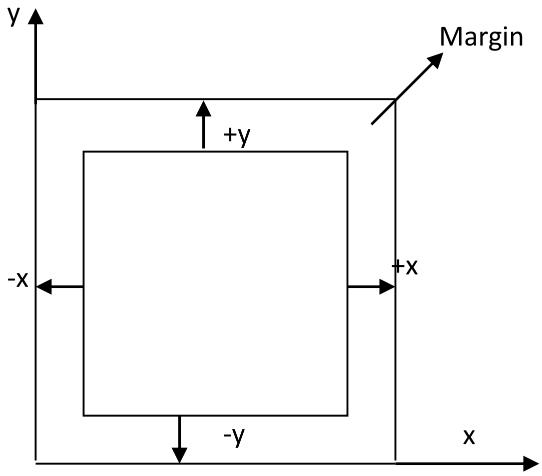


7. Click Create Project icon → click Next → select Material – ポリアセタール → click Next → confirm the end-mill from Z direction → click Next → confirm starting point at Zero → click Next → click Next →click Next → click Next → click centre button

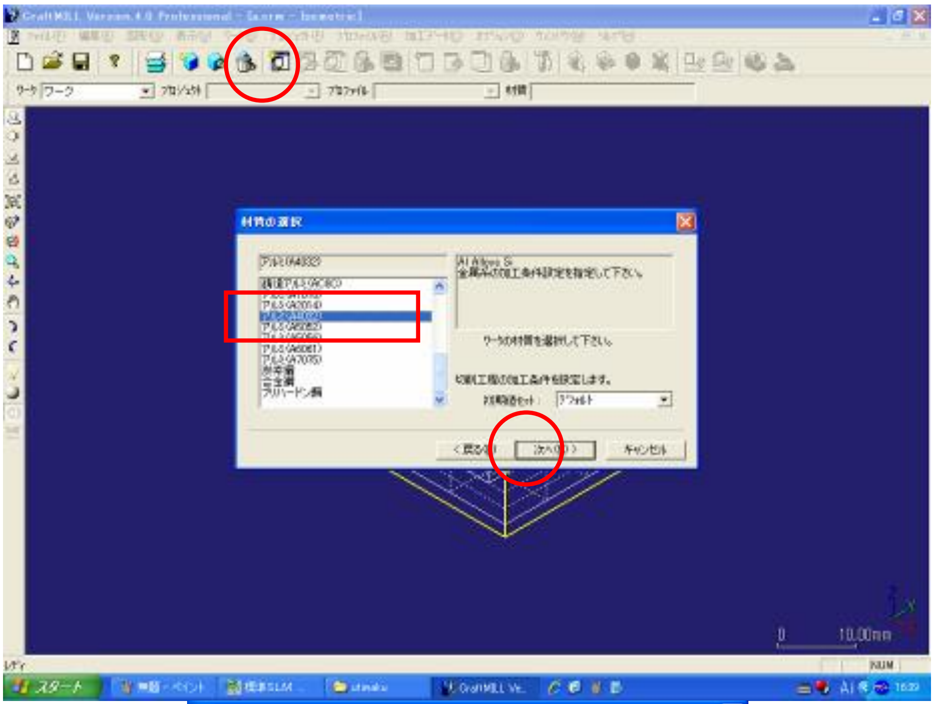

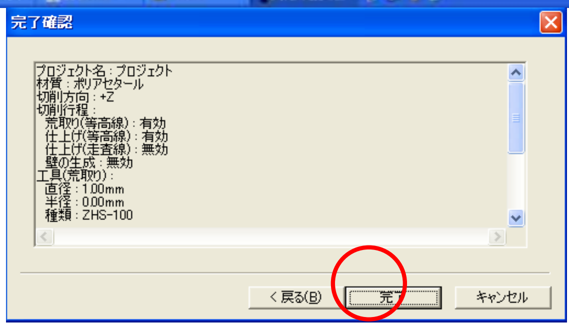


**Configure the end-mill**

8. Click the first end-mill → click End-mill Profile icon → click the first column to arrange the End-mill → select you corresponding end-mill → enter the rotation speed according to the table → click OK → click Yes

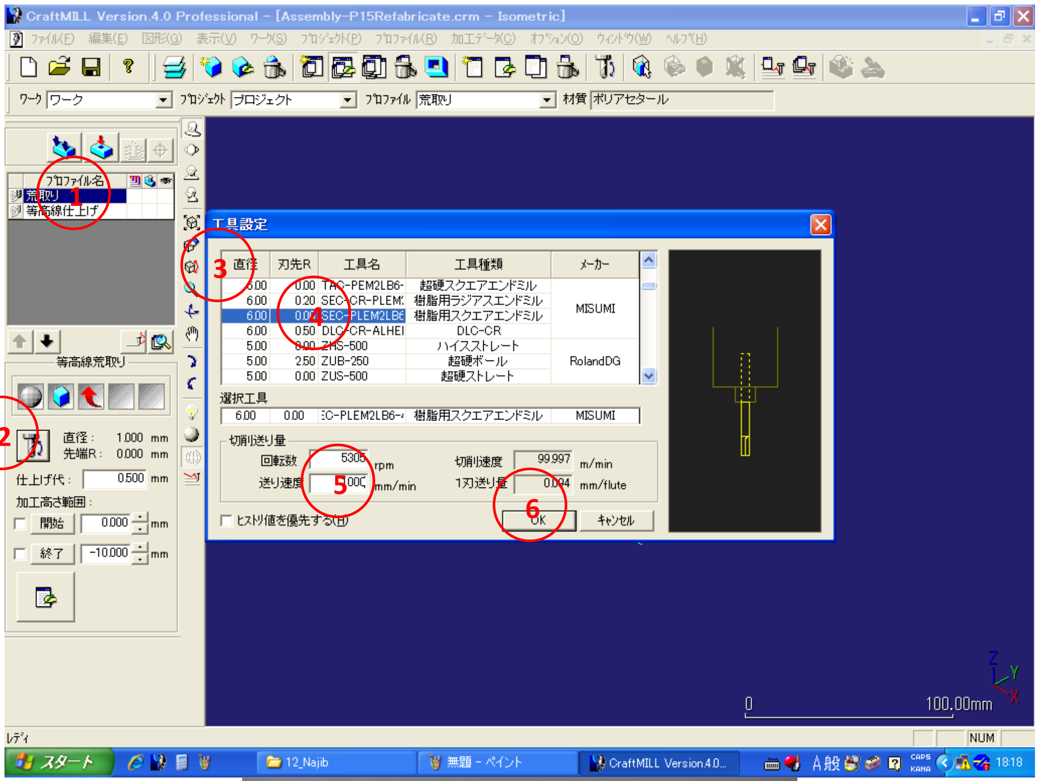


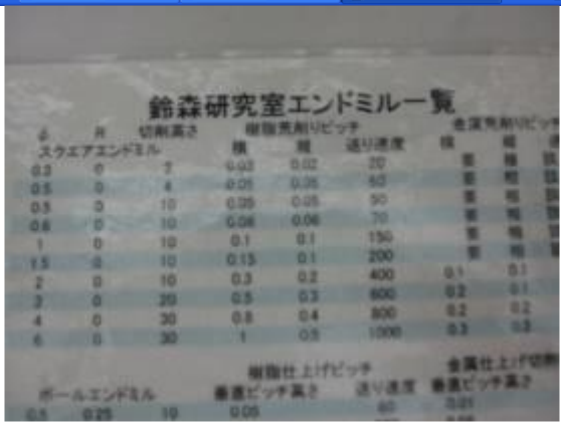


9. Click Edit Profile icon, 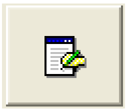 → enter the vertical (P) value (from table) → Click next tab → enter planar (P) value (from table) → click オプション tab → unchecked the first right option → click OK

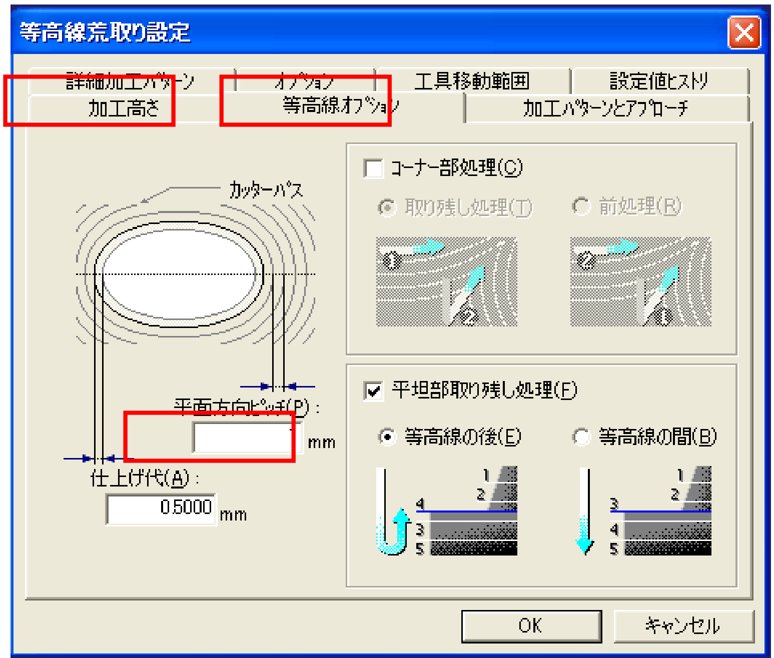


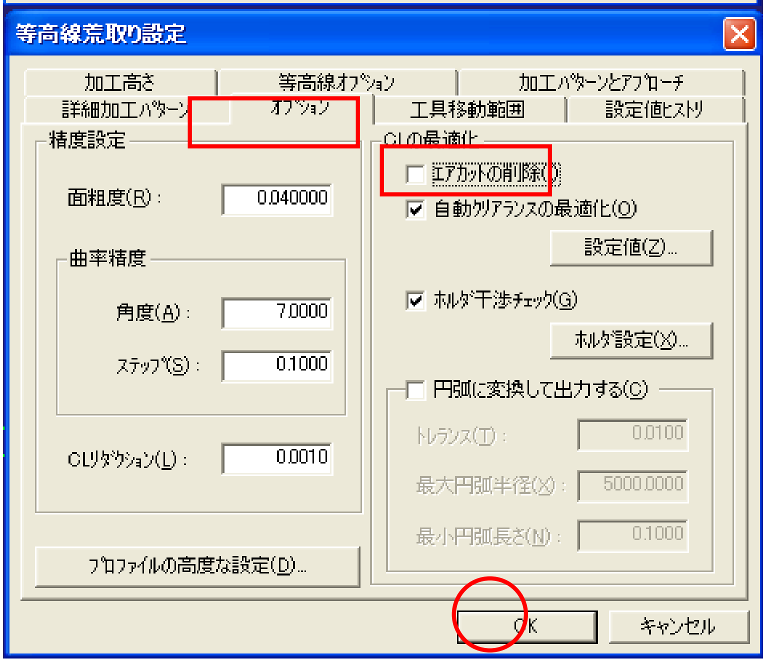


10. Repeat Step 8 & 9 for second end-mill. However, in Step 9, check Delete Air Cut under Option tab → click OK

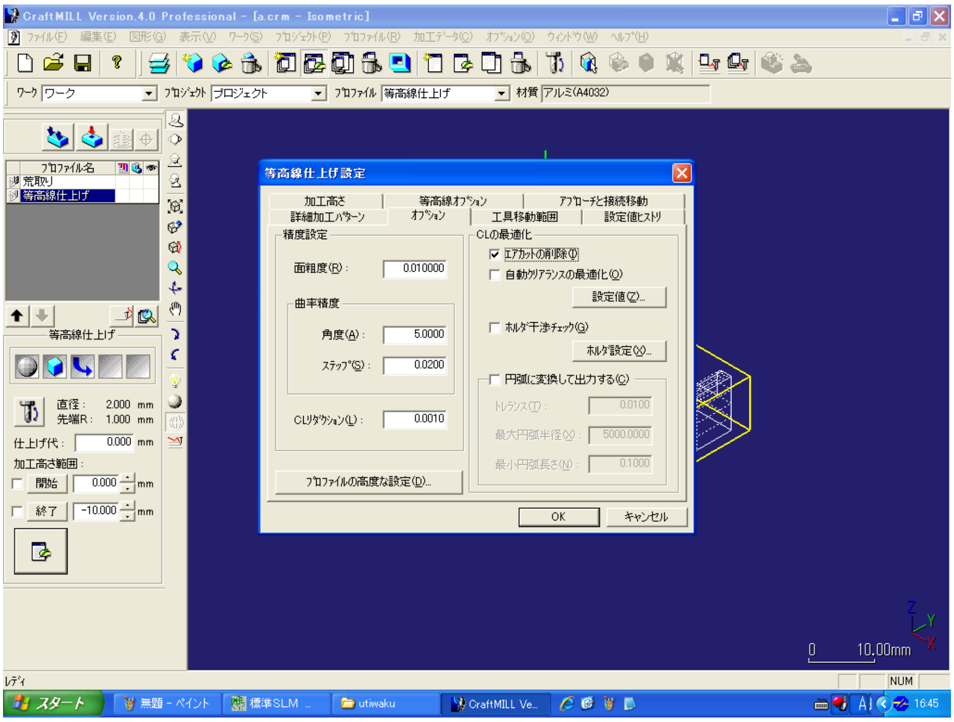


11. To add the third end-mill, click the second end-mill → right click → select (I) – Insert

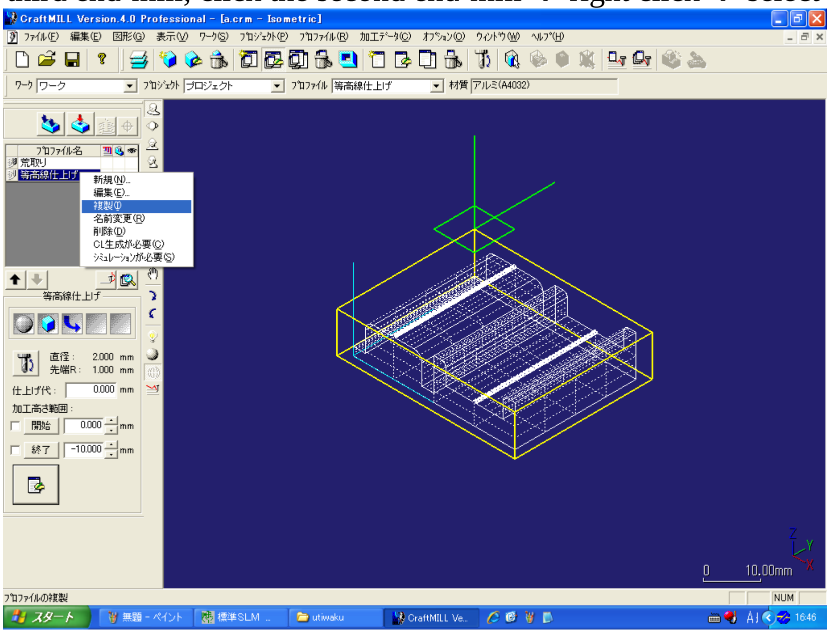


12. Repeat Step 8&9. Since we copy the setting by selecting (I), Step 10 can be ignored.
13. If you want to cut the processing time, you can specify the processing area. Select the last end mill → click Area Setting  → select the particular area you want to apply precise milling so the result will be accurate (including pin hole area) by click left mouse once, move the mouse, click again and continue until rectangle is achieved (covering the area), right click & select Enter → click OK 2 times

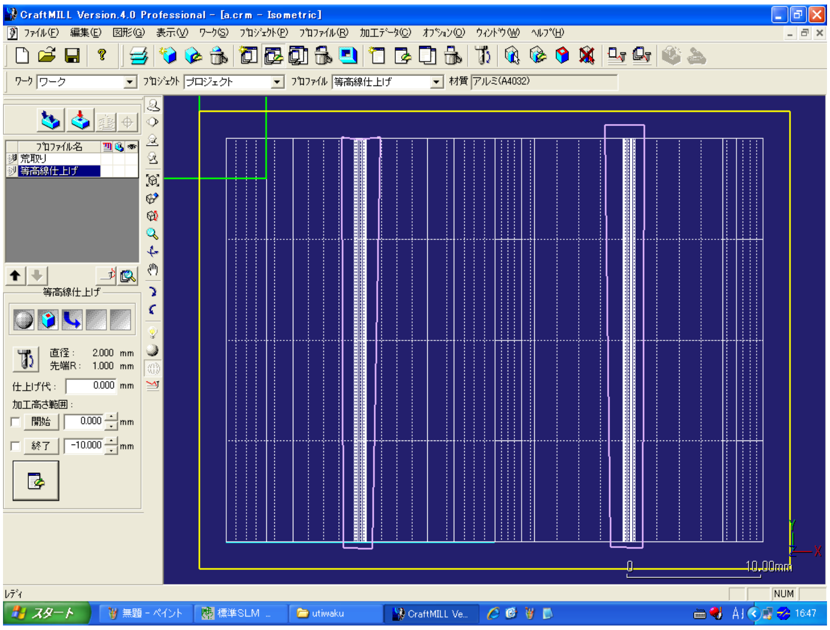

Purple line indicate specified processing area

**Generate Project**

14. Click Generation Project icon,  → click Yes → click Yes → computer will process the project & wait for few minutes → click OK. The blue Right sign indicates correct process. The orange Right sign indicates the length from simulation is not match with the length of end-mill. *can be ignored.

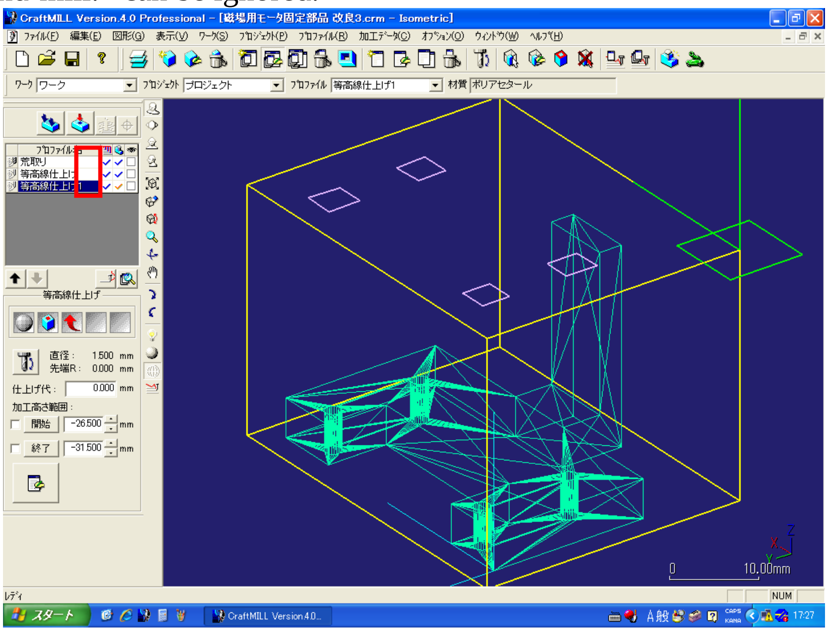


15. Click Simulate Project icon,  . You can select which end-mill you want to see the simulation → click the end-mill → click Simulate Project icon → click the top first right icon → click cancel after finish.

**Option**

16. Click the processing time icon,  to confirm the estimation processing time and any presence of error.

17. Select the end-mill and click the display processing path icon, 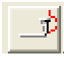 (next to processing time icon) to display the processing path of the end-mill.

**Execute project**

18. Click the Execution icon,  → select Kurando → select end-mill → click OK

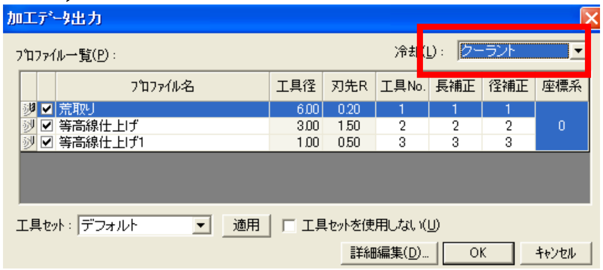

19. Click execution (E) → click OK

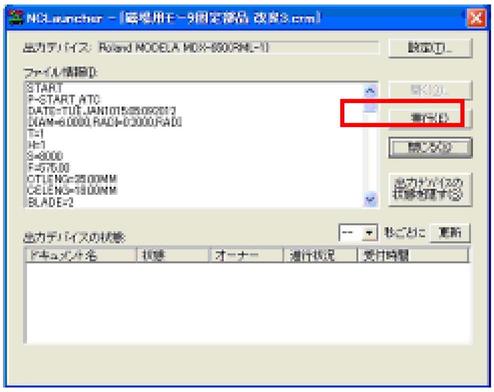

**For more than 4 end-mill**

20. Click Execution icon→ uncheck the 1-4 tools → change the no. for end-mill no. 5 to no.1 in all the column → select Kurando → click OK → click (E)

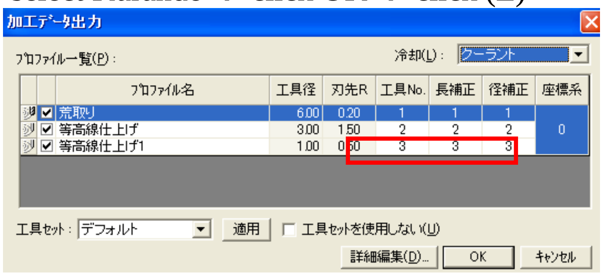

**Note:** Roland machine only understand tools no. from 1 to 4 and CraftMILL understand 1 to greater than 4. Hence, adjusting the no. 5, 6, 7… to 1, 2, 3… in CraftMILL in important for Roland to execute the instruction.

21. Dismantle the tools and clean Roland machine after the process is finish.

# APPENDIX B

## Using Mixer

This mixer is used for 2 purposes. In automatic mode, the mixer mixes the substance and release the bubble inside the container. In manual mode, the bubble appears during the pouring into molding is vacuumed to ensure good result is produced.

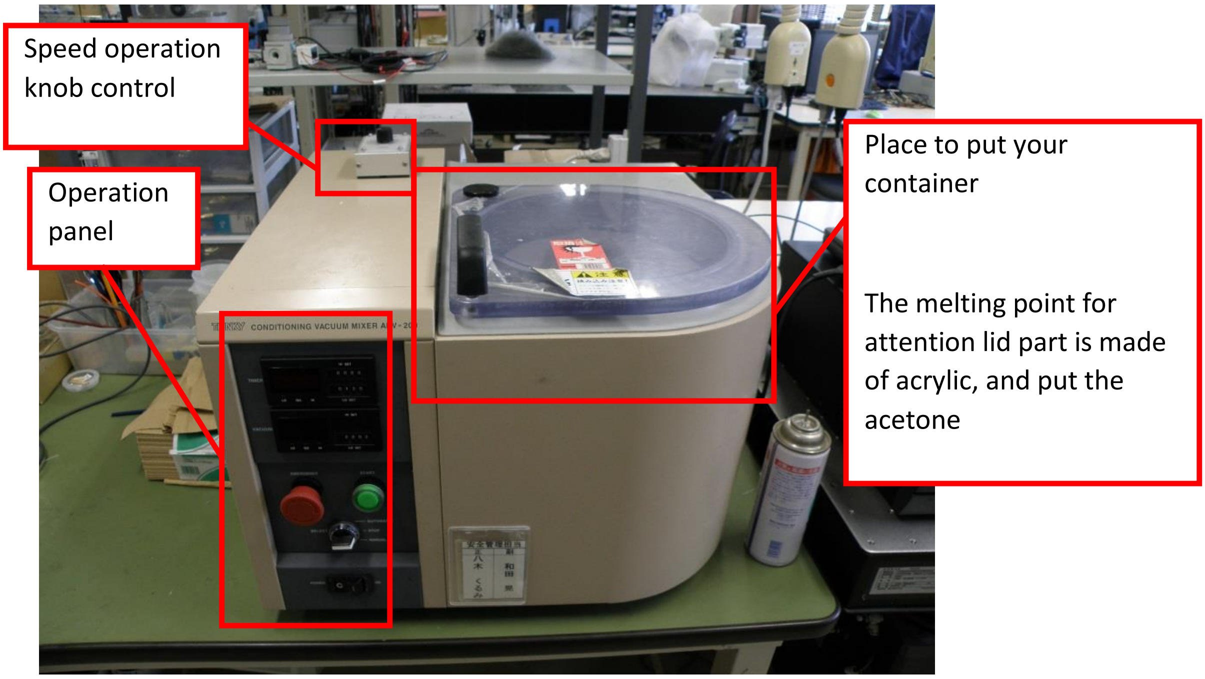


1. Ensure the Power switch is not ON.
2. Ensure the SELECT knob is in STOP.

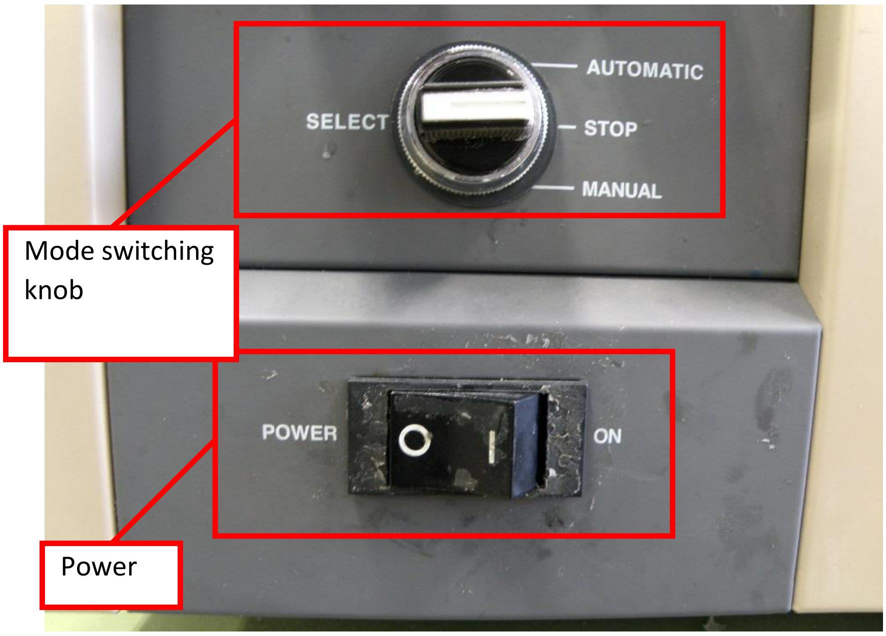

3. Check the knob of rotational speed control as shown in the photo. Ensure the value is not too high as standard revolution is at 600rpm.


4. Put a rubber container into the mixer. Uplift the handle and then slide to the right to open the lid.

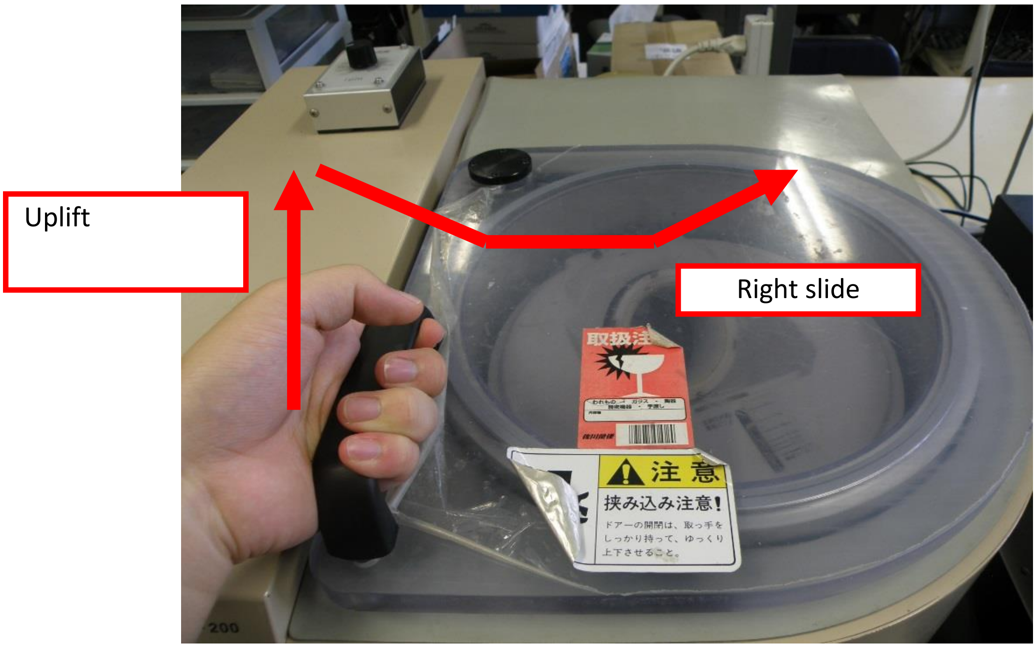


5. Put the container into the slot. Change the weight to match the total amount of adapter and rubber container.

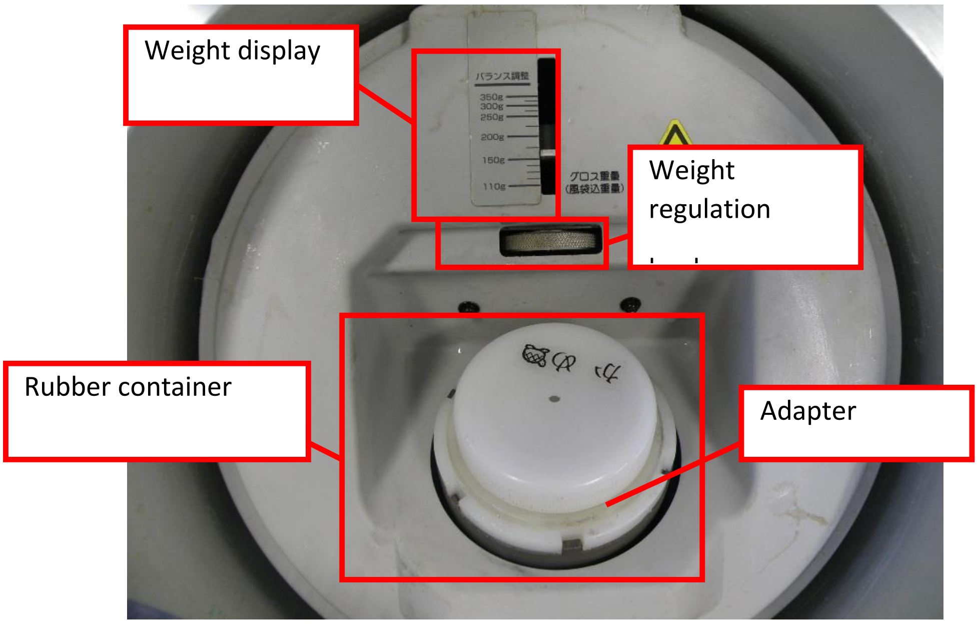


6. Close the lid. There is a possibility that it is not sealed (make sure that you closed it firmly).
7. Switch on the POWER.
8. The SELECT has two modes and divided according to its application.
   Beginners are recommended to use Automatic mode.
   - Automatic Mix + deaeration Recommendation

   Advanced users can use the Manual mode
   - Manual Only defoaming (vacuuming)
9. Setting confirmation
   - Timer Can be set according to your application. Usually it has been set to 120 seconds but can be changed.
   - Emergency EMERGENCY button is an unpowered state It is not possible to press and not from twist to the right and. However, after you press the START button, you can push it without having to twist. I will confirm that the EMERGENCY button is not pressed
   - Vacuum Said を confirmation

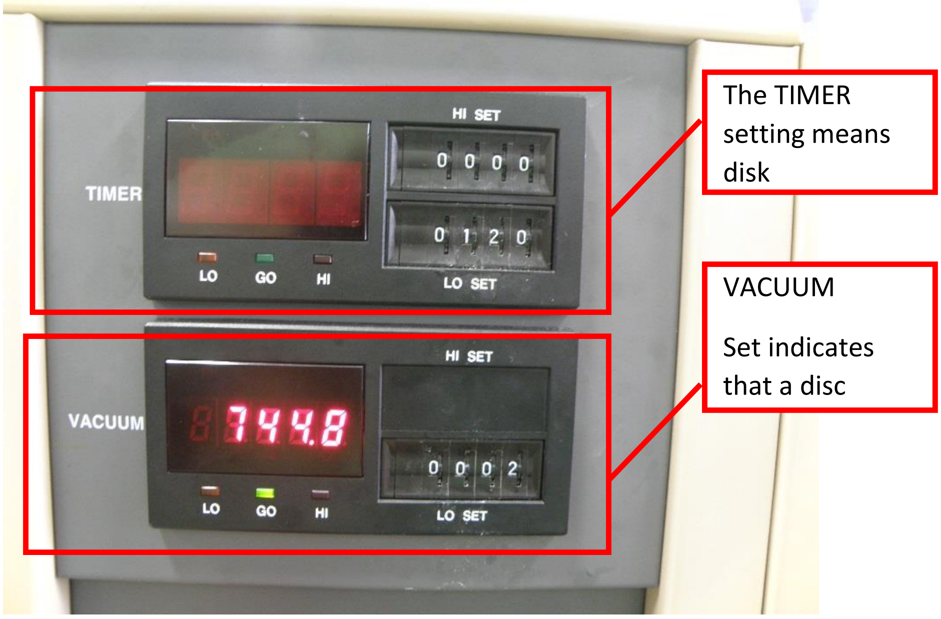


10. Press the START button. The rotation will begin. Press the EMERGENCY button if you want to stop it in emergency.


11. When the rotation stops, turn the SELECT control knob to STOP to turn OFF the power.
12. Take out the rubber container.